BROADBAND HIGH EFFICIENCY ACTIVE INTEGRATED ANTENNA

Yi Qin

A thesis submitted to the Faculty of the

Graduate School of Northumbria University

in partial fulfilment of the requirements

for the degree of Doctor of Philosophy

School of Computing, Engineering and Information Sciences,

Northumbria University, Newcastle Upon Tyne, UK

December 2006

Acknowledgments

I am deeply grateful to my PhD supervisor Dr. Steven Gao. He had provided me inspiration encouragement, strength, advice and research support during the years. The work would not have been possible without his academic guidance. It was such a pleasant and enlightening experience to work under his tutelage.

I am glad to thank my co-supervisor Professor Alistair Sambell, for his support of my research and his valuable comments that lead to completion of my work.

I also would like to give thanks to Professor Fary Ghassemlooy. He had provided kindly support my research work in many ways.

I would like to thank the past and present member of the group and technical support team in my research and class work.

I am deeply appreciative of my colleagues Lee. Dodson, David Tingy, Omar Veledar, Patrick Johnson and Michael Elsdon who gave friendly guidance and support at critical moments in my life. Special thanks should be given to Peter Elsdon for his unfailing technical advices on building practical circuits in the laboratory.

Also, I thank my father, Hongyao Qin, my mother, Huiping Zhen and my Brother, Wei, for being positive influences in my life. I could not imagine life without any of them.

Finally, I would like to give heart-felt thanks to my lovely wife Hui Ma, for her love, understanding and contribution to my success in my PhD. She has provided me with

limitless support in a difficult environment. Her selfless investment in my success has earned my life long respect and loyalty.

TABLE OF CONTENTS

LIST OF TABLES

LIST OF FIGURES

List of Symbols and Abbreviations

AIA.....active integrated antenna

VSWR.....voltage standing wave ratio

LP..... linearly polarization

CP..... circularly polarization

AR..... axial ratio

ac .....alternating current

dc .....direct current

FET..... field effect transistor

MESFET .....metal/semiconductor field effect transistor

PHEMT.....pseudomprphic high electron mobility transistor

RF .....radio frequency

Cs..... the drain to source capacitance of a FET

Cg .....the gate to drain capacitance of a FET

dB .....decibel

dBi.....decibels with respect to a isotropic source

dc .....direct current

ϕ .....Schottky barrier capacitor potential

FET..... field effect transistor

GaAs..... gallium arsenide

GHz .....10^9 Hertz

I .....current

V.....voltage

Ids..... drain to source current

Pout..... output power

Rd .....drain resistance of a MESFET

Re .....the real portion of a complex number

Im.....the imaginary portion of a complex number

I() .....a general error function

V..... voltage

Vg .....gate dc bias voltage

Vd .....dc drain voltage

Vds..... drain to source voltage

Vs .....dc gate voltage

V_g.... instantaneous ac gate voltage

V_{gs} .....gate to source voltage

Z_{load} .....the load impedance

Z_{opt} .....Optimum impedance

dBm .....decibels with respect to a milliwatt

PA..... power amplifier

PAE.....power added efficiency

Vin.....amplifier input voltage

α .....the Statz model Vds saturation voltage parameter

Idss .....drain to source current for 0 gate to source voltage

Igs .....gate to source current

RL.....load resistance

Vgs.....gate to source bias voltage.

C .....capacitance

α..... transmission line loss constant

Pin..... input power

Zo..... transmission line characteristic impedance

Abstract

Active integrated antenna (AIA) is a very popular topic of research during recent decades. This is mostly due to its advantages, such as compact size, multiple functions and low cost, etc. The AIA system can be regarded as an active microwave circuit which the output or input port is free space instead of a conventional 50-ohm interface. The major drawbacks of the conventional AIA include narrow bandwidth, low efficiency, etc.

An experimental investigation on broadband slot-coupled antenna is carried out, which results an impedance bandwidth of 50 % is achieved by both a ring slot-coupled and square ring slot-coupled patch antenna. An improved design technique for broadband class-E power amplifier (PA) design, based on the theoretical analysis done by Mader [2], is introduced to calculate the circuit parameters. The technique is applied to a RF microwave class-E power amplifier design (PA) that results a bandwidth of 12 % power added efficiency (PAE) greater than 60 % is achieved.

The aim of this work is to design broadband high efficiency linearly polarized (LP) and circularly polarized (CP) AIA and arrays that will be useful for mobile communication system. The AIA does not need conventional matching network between the amplifier and the antenna, because the antenna serves as both a harmonics-tuning network and a radiator. A novel high efficiency broadband LP AIA

is demonstrated using a ring slot-coupled patch antenna with a class-E PA. It exhibits a PAE over 50 % within a 14.6 % bandwidth. For the first time, a high efficiency broadband CP AIA is designed using a class-E PA integrated with a broadband CP antenna. The CP AIA achieves a PAE over 50 % within a 14 % bandwidth. The axial ratio of the CP AIA is below 3 dB over a 9 % bandwidth. For further improve the performance, a novel L-shaped slot-coupled broadband CP AIA is employed in a 2×2 array. The array consists of four sequentially rotated broadband CP antenna elements with an element spacing of half a free space wavelength. The antenna was designed to operate in the 3G band around 2 GHz. A bandwidth of 22.7 % PAE greater than 50 % is achieved together with a peak PAE of 71.35%. A bandwidth of 27 % axial ratio below 3 dB is resulted.

CHAPTER 1

Active integrated antennas (AIAs) combine prominent features that make them usable for both military and commercial applications. The most important feature is that the antenna and the active device are treated as a single entity, and accordingly active antenna in its minimum configuration consists of a passive antenna, typically, a rod or a dipole and an integrated amplifying device allowing compactness, low cost, low profile, minimum power consumption, and multiple functionality. A typical active antenna consists of one or more electronic devices such as diodes (Gunn, IMPATT (IMPact ionization Avalanche Transit-Time), Schottky, and varactor) and/or three terminal active devices, such as MESFET (Metal-Semiconductor Field Effect Transistor), HEMT (High Electron Mobility Transistor), or HBT (heterojunction bipolar transistor), integrated with planar antennas such as microstrip patches, printed dipoles, bowties, or slot antennas.

Most of AIAs reported so far have the drawback of narrow bandwidth, low efficiency, and/or high cost which limit their applications in mobile communication,

radars, etc. The low-efficiency and losses in AIAs limit their applications significantly, as morden communications need compact devices with a longer battery life. Furthermore, modern communication systems demand a high rate of data transmission, which requires a wide operation bandwidth. Recently, good improvements have been achieved with the integration of antennas with narrow band high efficiency amplifiers such as class-F [1] and class-E [2] amplifiers.

In this work, the critical issues limiting the bandwidth and efficiency of the AIA are investigated. This research extends the previous works [1-3] and presents theoretical and experimental work on novel AIA designs. A systematic design methodology is proposed to develop a broadband high efficiency class-E PA. Several broadband high efficiency LP and CP AIAs and array are developed. But first, a brief history of AIA and other background information is presented here.

1.1 Historical Comments And Applications

The first wireless communication dated back to 1901, when a young Italian, Guglielmo Marconi, took the new science out of the laboratory and into the 'real' world, sent radio signals across the Atlantic Ocean. Since then, wireless communications aim at high speed and high power efficiency. Consequently, all of the associated electronic systems have been influenced by this trend toward smaller size and better performance. Figure 1.1 shows a road map of wireless communication's development.

The idea of using active antennas can be traced back to as early as 1928 [4]. A small antenna integrated with electron tube was commonly used in radio broadcast receivers around 1 MHz at that time. In 1960's and 1970's, due to the invention of

high frequency transistors, the study of active antennas received much attention and several pioneering works were reported [5-19]. There are several advantages by implementing an active device into a passive radiating element, such as, increasing the effective length of a short antenna, increasing the bandwidth, decreasing the mutual coupling between array elements, and improving the noise factor. The performance of antenna is greatly improved using this concept.

Figure 1.1: Road map of wireless communication's development [4].

AIA topology has been popular in a variety of application such as: active phase array, radar, satellite communication in both military and commercial applications [3-16]. Figure 1.2 shows an example of the Erieye SLAR, which is a long-range pulse Doppler radar, fitted with a fixed active phased array antenna and

Figure 1.2: Erieye is a long range pulse Doppler radar, fitted with fixed active phased array antenna [17].

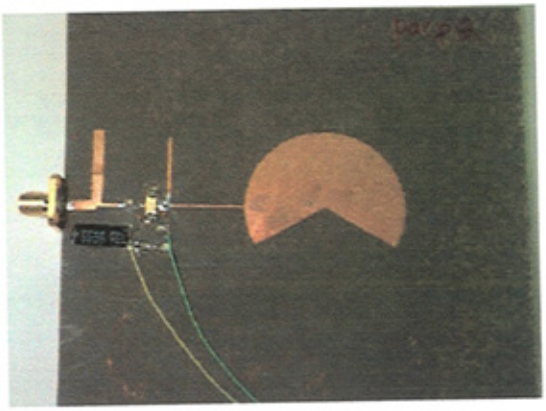

Figure 1.3: High efficiency AIA with class-F PA [2].

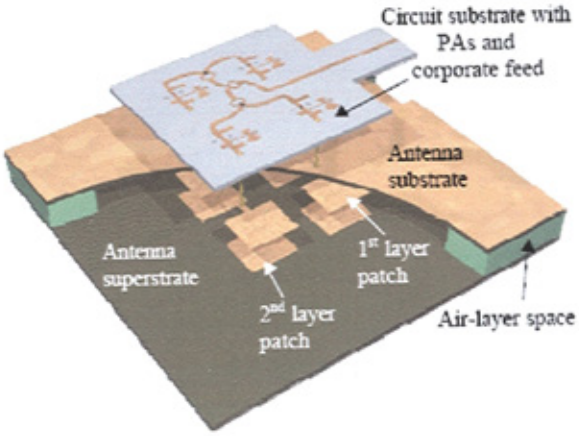

Figure 1.4: High efficiency AIA sub-array with class-E PA [3].

operating within the 2 GHz to 4 GHz, North Atlantic Treaty Organisation (NATO) E to F bands.

In more recent work, Itoh [2] and Popovic [3] reported high efficiency AIAs using class-F PA and class-E switch mode PA which are shown in Figure 1.3 and 1.4, respectively. Their works demonstrate that the AIA with switch mode PA is capable of achieving high efficiency performance.

1.2 Active Antenna In Radio Frequency (RF) Front-End

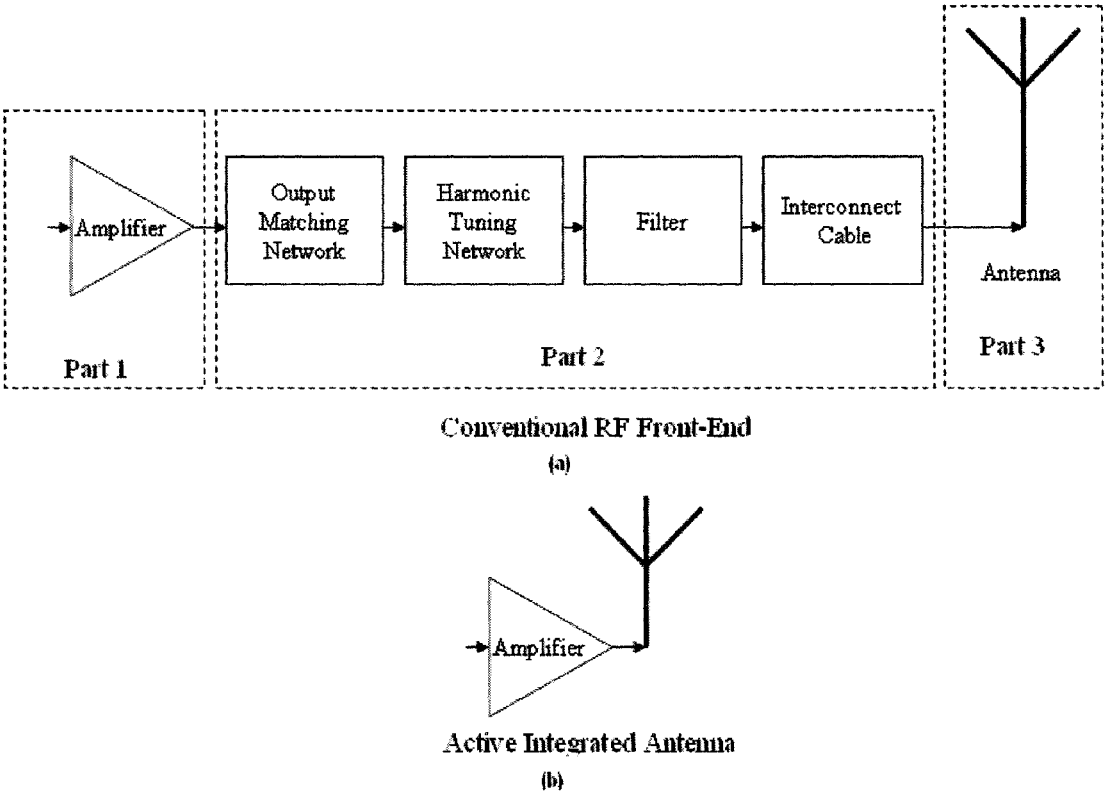

Figure 1.5: (a) Block diagram of conventional RF front end, and (b) active integrated antenna [20].

Advanced communications systems aim at low cost, high performance and low power consumption. The conventional radio transmitter RF front end can be divided into three parts, as shown in Figure 1.5(a). Part 1 is the RF power amplifier

(PA), which is typically designed separately and connected to part 3, *i.e.*, the antenna, through part 2. Part 2 includes many components, such as output matching circuits, harmonic tuning networks, filters and interconnecting cables. At high frequencies, these components in part 2 become quite lossy, which will directly increase the required amplifier power output for a given radiated transmitter power. To reduce the loss in part 1 and 2, AIA could be employed. In the AIA, the loss in part 2 is eliminated, as the antenna is directly integrated with the high-efficiency PA, as shown in Figure 1.5(b). The antenna is used as a harmonic tuning load of the PA, in addition to its original role as a radiator.

The main purpose in this project is to develop novel compact high performance AIAs which could reduce the power consumptions in all above three parts, and achieve high performances (such as high efficiency, broad bandwidth, high gain, high polarization purity, *etc*). As a key component in radio transmitters, the AIA in this project will significantly improve the performance of mobile communications systems while reduce the power consumption, the cost and the size. The most power-hungry component in transmitter designs is the PA. Since higher dc power adds to both system costs and weight, high-efficiency PAs are the essential key components for highly compact and light-weight transmitters in wireless communications systems. Even a few percent of improvement in power-added efficiency (PAE) can be significant if it can be designed without the major degradation in linearity. It has been shown that improving the PAE of an onboard 2-kW solid-state power amplifier in a communication satellite from 25 % to 30 % will reduce the waste heats substantially from 6 to 4.7 kW. Amongst various kinds of power amplifiers, class-E PA has been shown to be very promising for high-frequency applications, with a maximum

theoretical efficiency of 100 %. In this project, we will investigate novel configurations of AIAs which integrate high-efficiency Class-E microwave power amplifiers with broadband microstrip antennas. Different kinds of broadband microstrip antennas suitable for this application will be studied. The antenna will also serve as harmonic terminations for the class-E PA, in addition to its original function as a radiator. Harmonic radiation will be reduced by suppressing higher harmonics.

1.3 Motivations of This Research

For applications in microwave and millimetre wave communication system such as GSM (global system for mobile communications) and GPS (global position system), it is very important for AIAs to achieve both high efficiency and broad bandwidth. Several AIAs are proposed in [1-3], through the integration of antennas with class-B, class-E and class-F PA. However, class-E and Class-F designs are for narrow band applications. A bandwidth of 6% for class-E [3] AIAs and 5.8% for class-F [1] are achieved. So that it is necessary to develop a broadband high efficiency class-E PA. How to develop broadband high efficiency class-E PA is a challenging task.

Circularly polarized antennas are useful for satellite communications and GPS system, as polarization of a linear polarized radio wave may be rotated as the signal passes through any anomalies in the ionosphere. Furthermore, due to the position of the Earth with respect to the satellite, geometric differences may vary especially if the satellite appears to move with respect to the fixed Earth bound station. Circular polarization will keep the signal constant regardless of these anomalies. Therefore, the integration of high efficiency PA with broadband CP antenna will be very useful for

advance wireless system. However, high efficiency AIAs represented in [1-3] are producing limited bandwidth only.

1.4 Objectives of This Research

This work aims at the development of a novel broadband high efficiency RF/microwave PA and a broadband high efficiency AIA for applications in broadband communications.

Objectives include:

- To develop new broadband microstrip antenna for further integration with RF PA module
- To develop a design methodology for improving the bandwidth of high efficiency class-E RF PA
- To optimize the circuit configuration of the conventional class-E power amplifier in order to compromise the tradeoff between the efficiency and bandwidth
- To develop a prototype of novel RF/microwave broadband high efficiency class-E PAs
- To develop a novel LP broadband high efficiency AIA for radio transmitter's in future mobile communication systems
- To develop novel CP broadband high efficiency AIAs for radio transmitter's in future mobile communication systems
- To develop novel CP AIA arrays for achieving high output power and broad impedance bandwidth. A proposed layout is shown in Figure 1.6.

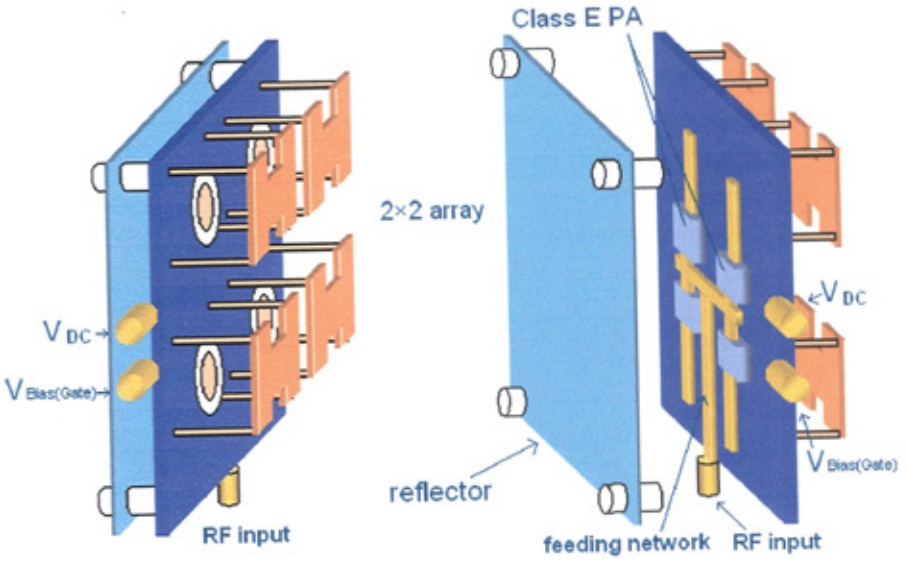

Figure 1.6 Layout of 2×2 AIA array.

1.5 Key Contributions

Key contributions of this work include:

- Development of two novel broadband high efficiency CP AIAs. The cross slot-coupled CP AIA achieves a PAE above 50 % over a 14 % bandwidth from 1.92 GHz to 2.21 GHz. A peak output power of 22.3 dBm is obtained. The axial ratio of the CP AIA is below 3 dB over a 9 % bandwidth from 1.99 GHz to 2.18 GHz. This is the first demonstration of broadband high efficiency CP AIA. State of the art performance has been achieved. The AIA with an L-shaped feed line achieves an AR value below 3dB within a 9 % bandwidth, i.e., from 1.84 GHz to 2.01 GHz. A peak drain efficiency of 73.3 % is achieved. A 12 % bandwidth for PAE over 60 % is obtained, with a peak output power of 21.7 dBm

- Development of broadband high efficiency LP AIA, which achieves a PAE above 50 % over a 14.6 % bandwidth from 1.78 GHz to 2.06 GHz
- Development of a novel broadband high efficiency CP AIA array, which achieves a PAE over 50% within a 22.6% bandwidth from 1.72 GHz to 2.16 GHz. The drain efficiency is over 60% from 1.82 GHz to 2.14 GHz. The AR value below 3 dB is obtained over a 27% bandwidth from 1.73 GHz to 2.26 GHz
- Development of two novel broadband slot-coupled microstrip patch antennas at 3 GHz, which achieve a return loss bandwidth of 50%
- Development of three broadband high efficiency class-E PA at different frequencies. The first one achieves a PAE greater than 50 % over the frequency range between 540 MHz and 890 MHz. The second one achieves a PAE above 50%, within a frequency range between 1.52 GHz and 2.16 GHz. The third one achieves a PAE above 60 % between 1.73 GHz and 2.16GHz
- Development of an improved design methodology for broadband high efficiency class-E PA. This work extends Madder's [4] work on class-E PA for boradband operation.

1.6 List of Publications on Results of This Work

Journal:

1. Y. Qin, S. Gao and A. Sambell, "Broadband High Efficiency Linearly and Circularly Polarized Active Integrated Antennas", **IEEE Transactions on Microwave Theory and Techniques,** vol. 54, no. 6, pp: 2723-2732, Jun 2006

2. Y. Qin, S. Gao and A. Sambell, "Broadband High Efficiency Circularly Polarized Active Integrated Antenna and Array for RF Front-End Applications", **IEEE Transactions on Microwave Theory and Technique,** vol. 54, no. 7, pp: 2910-2916, July. 2006

3. S. Gao, Y. Qin and A. Sambell, "Low-cost Broadband Circularly Polarized Printed Antenna and Array", **IEEE Antennas and Propagation Magazine,** *(accepted)*

4. Y. Qin, S. Gao, E. Korolkiewicz and A. Sambell, "Broadband patch antenna with ring slot coupling" **IEE Electronic Letters,** vol. 40, Issue. 1, pp: 5 – 6, Aug 2004

5. Y. Qin, S. Gao, E. Korolkiewicz and A. Sambell, "Broadband patch antenna with Square ring slot coupling", **Microwave and Optical Technology Letter,** vol. 47, no. 5, pp: 454-457, Dec 2005

6. Y. Qin, S. Gao, E. Korolkiewicz and A. Sambell, "Design of Low Cost Broadband Class-E Power Amplifier Using Low Voltage Supply", **Microwave and Optical Technology Letters,** vol.44, no.2, pp: 103-106, Jan 2005

7. S. Gao, Y. Qin and A. Sambell, "Broadband circularly polarized high efficiency active antenna", **IEE Electronic Letters,** vol. 42, pp: 258-260, No. 5, Mar 2006

Conference:

8. Y. Qin, S. Gao, E. Korolkiewicz and A. Sambell, "Improved Design Technique of a Broadband Class-E Power Amplifier at 2GHz", **European Microwave Conference**, Paris 2005, vol. 1, pp: 453 – 456, Oct 2005

9. Y. Qin, S. Gao, E. Korolkiewicz and A. Sambell, "Design of Low Cost Broadband Class-E Power Amplifier Using Low Voltage Supply at 2GHz", **2004 IEEE High Frequency Postgraduate Student Colloquium**, vol. 1, pp:101-106, Sep 2004. Su Zhou, China

10. Y. Qin, S. Gao, E. Korolkiewicz and A. Sambell, "Improved Design Technique of a Broadband Class-E Power Amplifier", **House and Common Annual presentation by Britain's top younger Scientists, and engineers and technologists London,** May. 2005

11. Y. Qin, S. Gao and A. Sambell, "Broadband high efficiency circularly polarized active antenna", **IEEE Asia Pacific Microwave conference,** vol. 3, pp: 4, Dec 2005

12. S. Gao, Y. Qin and A. Sambell, "Broadband high-efficiency active integrated array antenna", **Loughborough Antennas and Propagation International Conference 2006**, pp. 29-32, Apr 2006, Loughborough, UK
13. S. Gao, Y. Qin and A. Sambell, " Low-cost circularly polarized broadband high efficiency active integrated antenna", **IEEE Antennas and Propagation International Symposium,** New Mexico, USA, July 2006 *(accepted)*

Related to this work the author has also been involved with the following publications:

Journal:

14. M. Elsdon, Y. Qin and A. Sambell, "Compact circular polarised patch antenna with relaxed manufacturing tolerance and improved axial ratio bandwidth" **IEE Electronic Letters**, vol, 39, Issue. 18, pp: 1296-1298, Sep 2003

15. Y.Qin and E. Korolkiewicz, "Design of Microstrip Offset Feed Circular polarised Nearly Square Patch Antenna Operating at 2.45GHz", **IEE Electronic Letters,** vol. 38, no. 16, pp: 844 – 845, Aug 2002

16. S. Lee, Y. Qin, E. Korolkiewicz and A. Sambell, "Reduction of the second and third harmonics for a rectangular Microstrip patch antenna", **Microwave and Optical Technology Letters**, vol. 40, no. 6, pp: 455-460, Feb 2004

17. M. Elsdon, A. Sambell, S. Gao and Y. Qin, "Planar Fed Compact Circular Polarised Microstrip Antenna with Triangular Slot Loading", **Microwave and Optical Technology Letters**, vol.41, Issue. 3, pp: 226-228, May 2004

18. M. Elsdon, A. Sambell, S. Gao and Y. Qin, "Compact Circular Polarised Patch Antenna with Relaxed Manufacturing Tolerance and Improved Axial Ratio Bandwidth", **IEE Electronic Letters**, vol. 39, no. 18, pp: 1296-1298, Sep 2003
19. M. Elsdon, A. Sambell and Y. Qin, "Reduced Size Direct Planar Fed Patch Antenna", **IEE Electronic Letters**, vol. 41, no. 16, pp: 884-886, Aug 2005

20. M. Elsdon, and Y. Qin, "Dual Frequency Planar Fed Microstrip Patch Antenna", **Microwave and Optical Technology Letters,** vol. 48, issue. 6, pp: 1053-1054, Jun 2006.

1.7 THESIS OUTLINE

This thesis presents the designs, simulation, fabrications, and measurements of novel broadband antennas, broadband high efficiency class-E PA, broadband high efficiency AIAs and active array.

The introduction of this project, motivations of this work for using high efficiency active integrated antenna, as well as the key contributions of this work have been presented in Chapter. 1.

A literature review of broadband microstrip patch antennas with different techniques of realizing broadband operation is presented in Chapter 2. Designs and simulations of novel LP and CP broadband slot-coupled microstrip patch antennas are presented in Chapter 3 together with practical measurements.

The Chapter 4 provides a review of class-E PA and its theoretical analyses of class-E PA. The investigations of the practical effects on the performance of class-E PA are discussed. Chapter 5 presents design, fabrications and measurement of two broadband class-E PA. An improved design methodology for broadband class-E PA is introduced and verified by a class-E PA design at 2GHz. Experimental results are presented in this chapter.

The focus of Chapter 6 is to present the background of AIA as well as the early work on high efficiency AIA. Designs and fabrications of broadband high efficiency LP and CP AIAs and active array are presented in Chapter 7.

Finally, Chapter 8 provides a summary of this work and suggestions for future work on high efficiency AIAs for RF front-end.

CHAPTER 2
Review of Broadband Microstrip Patch Antenna

The broadband microstrip patch antenna is capable of operation within a broad frequency range which is useful for broadband communication and radar system. In communication systems, broad bandwidth means more capacity and high data rate. The purpose of this chapter is to present a general overview of design techniques used to enhance the bandwidth of the microstrip patch antenna, including: reactive load, multi-layered aperture-coupled structure, multi-resonators and broadband CP antennas.

2.1 Introduction

In industry today, microstrip patch antennas are widely used because of several major advantages such as low profile and light weight. However, the conventional single-layer microstrip patch antenna has a main disadvantage of narrow bandwidth which significantly limits its application. On the other hand, the modern communication system often needs a single antenna which can operate within a broad

frequency range or in multiple channel communication. To achieve broadband operation, the patch antenna should operate with good impedance matching and a stable radiation pattern within a broad frequency band. To achieve this, a large number of structures have been proposed and applied to practical designs.

During the past few years, many configurations have been suggested and developed to extend the bandwidth. In the following sections, the different techniques for realising the broadband microstrip patch antenna are briefly discussed, with special emphasis on configurations that are particularly attractive for integration. This chapter focuses on the configurations of the antennas used to improve the bandwidth performance. After introducing the reactive load to the single element, such as U-slot [22], E-shaped [23], H-shaped [24], the broad operation bandwidth can be achieved. The most attractive design is the aperture-coupled broadband microstrip antenna. This configuration [25-26] avoids the main disadvantage of the probe feed, thus performing with a broader bandwidth and a high level of radiation gain amongst existing designs. Multi resonant structures are used when the resonant frequencies of each elements are close to together, thus to achieve a wider bandwidth operation. The structures of broadband circularly polarized (CP) antenna are discussed in the following section. A summary is given at end of this chapter.

2.2 Broadband Techniques for Single Patch Antenna with Reactive Loading or L-Probe

It is possible for a single element microstrip patch antenna to operate over a broad frequency band corresponding to the various modes pertaining to the structure. One of the most popular techniques used to obtain a broadband operation is to introduce a reactive load in the patch combined with a thick air gap between the

radiating element and the ground plane. The effective permittivity of the cavity will be changed to a lower value, which means a broad impedance bandwidth could be achieved.

2.2.1 U-Slot On The Patch

Embedding a suitable U-shaped slot in a radiating patch [22] is a very effective method for achieving a broad bandwidth for a probe-fed microstrip antenna with a thick air substrate as shown in Figures 2.1 & 2.2. The maximum bandwidth achieved by this design is 27%, centre around 3.1 GHz, with good pattern characteristics. It is also noted that the operating frequencies over the wide impedance bandwidth are usually with a relatively large cross-polarization radiation, especially in the H-plane in which the cross-polarization levels (XPLs) are usually only about -10 dB or less, which is a common characteristic of this kind of probe-fed microstrip antenna with a thick air substrate. To improve the cross-polarization radiation to obtain a linearly polarized wave with better polarization purity, the technique of adding an additional feed or equal amplitude and 180 ° phase shift has been suggested [27].

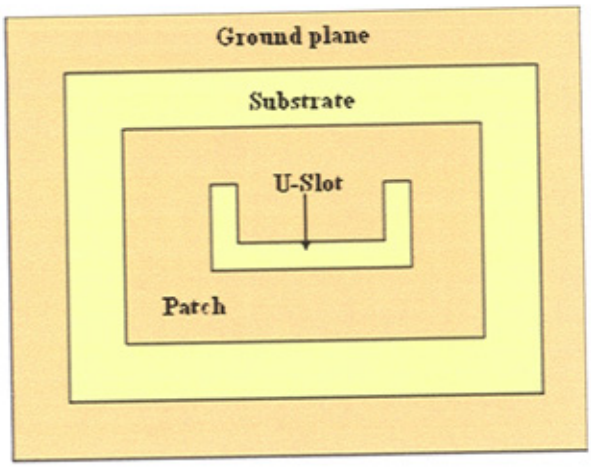

Figure 2.1: U-slotted broadband antenna [22].

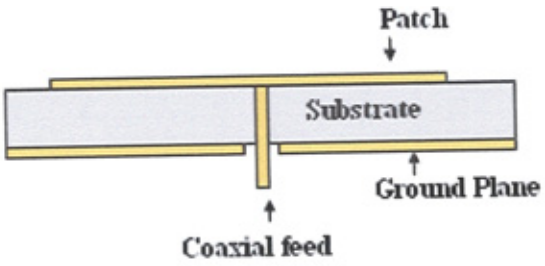

Figure 2.2: Side view of U-slotted broadband antenna [22].

2.2.2 A E-Shaped Broadband Microsrtip Patch Antenna

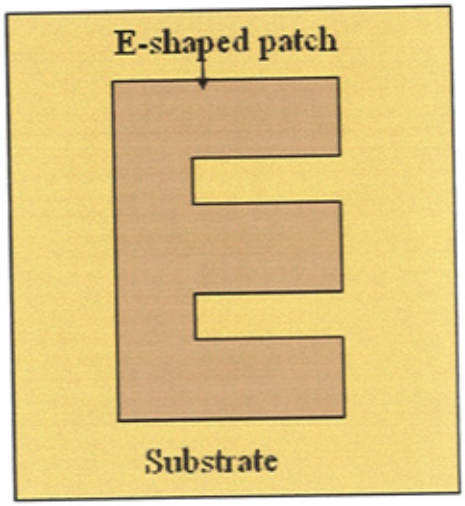

Figure 2.3: E-shaped broadband antenna [23].

When two parallel slots are incorporated in the patch [23] (Figure 2.3), it is found to have a much broader impedance bandwidth as compare to the conventional U-slot antenna. By properly adjusting the parameters of the slots and the feed position, an impedance bandwidth of 32.3% is achieved.

The ordinary microstrip patch antenna can be modelled as a simple *L-C* resonant circuit. Due to the two slots being placed at the edge of the rectangular patch, the resonant features change. The current has to flow around the slot at the edge, so the length of the current path is increased. This effect can be modelled as an

additional series inductance ΔL [23]. So the equivalent circuit of the edge part resonates at a lower frequency. Therefore, the antenna changes from a single *L-C* resonant circuit to a dual resonant circuit. These two resonant circuits couple together and form a wide bandwidth. The two operating frequencies are related to the resonant frequencies of the fundamental TM_{10} mode and the new resonant frequencies denoted as $TM_{\delta 0}(1 < \delta < 2)$. Both of the two modes also have the same polarization planes and similar radiation patterns.

2.2.3 Dual U-Slotted Broadband Microstrip Patch Antenna

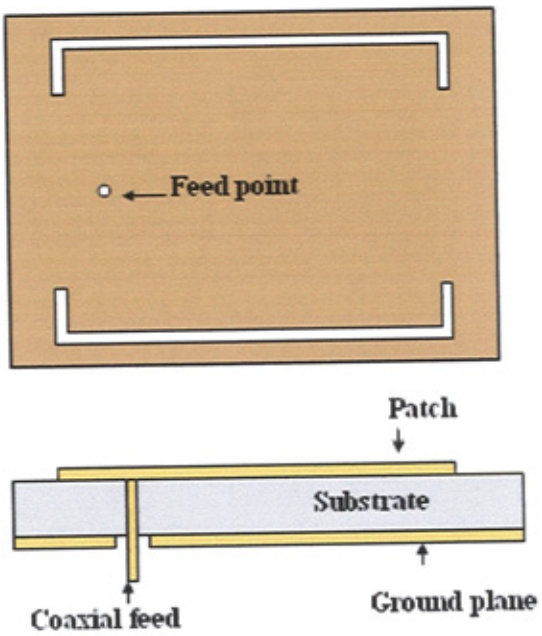

Figure 2.4: U-slotted broadband antenna [24].

When embedding a pair of u-slots parallel to the non radiating edges [24] (Figure 2.4) of the rectangular patch, a new resonant mode between the TM_{10} and TM_{20} modes of the conventional rectangular patch antenna can be excited. The second resonant frequency decreases rapidly with increases in the length of the slot.

The first resonant frequency is very slightly affected by the variation of the slot dimension, which results in a lower frequency ratio. The experiment results show the impedance bandwidth, determined from the -10 dB return loss, is as large as 95 MHz of which about 4.9% is obtained, which is about 2.6 times that 1.9% of the simple rectangular microstrip antenna without the slots.

2.2.4 A Broadband Circular Microstrip Antenna with Two Open-Ring Slots

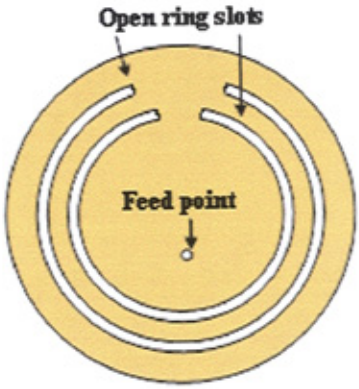

Figure 2.5: Circular broadband antenna with two open slots (top view) [25].

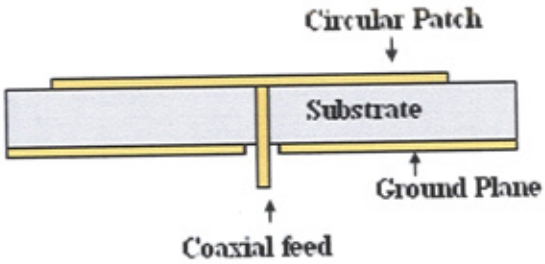

Figure 2.6: Circular broadband antenna with two open slots (side view) [25].

Figures 2.5 and 2.6 present a new design of probe circular microstrip antenna with two open-ring slots for broadband operation [25]. Due to the two embedded open-ring slots in the circular patch, two resonant modes of similar radiation

characteristic are found to be excited at frequencies in the vicinity of the fundamental resonant frequency of a corresponding simple circular microstrip antenna without slots. The two closely excited resonant modes can cause the enhancement of the impedance bandwidth of the proposed antenna. This design is related to the dual-frequencies operation. The advantage of this design is that it can be printed on an inexpensive substrate.

The experimental results of the impedance bandwidth, determined from -10 dB return loss, is found to be 90 MHz or about 4.14 % with respect to the centre frequency. The radiation characteristics of the operating frequencies within the 10 dB impedance bandwidth formed by the two resonant modes are also studied. Low cross polarization level less than -20 dB has been obtained.

2.2.5 Broadband Equilateral Triangular Microstrip Antenna With Asymmetric Bent Slot

A broad operating bandwidth for a single-layer equilateral triangular microstrip antenna can be obtained by embedding a pair of asymmetric bent slots inside the patch and inserting an inset microstrip line section at the patch edge as an integrate load [26] as shown in Figure 2.7 and Figure 2.8.

With this design, a group of three closely excited resonant modes of similar broadside radiation characteristics near the fundamental resonant mode of a corresponding simple equilateral-triangular microstrip antenna can be achieved. Results show that an impedance bandwidth as large as 4.5 times that of a simple triangular microstrip antenna can be achieved over 144 MHz.

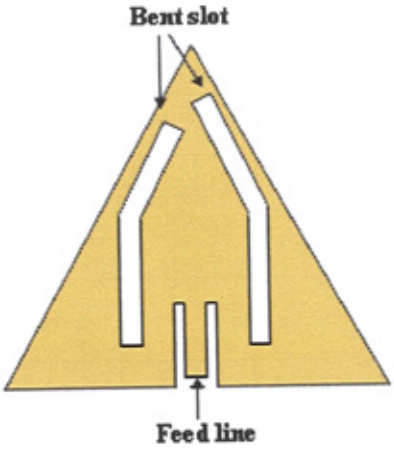

Figure 2.7: Broadband equilateral triangular with asymmetric bent slot (top view) [26].

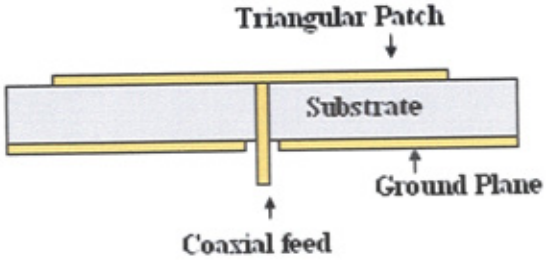

Figure 2.8: Broadband equilateral triangular with asymmetric bent slot (side view) [26].

2.2.6 A Wideband Circular Patch Antenna with A Pair of Wide Slits

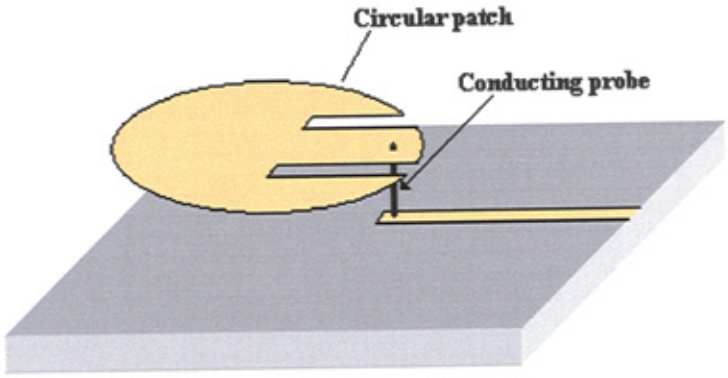

Figure 2.9: A wideband circular patch antenna.

A design of a circular patch antenna with an impedance bandwidth greater than 25% and a peak antenna gain about 8.3 dBi [27] is shown in Figure 2.9. A conducting post, which is also connected to the 50-ohm microstrip feed line, supports

the circular patch. The circular patch antenna has a thick air substrate and a pair of wide slits is cut in the circular patch to facilitate the antenna's impedance matching. The use of the wide slits is to compensate the large inductance of the conducting post. In this design, the feed substrate and the radiating patch are on the same side of the ground plane, thus no via holes in the ground plane are required for connecting the conducting post to the Microstrip line, which simplified the fabrication process.

This design, with an air substrate thickness chosen to be about 0.07 times the free-space wavelength of the centre operating frequency, means the proposed wideband circular patch antenna can have an impedance bandwidth of about 26%. Within the obtained impedance bandwidth, good radiation characteristics are also observed. It also shows a peak antenna gain of about 8.3dBi, with a gain variation less than 1.5dBi within the impedance bandwidth.

2.2.7 Broadband Microstrip Antenna with L-Shaped Probe Feed

A design of a rectangular microstrip antenna with an L-shaped probe feed [28] is shown in Figures 2.10 and 2.11. In this design, the L-shaped probe has been successfully applied into the rectangular patch by using a thick-substrate. However, the arising problem from using the long probe feed generates inductance limiting the achieved bandwidth to 10%. The horizontal portion of the L-probe acts as a transmission line with the ground plane, and thus with a proper adjustment in length, its capacitance can cancel out the feed inductance to enhance the impedance bandwidth. As a result, a 35% impedance bandwidth and an average gain of 7.5dBi can be achieved.

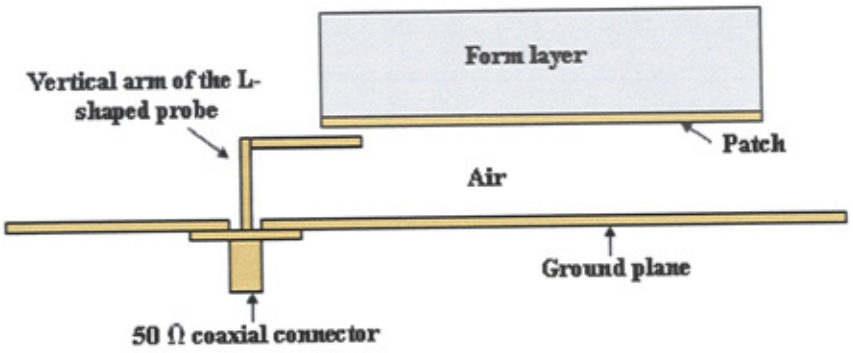

Figure 2.10: L –shaped probe single feed antenna (side View) [28].

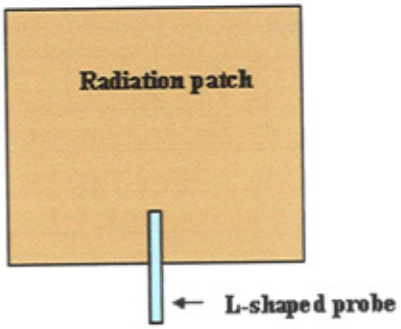

Figure 2.11: L –shaped probe single feed antenna (top view) [28].

2.3 Broadband Techniques for Aperture-Coupled Microstrip Patch Antenna

In the aperture-coupled microstrip antenna, the field is coupled from the microstrip feed line placed on the other side of the ground plane to the radiating patch through an electrically small aperture/slot in the ground plane, as shown in Figure 2.12. Two different dielectric substrates can be chosen, one for the patch and the other for the feed line to optimize the individual performances. The coupling to the patch from the feed line can be maximized by choosing the optimum shape of the aperture [29–30]. The aperture-coupled microstrip antenna has several advantages over the transmission line or probe fed patch antenna. Separate substrates can be used for the

feed circuit and the antenna element to isolate spurious feed radiation from the antenna element by use of a common ground plane, and to allow more space for the feeding network [23]. This is feature make aperture-coupled antenna as one of the most popular choice for integrating with active circuit. Further more, the input impedance is easily controlled by the size and the position of the aperture, and any excess reactance caused by the coupling aperture can be removed through the use of a tuning stub. Also, the aperture-coupled antenna provides low cross-polarization level. A cross slot can be used for exciting two orthogonal linearly polarized elements with 90 deg phase shift to produce circular polarization.

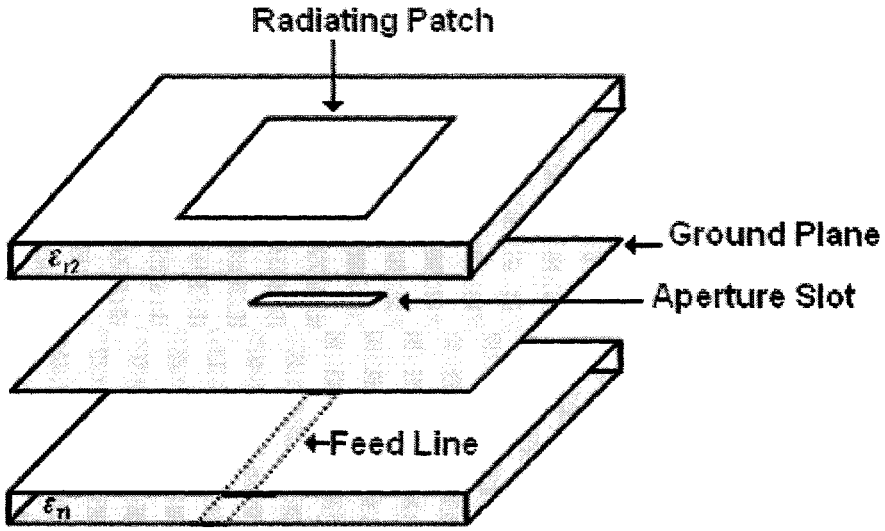

Figure 2.12: Aperture coupled microstrip patch antenna.

2.3.1 Wideband Linearly Polarized Aperture Coupled Antenna

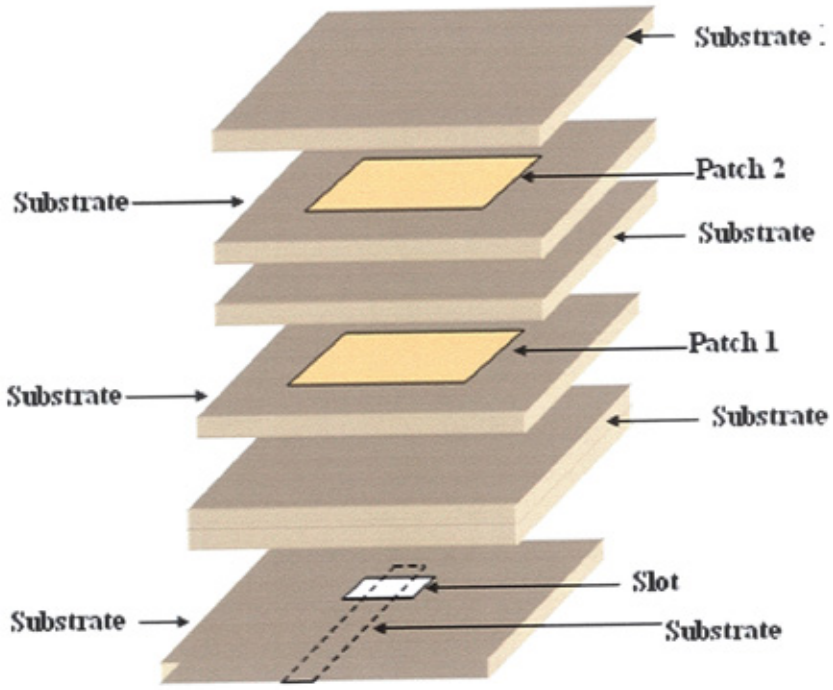

Figure 2.13: Geometry of multilayered aperture stacked patch antenna [29].

The design of wideband aperture coupled microstrip patch antenna is presented in [29]. The design utilizes a resonant aperture with stacked patches. The characteristics and impedance matching techniques of the designs are discussed. This work focus on the characteristics of the resonant aperture with the stacked patches. The performance of a single patch is compared with stacked patches. A wide-band aperture-stacked patch Figure 2.13 is designed and measured. A bandwidth of 50% is achieved. To further improve the impedance bandwidth, different feeding techniques are employed and compared. Figure 2.14 shows that two different feeding networks are used in the aperture-coupled stacked patch antenna. Significant improvement has been achieved by aperture stacked antennas. A bandwidth of 67 % is resulted with the dual offset feeding technique. Another significant feature of the aperture-stacked patch antenna is that it exhibits a lower front to back ratio than a typical aperture coupled patch antenna due to the use of a resonant aperture. As a result, a linearly

polarized experimental design is presented from which an octave bandwidth was realized.

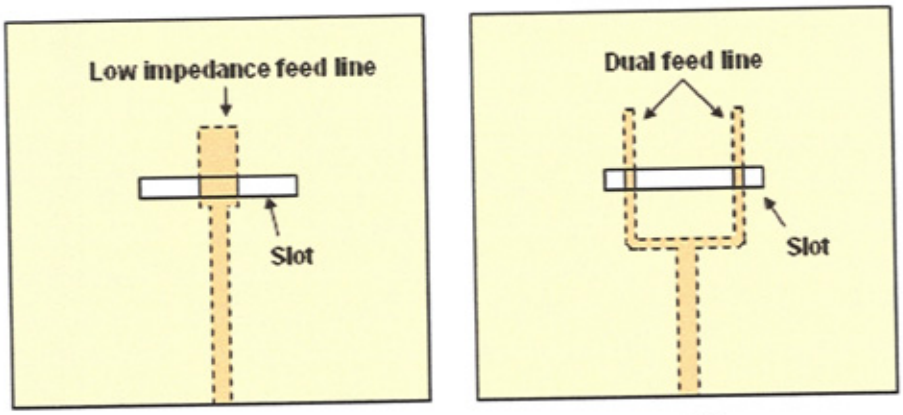

Figure 2.14: Impedance matching techniques for the aperture stacked patch antenna.; (a) wide centred feed line, and (b) dual feed line [29].

2.3.2 Broadband Aperture-Coupled Wideband Microstrip Antenna With Low Backward Radiation

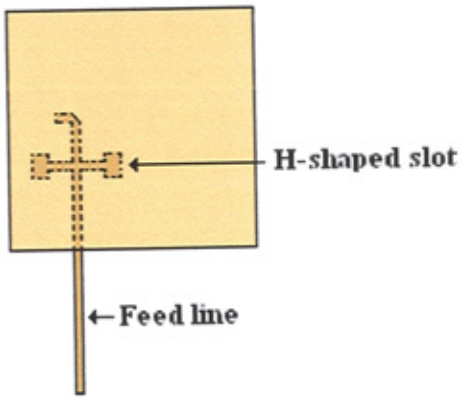

Figure 2.15: The top view of the H-shaped broadband antenna [30].

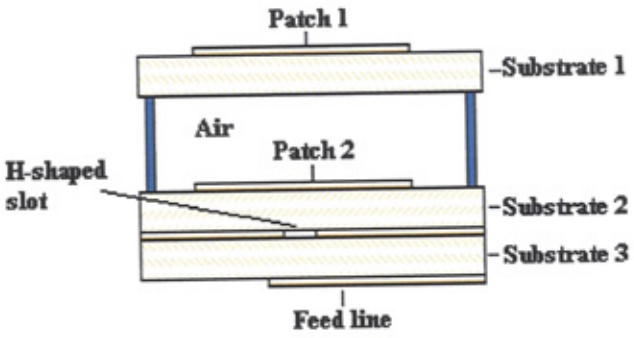

Figure 2.16: The side view of the H-shaped broadband antenna [30].

The aperture coupled microstrip patch antenna can improve the bandwidth by coupling the resonant patch to the aperture near its resonance [29]. This technique, however, also introduces a high level of backwards radiation due to the proximity of the resonance of the aperture that radiates on both sides of the ground plane. To avoid this disadvantage, the resonance of the aperture as far from the operation band of the antenna as possible was chosen, so that its radiation level is smaller compared with using the stacked patches which broadens the bandwidth.

A novel broadband Microstrip patch antenna Figures 2.15 and 2.16 is reported [30] by using a non-resonant H-shaped aperture coupled with stacked square patches. A thick air layer is inserted in between the two radiating patches. The measured return loss exhibits an impedance bandwidth of 21.7 %. The cross-polarization levels in both E and H planes are better than -23 dB. The front to back ratio of the antenna radiation pattern is better than -22 dB.

2.4 Broadband Techniques For Multi-Resonator Patch Antenna

In principle, every single element is operating at approximately 2% frequency bandwidth. To extend the operation bandwidth, multiple patches are combined together, each element operating at closely resonant frequencies and supporting strong

current and radiation. In order to avoid the effect between every element, the size of each element should be very close. These configurations provide wider frequency operation bandwidth, multi-polarization, and lower side lobe. This is called multiresonator broadband antenna.

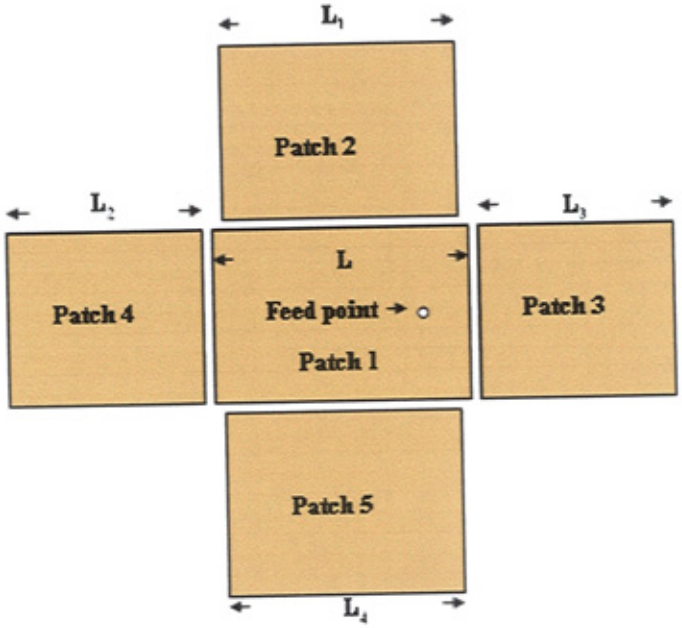

Figure 2.17: multi-resonators broadband antenna [31].

Multiresonator broadband antenna consist of two or more metallic resonator patches on a single dielectric [31] Figure 2.17 or supported by one or more dielectric layers [28] Figure 2.18. As shown in Figure 2.17, four additional patches are gap-coupled to every edge of the main rectangular patch antenna. However, the resulting broadband microstrip antenna also has a much increased antenna size compared to a single rectangular microstrip antenna. The lengths L_2, L_3, and L_4 of patches 2-4 in the excitation direction are selected to be slightly different from that (L_1) of the excited patch 1, which can result in three additional resonant modes closely excited at frequencies near the fundamental resonant frequency of the excited patch. A 6.9% impedance bandwidth can thus be obtained. Also, good impedance matching for the

excited resonant modes can be achieved by placing a probe feed at a position along the centre line (y axis) of patch 1 a distance from the connecting strip.

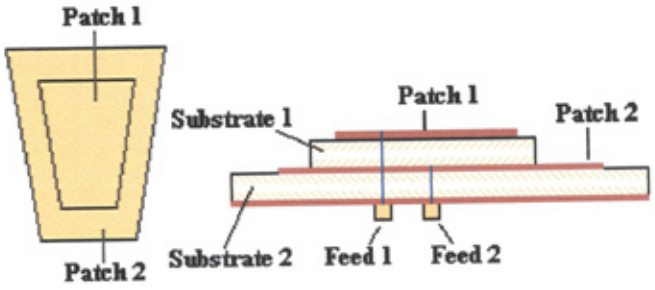

Figure 2.18: multi-resonators stacked broadband antenna [32].

All of the multi-resonators of this design only allow a limited value of the frequency ratio, in order to be suitable for short-range communication systems. For the application of far range communication systems such as radar applications, a wide separation between the frequencies is often required. Hence, the difference of the dimensions between every single element will be large. In order to obtain the large separation, the patch can be stacked on two different substrates, thus creating two independent antennas [32]. The advantage of this arrangement is that the sub-element provides a wider frequency bandwidth with the resonant frequency of the main patch. As shown in the Figure 2.18, the probe crosses through a clearance hole in the lower patch and is electrically connected to the upper patch. If one considers the two regions under the patch as two resonant cavities it is clear that the system behaves as a pair of coupled cavities. Since the fringing fields are different between the upper and lower cavities, two resonant frequencies are expected.

In this case two options should be investigated. The first is when the smaller patch printed on the dielectric layer is above the larger patch. This could have the

advantage of limiting the blockage of the low frequency radiation. On the other hand, the larger patch works on a substrate presumably thin in terms of a wavelength, so that their bandwidth could be too narrow. The second possibility is to print the larger patch on the upper layer, to broaden their bandwidth. This configuration solution has the impairment of causing the blockage of the upper frequency radiation, and possible excitation of cross-polarization.

2.5 Broadband Techniques for Circularly Polarized Patch Antenna

2.5.1 L-Shaped Probe-Feed Circularly Polarized Microstrip Patch Antenna With A Cross Slot

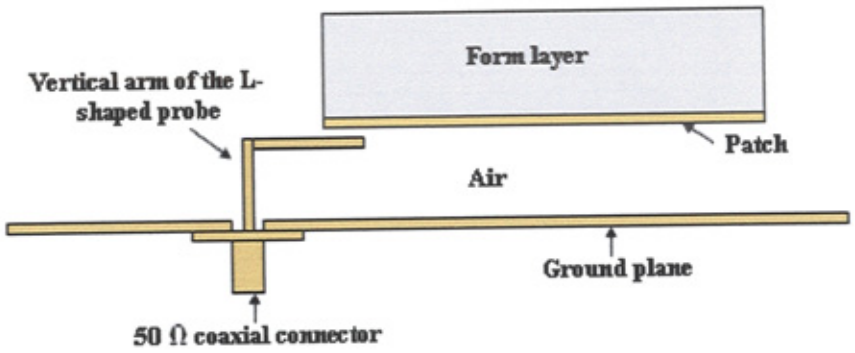

Figure 2.19: L –shaped probe single –feed CP antenna (side view) [34].

As introduced before, the L-shaped probe feed patch antenna can achieve the wider bandwidth. A modified design of a circular patch with cross slots using the probe feed is shown in Figures 2.19 and 2.20.

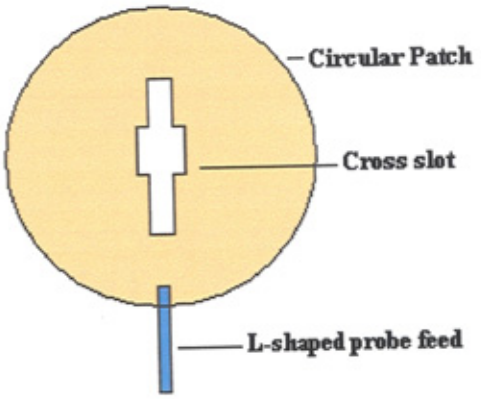

Figure 2.20: L –shaped probe single –feed CP antenna (top view) [34].

This design of an L–shaped probe single feed CP antenna can achieve a wider impedance bandwidth, axial ratio bandwidth, and gain bandwidth without using the phase shifter or hybrid couplers.

It is well known that the circular microstrip patch antenna with a cross slot fed by a transmission line can excite two orthogonal modes with equal amplitude in order to obtain the circular polarization. The main disadvantage of this single feed CP antenna is that its impedance and axial ratio bandwidth are narrow when compared to those of the conventional CP microwave antennas. The flexibility of the antenna design is attained only by adjusting the length of the cross slot to excite the circular polarization.

In this design the horizontal portion of the L-probe acts as a transmission line with the ground plane [34]. Thus with proper adjustment in length, its capacitance can cancel out the feed inductance to enhance the impedance, axial ratio and gain bandwidth effectively. The use of the cross-slot is to reduce the physical size of the circular patch.

The antenna achieves an impedance bandwidth (Voltage standing wave ratio (VSWR) < 2) of about 29 %. The 3 dB axial ratio also improved to 4.5 %. The

antenna highest gain of this L-shaped probe feed antenna is 6.8 dBi. The 3 dB gain bandwidth is about 24 %.

2.5.2 Wideband Circularly Polarized Aperture Coupled Antenna

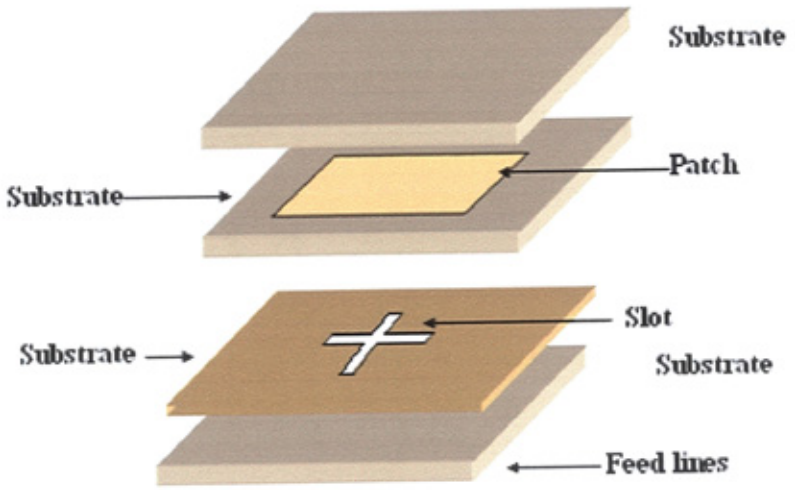

Figure 2.21: Geometry of the cross slot aperture-coupled microstrip antenna [37].

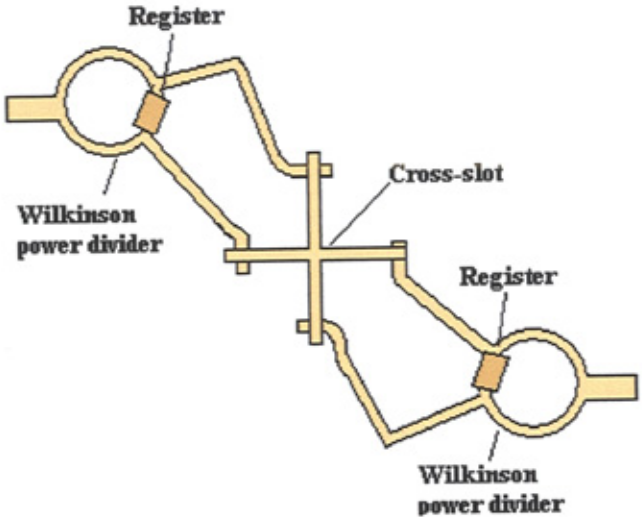

Figure 2.22: Feeding network of the cross slot aperture-coupled antenna [37].

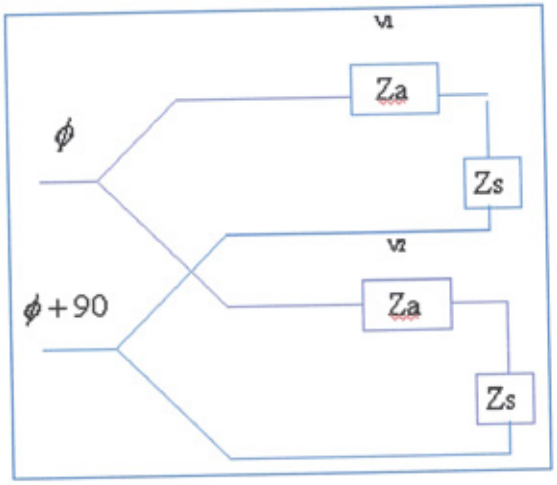

Figure 2.23: The equivalent circuit of the feeding network [37].

The design with a pair of parallel feeding networks using the Wilkinson Power Divider fed into two slots has been discussed in [37]. The disadvantage of the conventional series feed is that the axial ratio degrades fairly rapidly with frequency because of the increased amplitude error in the excitation of the two apertures. The amplitude error has a much greater effect on the axial ratio than does the phase error. A parallel feed structure shows in Figures 2.21 and 2.22 along with its equivalent circuit shown in Figure 2.23 overcome these disadvantages. Because the reactive divider does not provide any isolation between the two output ports, reflected power from one aperture can couple through another aperture. This coupling can cause enough error to destroy the axial ratio. Thus the use of the Wilkinson Power Divider is to provide high isolation between the output ports.

The results shown much improvement have been obtained by using parallel feed, exhibiting impedance and axial ratio (< 2 dB) bandwidth of 22 % and 25 %.

2.6 Summary

This chapter gave a brief review of several techniques for realizing broadband microstrip patch antenna operation, such as slot loaded antenna, slot-coupled broadband antenna, multi resonator antenna using stacked patch antenna. A brief description of broadband CP antenna was also presented. There are many other types of broadband antennas such as slot antennas, and many other, such as spiral antenna , monopole antenna, ultra wide band antenna, very useful for communication systems, are presented else where [38-43]. Because the slot –coupling structure is useful of active integration with RF/microwave circuit, such as oscillator and amplifiers, I will investigate broadband slot-coupled microstrip antennas and their integrations with RF/microwave power amplifier in the following chapters.

CHAPTER 3

Broadband Slot-Coupled Microstrip Patch Antennas

3.1 Introduction

The conventional single layer microstrip patch antenna has a very narrow bandwidth. In recent years, much attention has focused on the development of broadband antenna for modern communication systems. Current techniques of achieving enhanced bandwidth include the use of co-planar parasitic patches and stacked patches [37]. It has been reported that such designs can achieve a bandwidth of approximately 20% while single layer probe or microstrip line-fed elements are typically limited to bandwidths of 2%-5%, slot-coupled elements have been demonstrated with bandwidths up to 10%-15% with a single layer. By separating the feeding network from the antenna using the ground plane, slot-coupled antenna offers two advantages. First, the slot-coupled microstrip antenna can provide substantially improved impedance bandwidths. Secondly, the feeding circuit and the antenna are

based on different substrates; thus, the ground plane serves to eliminate the interference between them. Therefore, the slot-coupled antenna is an ideal candidate for active circuit integration. Wideband operation of more than 50% through the use of a slot-coupled design has been reported [37]. However, it involves the use of several patches stacked upon each other.

In this chapter, several novel broadband microstrip antennas with linear polarization (LP) and those with circular polarization (CP) will be presented. A novel broadband CP array will also be presented. The design procedures are discussed. The simulation and measured results are shown and discussed.

3.2 Circular Ring Slot-Coupled Broadband Antenna

In this section a novel structure consisting of a single patch coupled to a microstrip feed through a ring slot is presented, which can achieve a bandwidth of 54%. Enhanced gain and low cross-polarisation levels are achieved. Another significant advantage of this design is that only a single patch is used to achieve the wider bandwidth.

3.2.1 Antenna Design And Simulation

The use of a slot-coupled patch as shown in Figure. 2.13 is a well known technique for achieving a broad return loss bandwidth. This approach makes the input impedance easily controlled by the size and position of the aperture/slot.

To design a broadband slot-coupled patch antenna a number of parameters must be determined. These include: patch dimensions, slot dimensions, feed dimensions and position. The dimension of the patch is predetermined by the standard

equation in [36] for rectangular patch antenna operation at the fundamental frequency, given by:

$$f_o \approx \frac{c}{2L\sqrt{\varepsilon_r}} \tag{3.1}$$

where c is the speed of light, L is the patch length and ε_r is the substrate permittivity.

The antenna is designed on the substrate Duroid 5870 which has a permittivity of 2.33 and thickness of 1.57 mm. The resonant frequency of this rectangular patch is approximately 3 GHz.

The multiple resonant frequency characteristics of ring slot antennas have been reported [41]. With multiple resonant frequency characteristics it is possible to achieve broadband operation. The ring slot is introduced to the design to change the resonant feature with reference to the normal rectangular slot aperture-coupling antenna. The guided wavelength λ_{gs} of the ring slot can be determined by the equation from reference [42]:

$$f \approx \frac{c}{2(R_1 + R_2)} \times \left(\frac{1+\varepsilon_r}{2\varepsilon_r}\right)^{\frac{1}{2}} \tag{3.2}$$

where R_1 is the outer slot width, R_2 is the inner slot width and ε_r is the permittivity of the substrate.

The operating frequency of the ring slot can be determined from the guided wavelength of the slot because the circumference of the ring slot is approximate one guided wavelength of the slot. The ring slot is simulated in Ensemble® by using full wave analysis moment method. Figurer 3.1 shows the return losses of the ring slot fed

by a 50 Ω microstrip feed line. Two resonance frequencies at 2.5 GHz and 3.5 GHz are generated by the ring slot. By adding the resonance of the patch (3 GHz) on the top of the ring slot, a broadband operation from 2.5 GHz to 3.5 GHz can be achieved.

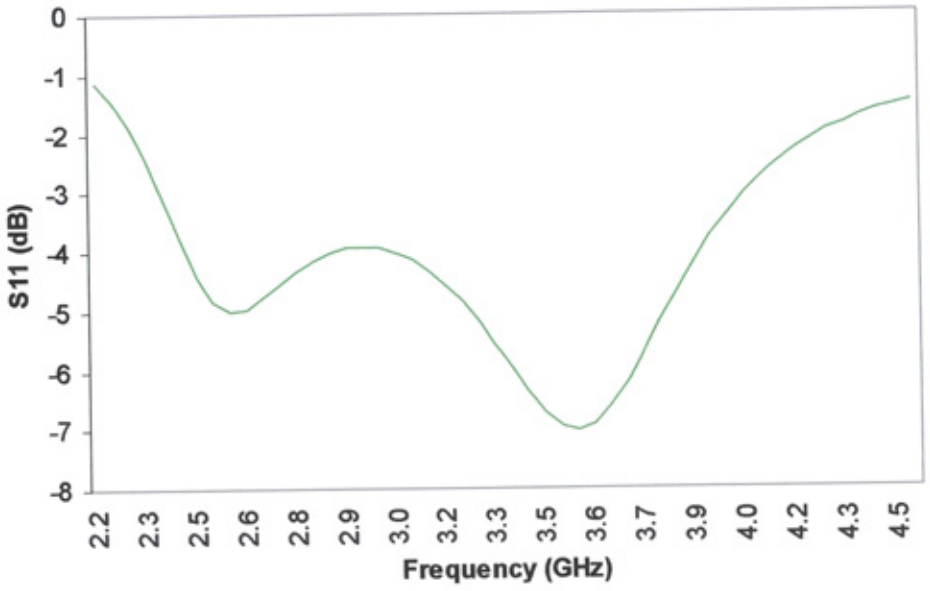

Figurer. 3.1: Simulated return losses of ring slot with a 50 Ω microstrip feed line.

A 10 mm high air layer between the ground plane and patch is used to prevent the appearance of surface waves while enhancing radiation, and also widen the frequency bandwidth. The H-shaped geometry of the antenna patch was arrived at by first examining experimental results using a square geometry. These results showed non-uniformity in the VSWR, which oscillated about a ratio of 2. It was necessary to narrow the bandwidth between the lower and upper resonant frequency to reduce the VSWR. This was obtained by decreasing the cavity volume under the antenna geometry by deleting rectangular segments along the two radiating edges. Thus the resultant H-shaped patch was designed.

The use of step microstrip feed line further enhances the bandwidth. In Figure. 3.2(b), the metallic H-shaped patch is attached to the underside of the upper supporting substrate, which is held in position by vertical supporting rods. In the top view, Figure 3.2, the relative positions and dimensions (Table. 3.1) of the feed, ring slot, and, H-shaped patch are shown. The upper patch support substrate is very thin (1.5 mm) and its effect on the radiation characteristic is negligible. A 1.575 mm thick Duroid (5870) substrate is used to attach the feed line.

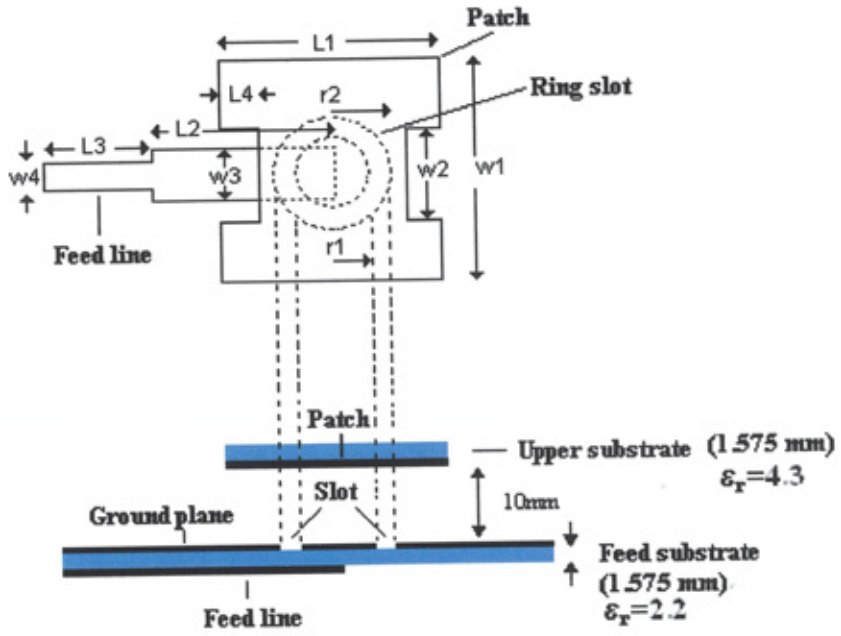

Figurer 3.2 (a): The top view of the ring slot-coupled antenna, and (b) the side view of the ring slot-coupled antenna.

W_1 = 33 mm	W_2 = 9.5 mm	W_3 = 9.93 mm	W_4 = 4.4 mm	L_1 = 33 mm
L_2 =40 mm	L_3 = 25 mm	L_4 =6.8 mm	R_1 =7.8 mm	R_2 =12.8 mm

Table 3.1: Dimensions of the antenna design.

The proposed antenna structure is shown in Figurer 3.2. This design uses only a single patch, which is simpler and more compact when compared to the conventional broadband antenna using stacked or co-planar parasitic patches. To establish the broadband operation, a ring slot coupled with a low permittivity value substrate (air) and H-shaped patch on the top has been proposed. It is fed by a microstrip line with matching network, which is placed underneath the ground plane. The dimensions of the design is characterised by (L,W,r) shown in the Figurer 3.2 and Table 3.1.

3.2.2 Experiment Results and Discussion

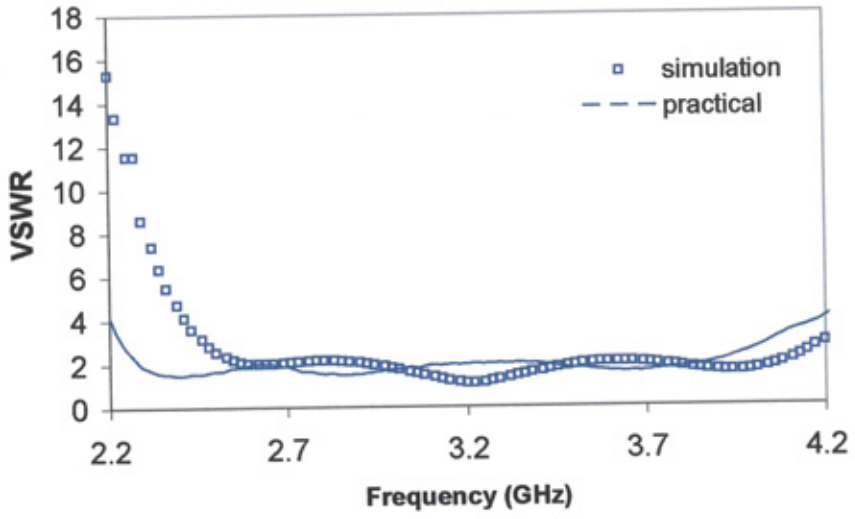

Figurer 3.3: Simulated and measured VSWR.

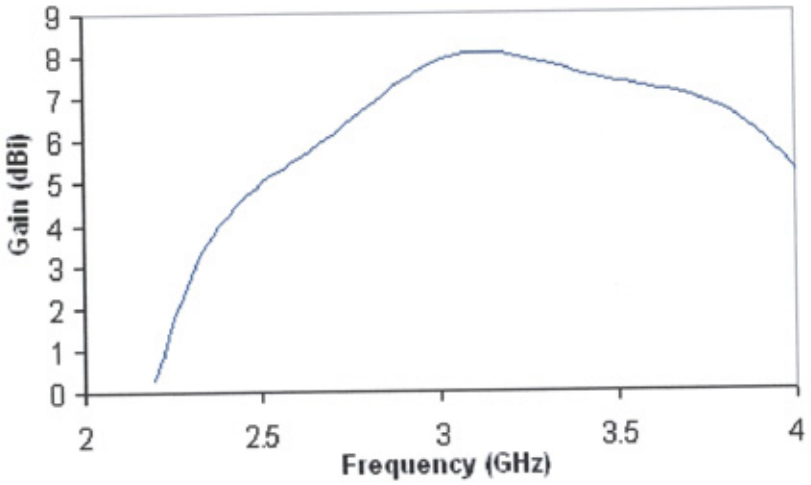

Figurer 3.4: Measured gain of the antenna versus frequency.

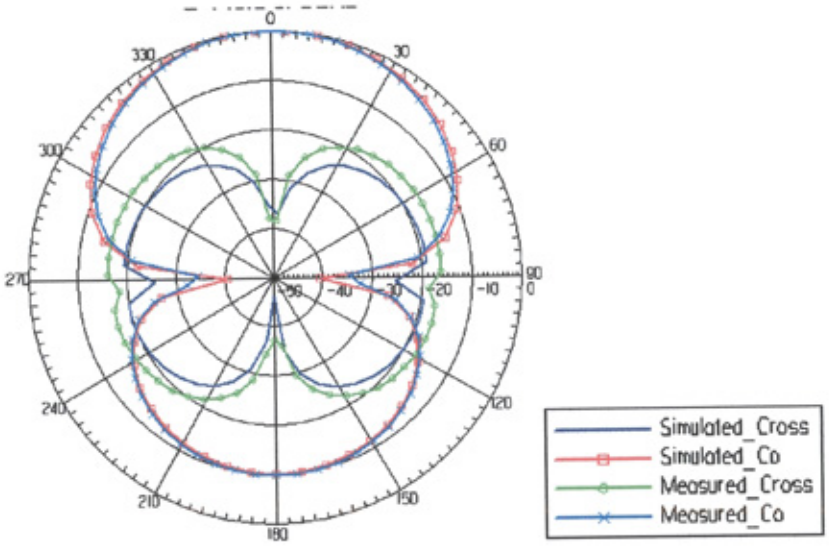

Figurer 3.5: The comparison of the radiation patterns between simulation result and practical measurement (E field at 3 GHz).

The antenna simulation is done by Ensemble® and measured by a vector network analyzer (Anritsu 37347c). The measured result of the antenna bandwidth is 54 % (2.3 GHz -3.845 GHz) for VSWR less than 2 and is shown in Figure 3.3. Good agreement was observed between the measured and simulation result, save a slight frequency shift, which is attributed to fact that the simulation does not take into

account the thickness of the copper. Figurer 3.4 shows the measured results of antenna gain. Three frequency points have been tested in simulation for backward radiation; maximum back to front radiation is below –10 dB at those frequency points (2.8 GHz, 3.2 GHz, and 3.8 GHz).

Figurer 3.5 gives measured and simulated results of the E-plane radiation pattern at 3 GHz, i.e., the centre frequency within the band. It shows that an excellent agreement was obtained between simulation and measured results. A symmetric radiation pattern is obtained in the E-plane and cross polarization levels are well below -20 dB in the broadside direction.

3.23 Discussion

In this section a new design of broadband microstrip antenna has been proposed and experimentally studied. An H-shaped patch is coupled to the feed through a ring slot in the ground plane. A wide bandwidth of 54% is obtained. Good broadside radiation is achieved within the wide frequency band and peak antenna gain can reach up to 8.1 dB. The new design is a suitable candidate for the modern communication and radar systems where a wide bandwidth is required.

3.3 Square Ring Slot-Coupled Patch Antenna

In contrast to the conventional rectangular slot coupled antenna, this new design employs a square ring slot coupling structure feeding to only a single H-shaped patch, but still achieves a bandwidth of more than 50 %. Indeed, the use of a low permittivity substrate largely prevents the appearance of surface wave effects allowing for a wider bandwidth. An improved design, including an additional ground

plane eliminates the unwanted backward radiation. Details of both design configurations are described and their respective simulation and practical results are discussed.

3.3.1 Antenna Design

As described in section 3.2.1, using a ring slot in a slot-coupled antenna has been used to achieve a broad impedance bandwidth. A square ring with similar resonant characteristics is used to achieve a comparable broad bandwidth in this section.

The geometry of the design is shown in Figure. 3.6. An H-shaped patch is printed on the 1.6 mm thick upper FR4 supporting substrate ($\varepsilon_r = 4.3$). Since the upper substrate is thin its effect on the radiation performance is negligible. A 50-ohm feed line with a tuning stub is located on the bottom side of the lower substrate (RT-Duroid 5880, $\varepsilon_r = 2.2$) and a square ring slot is etched on the upper surface, which is a ground plane. A 10 mm air filled substrate separates the ground plane from the H-shaped patch.

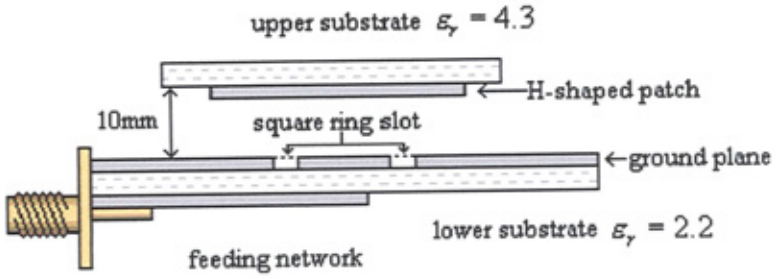

Figurer 3.6 (b): Side view of the square ring slot coupled patch antenna.

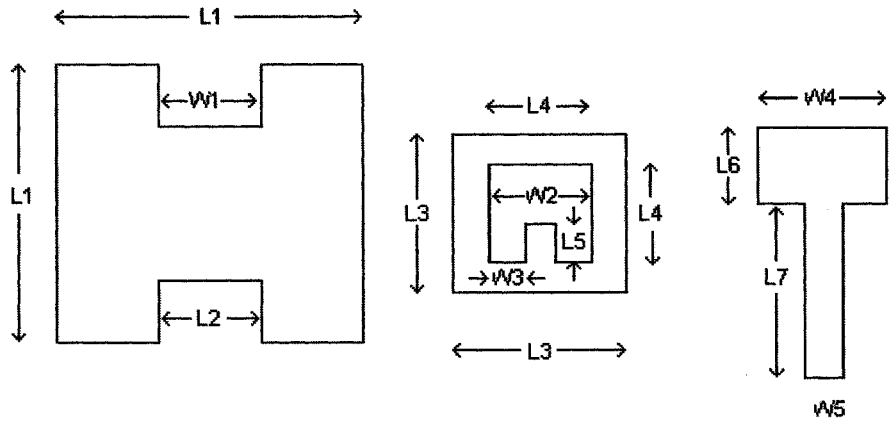

Figure 3.6 (c): Detailed dimensions of the proposed design.

L_1=28.0	L_2=9.5	L_3=23.0	L_4=14.8
L_5=6.5	L_6=10.6	L_7=15.7	W_1=9.5
W_2=6.5	W_3=5.7	W_4=11.8	W_5=3.0

Table 3.2: Dimensions of the design, in mm

This new structure consists of two resonators, which are a square ring slot and an H-shaped patch. To achieve a wide bandwidth, the multiple resonant characteristics of the two resonators must be exploited. A similar design method using in previous ring slot-couple antenna design is again used in this approach. The dimensions of the patch and square ring are initialized using equations 3.1 and 3.3:

$$f_o \approx \frac{c}{2(L_1 + L_2)} \times \left(\frac{1+\varepsilon_r}{2\varepsilon_r}\right)^{\frac{1}{2}} \tag{3.3}$$

where L_1 is the outer slot width, L_2 is the inner slot width and ε_r is the permittivity of the substrate.

The resonant characteristic of a square ring slot has been reported in [42]. The square ring slot is designed for 50 Ω impedance matching at multiple frequencies over a wide frequency range. The resonant frequency of the H-shaped patch is chosen to be the centre frequency of the desired operating band for the square ring slot antenna. The substrate between the top patch and the ground plane primarily affects the bandwidth of the proposed design. The air filled substrate is an ideal candidate for this design since its lower dielectric constant reduces surface wave generation. In order to maintain the high coupling efficiency, a 10mm high air substrate is finally selected. A further bandwidth improvement is obtained by removing a rectangular segment on the centre of the ground plane as shown in Figure. 3.6. The detailed dimensions are shown in Figure. 3.6 and Table 3.2. In the design process, the commercial software An soft® Ensemble v8 was used to optimize the dimensions of the design, in particular the height of the substrate and the dimensions of the deleted segments, which are the key design parameters required to achieve the desired bandwidth.

3.3.2 Experiment Results and Discussion

The antenna simulation was done with the 2.5D electromagnetic simulator Ansoft® Ensemble and the measurements are performed with a vector network analyzer (Anritsu 37347c). The design was fabricated based on the simulation results. The measured bandwidth of the antenna is 50.6 % (2.46-4.095 GHz) for a standing wave ratio (SWR) of less than 2 see Figure. 3.7. Good agreement was observed between the measurements and simulation, save for a slight frequency shift, which is

attributed to the fact that the simulation does not take into account the thickness of the copper. Figure. 3.8 shows the measured antenna gain. A greater than 6dB gain is obtained over the full frequency band with a peak gain of 8 dB. Figurers 3.9 and 3.10 show the measured results of the E-plane and H-plane radiation patterns at 2.8 GHz. A symmetric radiation pattern is obtained in both the E-plane and the H-plane, and cross-polarization levels are well above 25 dB in the broadside direction. The antenna gain is shown to be greater than 6 dB for the entire bandwidth. Due to limitations of the measurement setup, the backward radiation could not be measured in practice. Thus the back to front radiation ratio is only evaluated in simulation. The simulated backward radiation is found to be fairly poor with a value of only -10 dB.

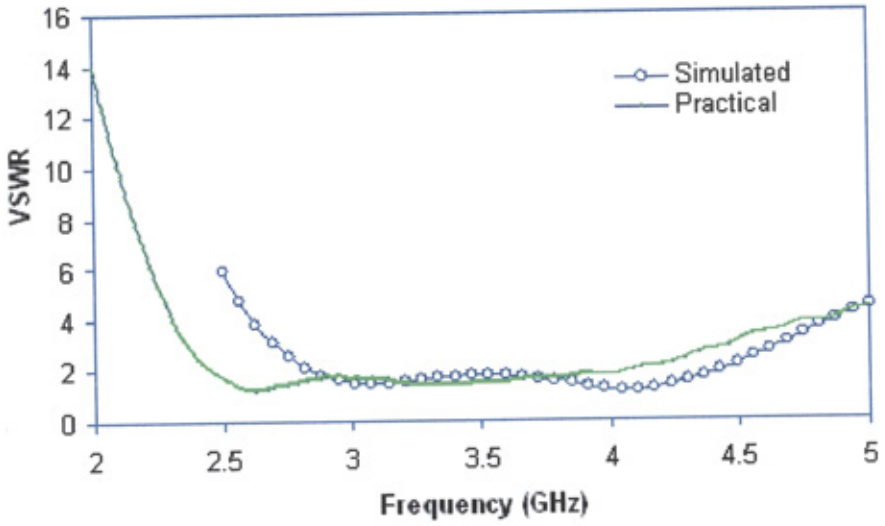

Figure 3.7: Predicted and measured VSWR.

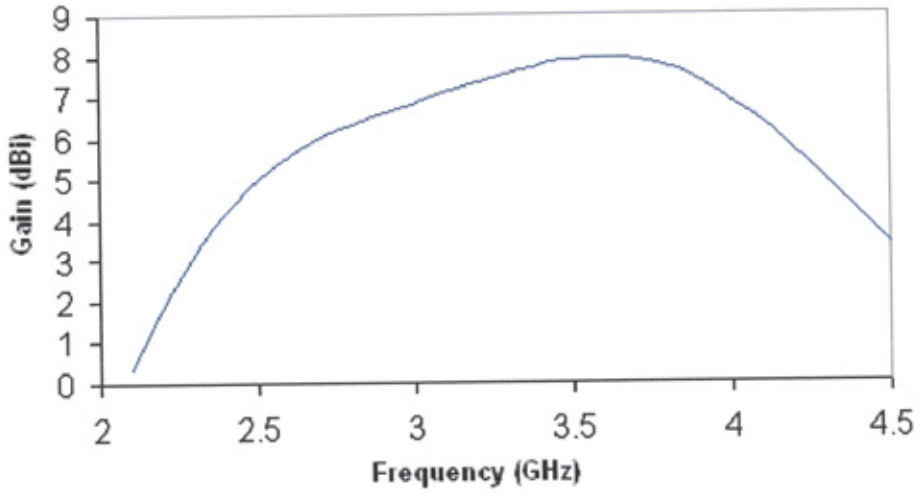

Figure 3.8: Measured gain of the antenna versus frequency.

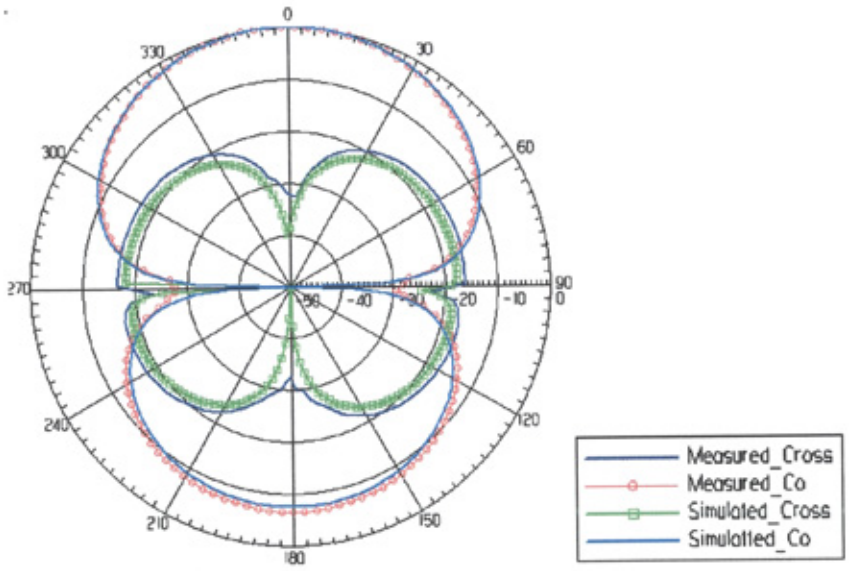

Figure 3.9: The comparison of the radiation patterns between simulation result and practical measurement (E-plane) at 2.8 GHz.

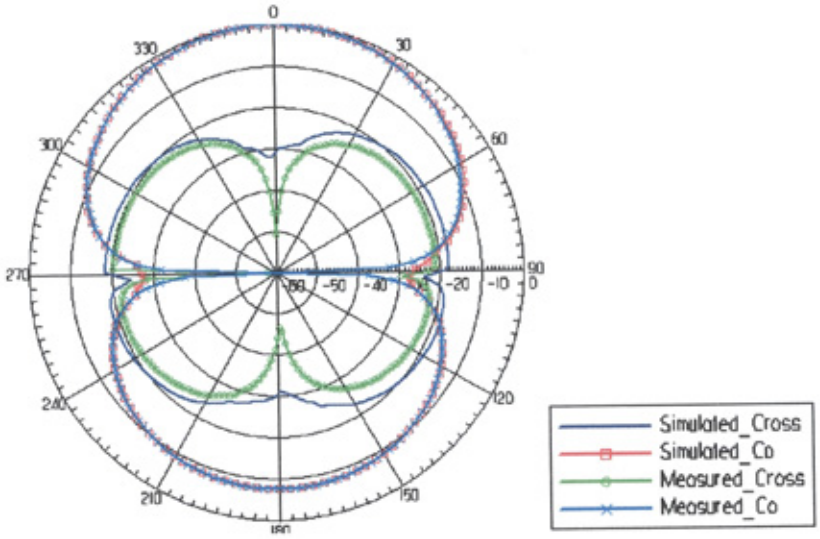

Figure 3.10: The comparison of the radiation patterns between simulation result and practical measurement. (H-plane) at 2.8 GHz.

3.3.3 Square Ring Slot-Coupled Antenna Design 2: Antenna with An Additional Ground Plane

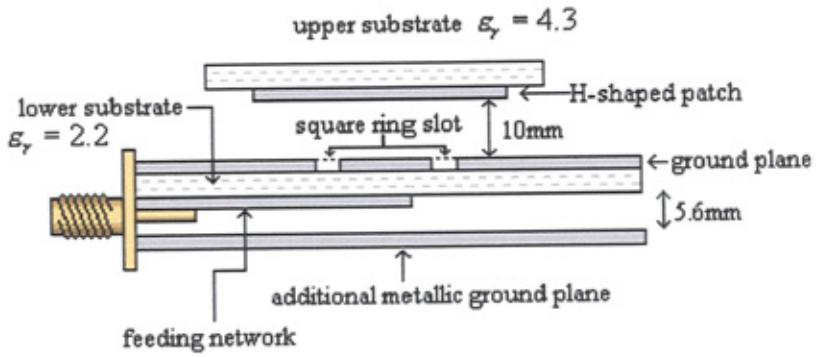

Figure 3.11: Side view of the improved design.

Since the design has a poor back to front radiation performance it is necessary to improve it by adding a ground plane, which is placed at the bottom of the previous configuration separated from the feed line by a 5.6 mm air layer Figure. 3.11. The additional shielding provided by the ground plane eliminates the backward radiation.

The modified design has been fabricated and tested. Figure. 3.12 presents the comparison of simulated and measured result of VSWR. Figures 3.13 and 3.14 present the comparison of measured and simulated radiation pattern.

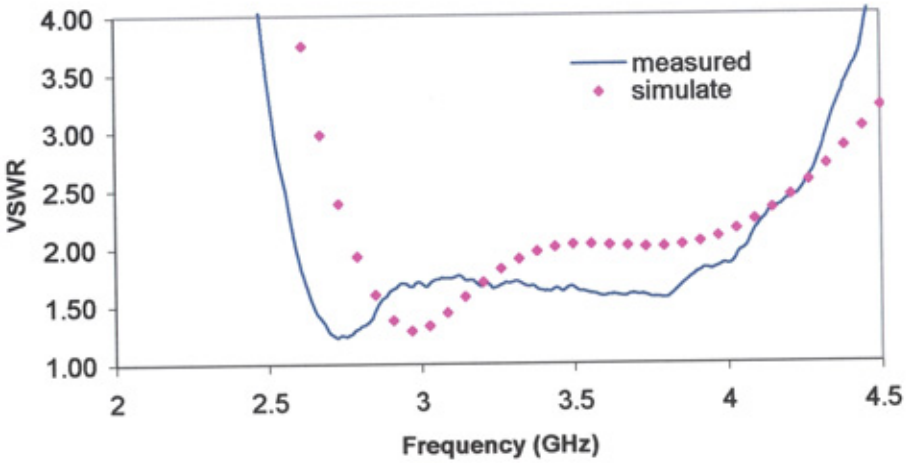

Figure 3.12: Voltage standing wave ratio versus frequency.

As shown Figure 3.12, a lesser impedance bandwidth (44 %) is achieved with the modified design, due to the additional ground plane causing a reduction of the parallel mode excitation. However, the modified design allows a significant improvement of the back to front ratio, while maintaining the radiation characteristics of the previous design (Figures 3.13 and 3.14). The performance of the two proposed designs is summarised (Table 3.3) and compared to the performance of the conventional aperture coupled antenna.

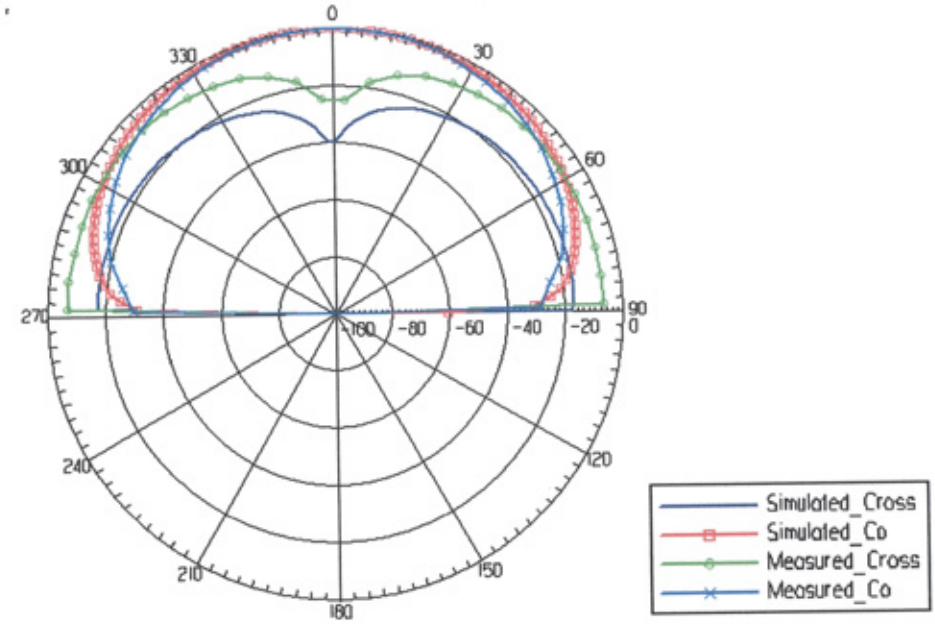

Figure 3.13: The comparison of the radiation patterns between simulation result and practical measurement (E field at 3.5 GHz).

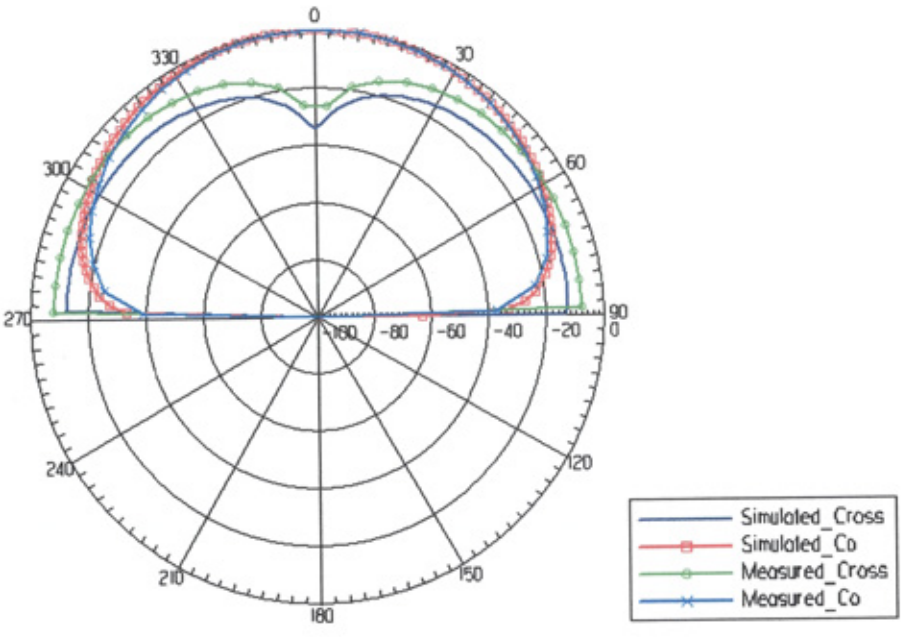

Figure 3.14: The comparison of the radiation patterns between simulation result and practical measurement (H-plane at 3.5 GHz).

	Bandwidth (%)	Peak Gain (dBi)	Back to front Ratio (dB)
Conventional aperture coupling design [4]	20 - 25	8.5	-15 to -20
First design	50.6	8.0	-10
Modified design	44.6	8.1	-100

Table 3.3: Comparison of the performance of the conventional aperture coupled antenna and the proposed designs

3.4 Broadband Circularly Polarized Antenna

This section presents the design, fabrication, and measurements of a low-cost broadband circularly polarized (CP) antenna and an array antenna at 2 GHz. A single circular patch is electromagnetically coupled by crossed slots, which are fed by a single L-shaped microstrip feed. By using the above CP element, a broadband CP 2×2 array antenna is then presented. Details of the antenna configuration, simulation and practical results for both structures are discussed.

3.4.1 Boadband Cp Antenna Element: Design And Results

The characteristics of a cross-slot coupled patch antenna have been reported in [44-45]. By using a cross slot for coupling the electromagnetic energy from the microstrip feed to the radiating element, circular polarization can be easily obtained. To achieve a broadband circular polarization operation, here a circular microstrip patch is put above an air layer with 10 mm thickness and electromagnetically coupled

using the cross-slot in the ground plane, which is fed by an L-shaped microstrip feed. The proposed design achieves right-hand circularly polarized radiation at a centre frequency of 2 GHz. The side view and top view of the antenna configuration are shown in Figure. 3.15. To ease the fabrication, an inverted structure is used, and a circular patch is printed on the Duroid 5880 substrate, which has a thickness 0.79 mm and relatively permittivity of $\varepsilon_r = 2.2$. This substrate does not affect much of the radiation performance, and acts as a kind of protection for the antenna against snow and fog. An L-shaped feed line is printed on the bottom of the lower substrate Duriod 5880 which has a thickness 0.79 mm and relatively permittivity $\varepsilon_r = 2.2$. A crossed slot with unequal dimensions is etched in the ground plane.

The substrate between the top patch and ground plane primarily determines the bandwidth of the proposed design. The air-filled substrate is an ideal candidate for this design since it has the lowest dielectric constant (1.0) and avoids the surface wave generation. In the design process, the commercial software Ensemble® v8, from Ansoft, is used to optimize the dimensions of the design. The design starts with calculating the initial dimension of the circular patch given by:

$$D = \frac{2\lambda}{1.36\sqrt{\pi\varepsilon}}, \tag{3.4}$$

for resonating at 2 GHz, based on the cavity model [45]. Two slots should have an average length of :

$$L_{avg} = \frac{\lambda}{1+\sqrt{\varepsilon}} \quad . \tag{3.5}$$

The slots have a fractional length difference ΔL to produce circular polarization, so their lengths are given by:

$$L = L_{avg}(1 \pm \frac{1}{2}\Delta L) \ . \qquad 3.6$$

The software Ensemble® is then used to optimize the dimensions of the antennas through electromagnetic simulations.

The crossed slots are used to excite the two orthogonal modes in the antenna, with equal amplitude and a 90°-phase shift between them. The length of the L-shaped feed line between two slots is adjusted to be approximately a quarter wavelengths. A tuning of the slot lengths is also used to achieve optimized performances, which leads to unequal lengths of the two slots as shown in Figure 3.15 (b). Detailed dimensions of the antenna are given in Figure. 3.15(c).

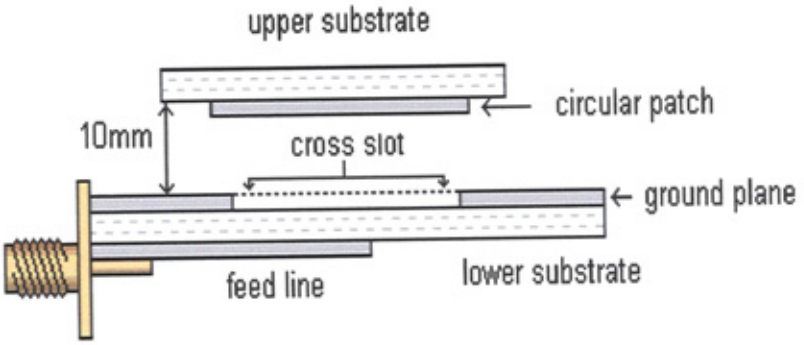

(a)

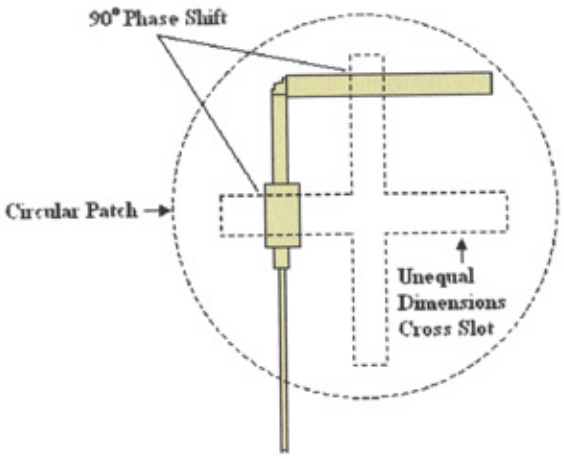

(b)

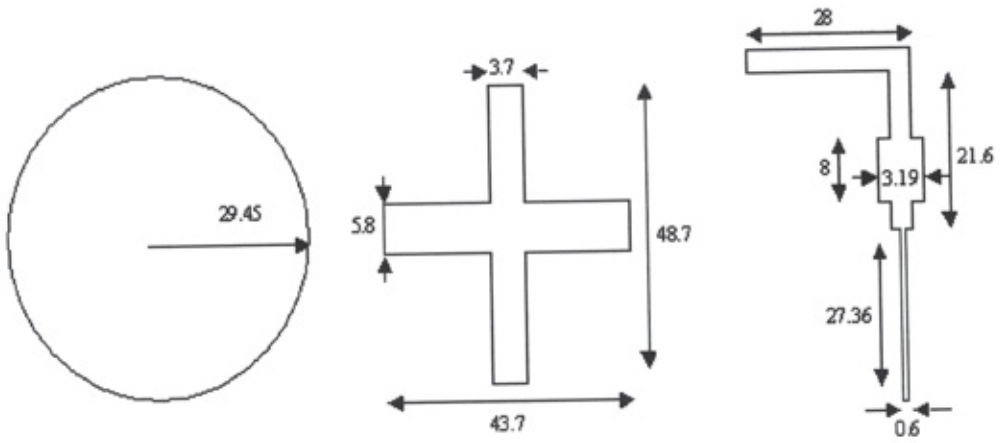

(c)

Figure 3.15: (a) Side view, (b) top view of the CP antenna, and (c) detailed dimensions of the proposed design (mm).

The antenna is fabricated and measured in anechoic chamber. The proposed design is operated in right-hand circular polarization. Figures 3.16 (a) and (b) show the measured return loss (S11) and 2:1 voltage standing wave ratio (VSWR) of the CP antenna element. It achieves a bandwidth of 0.53 GHz, i.e., a 26% bandwidth from 1.76 GHz to 2.29 GHz with a centre frequency of 2 GHz. The comparison of simulated and measured axial ratio is presented in Figure 3.16(c). The axial ratio bandwidth, defined as AR < 3 dB is found to be 9.6 % from 1.88 GHz to 2.07 GHz. The bandwidth for gain > 6 dBi is found to be 30 % from 1.86 GHz to 2.27 GHz.

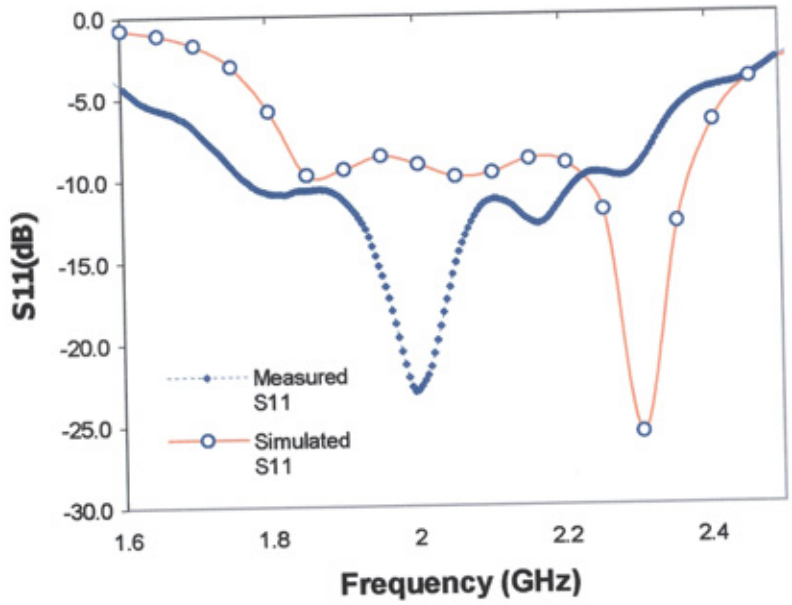
0.0
-5.0
-10.0
-15.0
-20.0
-25.0
-30.0
S11(dB)
Measured S11
Simulated S11
1.6
1.8
2
2.2
2.4
Frequency (GHz)

(a)

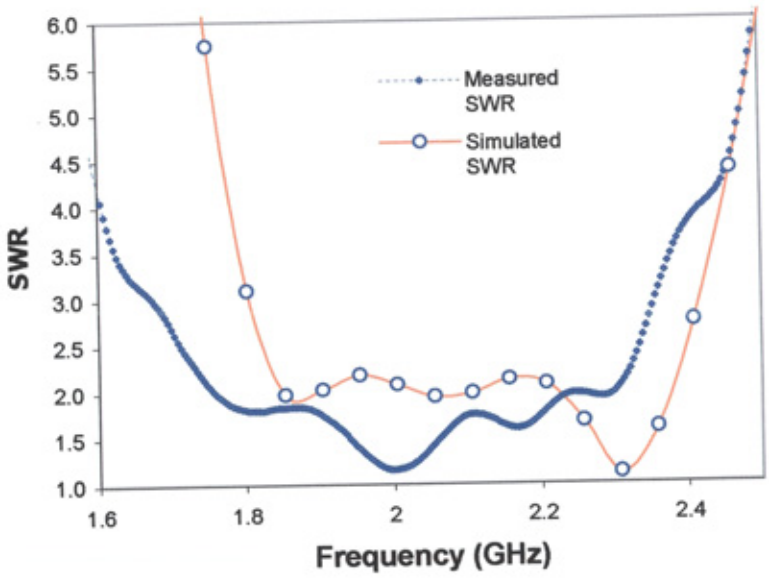
6.0
5.5
5.0
4.5
4.0
3.5
3.0
2.5
2.0
1.5
1.0
SWR
Measured SWR
Simulated SWR
1.6
1.8
2
2.2
2.4
Frequency (GHz)

(b)

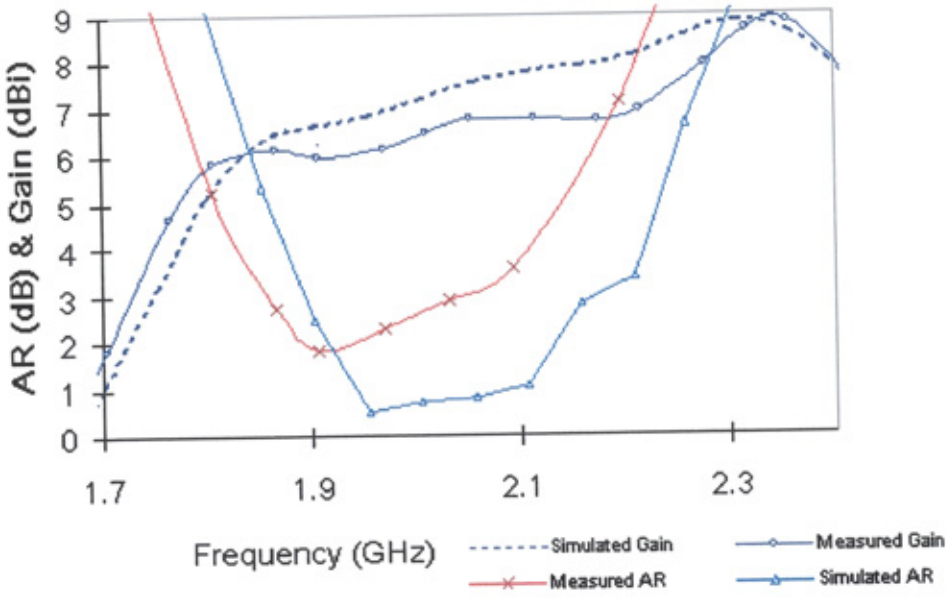

(c)

Figure 3.16: The comparisons between simulated and measured results (a) S11, (b) VSWR, and (c) axial ratio.

3.5 Broadband Cp Array Antenna

Application of sequentially rotated feeding in circularly polarized arrays leads to several advantages such as polarization, purity in the main beam and wide bandwidth [46-47]. To further improve the AR and impedance bandwidth of the CP antenna, the antenna proposed in the previous section is employed as an element in the four-element sequentially rotated array. The configuration of the proposed right hand circularly polarized cross-slot coupled array is shown in Figure. 3.17 (a). Four broadband CP antenna elements were arranged in a sequential rotation arrangement. The feed network consisting of seven-quarter wave transformers is designed to produce a match at the feed point for 50 Ω and produces a 90° phase difference between adjacent antenna feed lines ensuring that each one is fed with equal power.

The transmission line equivalent circuit of the array is shown in Figure 3.17 (b).

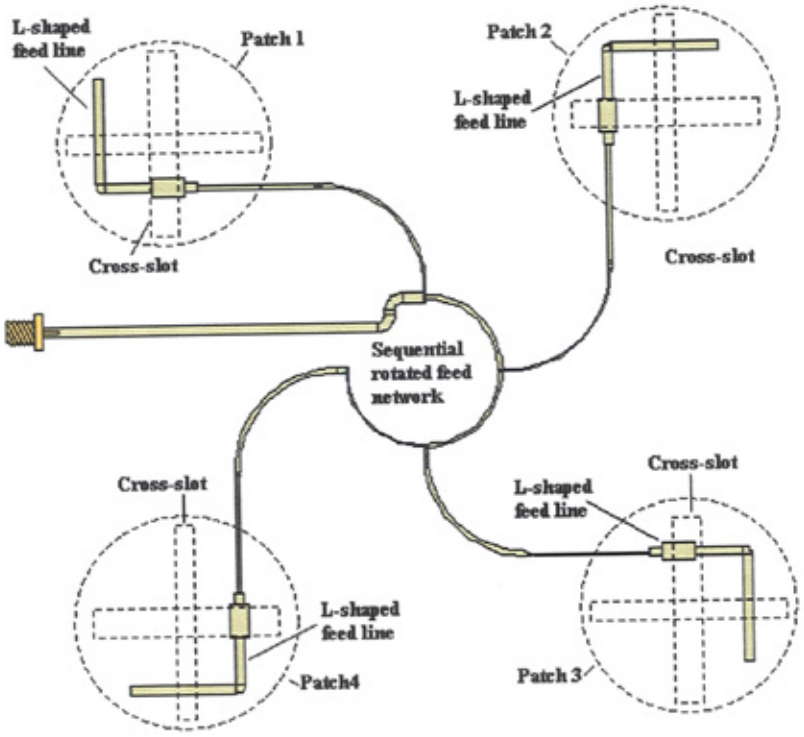

(a)

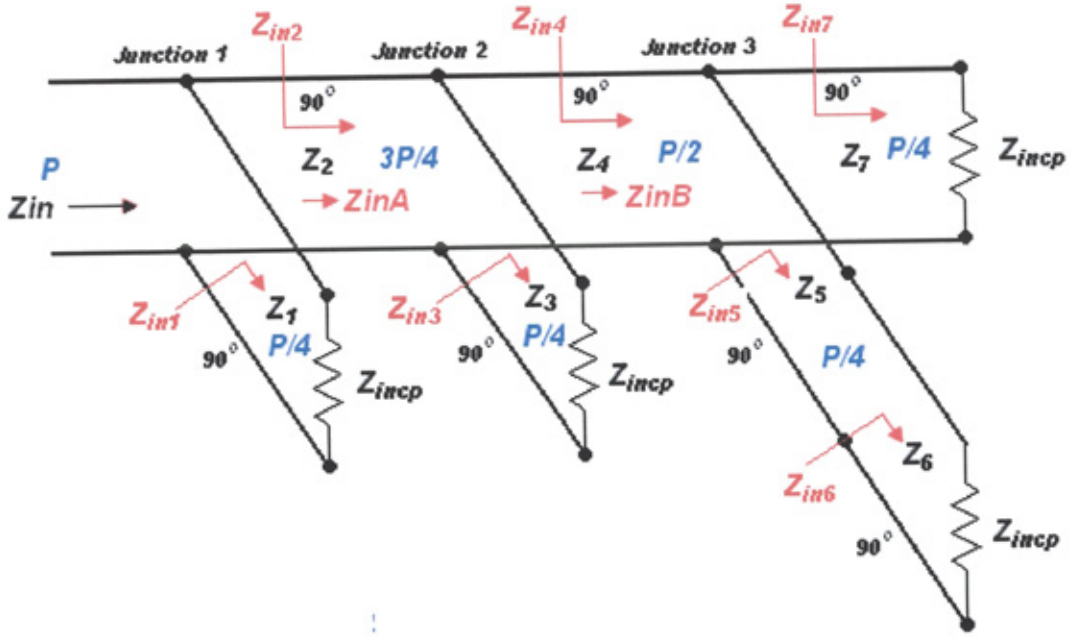

(b)

Figure 3.17: (a) Schematic of the 4-element CP array, and (b) the equivalent circuit for sequentially rotated antenna array.

To reduce spurious radiation and coupling effects, it is important for the width of the feed network to be as narrow as possible and consequently the characteristic impedance $Z_1, Z_2, \ldots Z_7$ should be as high as can be practically realized.

In the design of the feed-network, the following assumptions are made. The input impedance Z_{incp} of individual CP patch antenna element is 50 Ω. Each antenna element is sharing quarter of the total input power (P). Also the highest characteristic impedance that can be realized is 140 Ω using Duroid as a substrate.

Hence, the input power at Junction 1is given as:

$$P_{in} = \frac{|V_1^2|}{50}\frac{1}{4} = \frac{|V_1|^2}{Z_{in1}} \tag{3.7}$$

$$P_{in} = \frac{|V_1^2|}{50}\frac{3}{4} = \frac{|V_1|^2}{Z_{in2}} \tag{3.8}$$

Therefore, $Z_{in1} = 200\ \Omega$, and $Z_1 = 100\ \Omega$. And $Z_{in2} = 66.7\ \Omega$.

At Junction3:

Equal power is required to be supplied to patches 3 and 4 and to obtain narrow width feeds. It is assumed that $Z_5 = 120\ \Omega$. As Z_5 is now fixed, and equal power is fed into patches 3 and 4, hence $Z_7 = Z_6 = 77.5\ \Omega$, and $Z_{inB} = 60\ \Omega$.

$$Z_{in6} = \frac{Z_6^2}{Z_{incp}} \tag{3.9}$$

$$Z_{in5} = \frac{Z_5^2}{Z_{in6}} \tag{3.10}$$

$$\frac{1}{Z_{inB}} = \frac{1}{Z_{in5}} + \frac{1}{Z_{in6}} \tag{3.11}$$

Where $Z_{incp} = 50\ \Omega$

At junction 2:

One third of input power is fed into patch 2 and the remaining of the power is fed into patches 3 and 4 so that:

$$Z_{in4} = \frac{Z_{in3}}{2} \tag{3.12}$$

The feed network now reduces to three variables Z_2, Z_3, Z_4. It is now necessary to make an assumption for one of this impedance. If $Z_3 = 120\ \Omega$, hence it can be shown that $Z_4 = 92.95\ \Omega$ and $Z_2 = 80\ \Omega$.

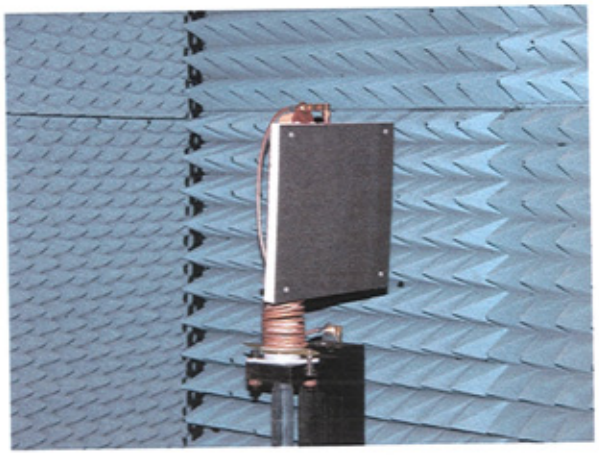

(a)

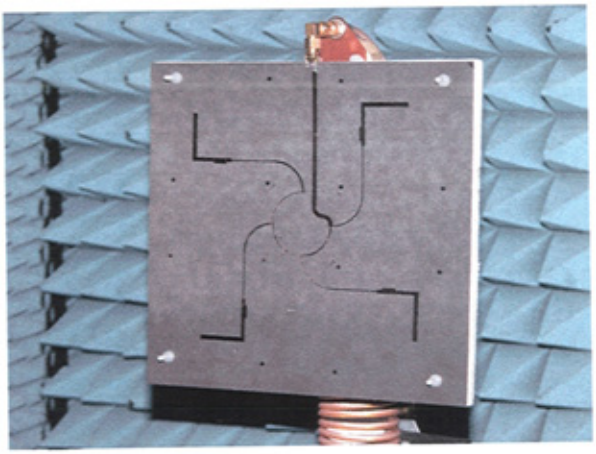

(b)

Figure 3.18: Photos of the CP array (a) View from front, and (b) view from the back.

The antenna simulation is performed by using Ensemble®, and practical S parameter results are obtained by using a vector network analyzer (Anritsu 37347c). The photographs of CP array design are shown in Figure 3.18. The measured antenna bandwidth for S11 below –10 dB is 41 %, from 1.68 GHz to 2.55 GHz, as shown in Figure 3.19 (a). Good agreement was observed between the measured and simulation, except a slight frequency shift, which is attributed to fact that the simulation does not take into account the thickness of the copper. Additionally, a VSWR < 1.5 bandwidth is found to be 33 % from 1.76 GHz to 2.45 GHz in Figure 3.19 (b). The antenna gain is above 10 dBi across the frequency band from 1.73 GHz to 2.5 GHz, as illustrated in Figure 3.19 (c). The axial ratio bandwidth Figure 3.19 (c), defined as below 3 dB, is found to be 27.2 % from 1.75 GHz to 2.3 GHz. Figure 3.19 (d) shows that the input impedance of the antenna array is flatness with very little variation. The measured results for E and H-plane radiation pattern at centre frequency 2 GHz are shown in Figures 3.20 (a) and (b) respectively. It has been shown that a symmetric radiation pattern is obtained in both E-plane and H-plane, and cross polarization levels are well below -30 dB in the broadside direction.

The practical measurements demonstrate the use of sequentially rotated structure in the broadband CP antenna array design. Excellent performance is achieved.

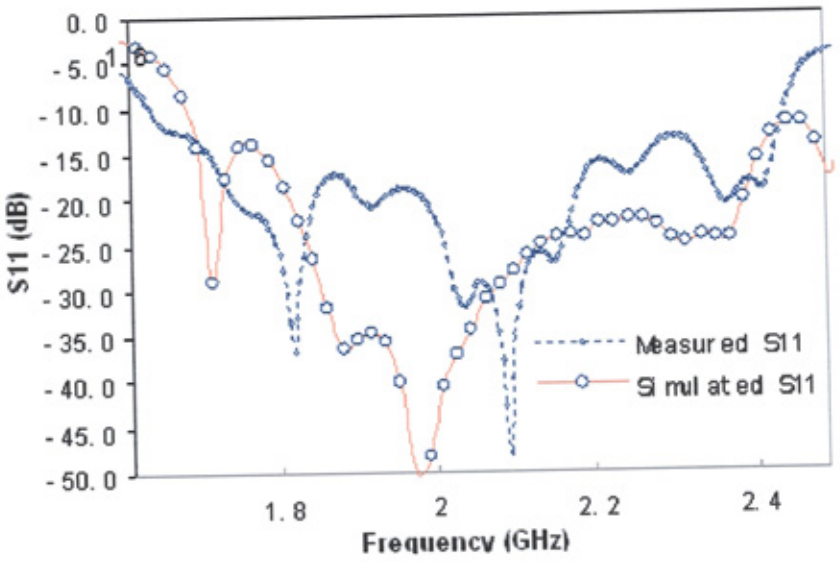
0.0
-5.0
-10.0
-15.0
-20.0
-25.0
-30.0
-35.0
-40.0
-45.0
-50.0
S11 (dB)
1.8
2
2.2
2.4
Frequency (GHz)
Measured S11
Simulated S11

(a)

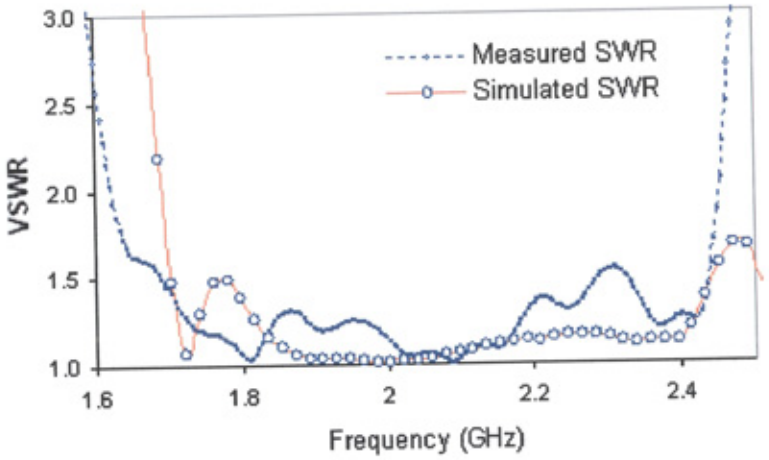
3.0
2.5
2.0
1.5
1.0
VSWR
1.6
1.8
2
2.2
2.4
Frequency (GHz)
Measured SWR
Simulated SWR

(b)

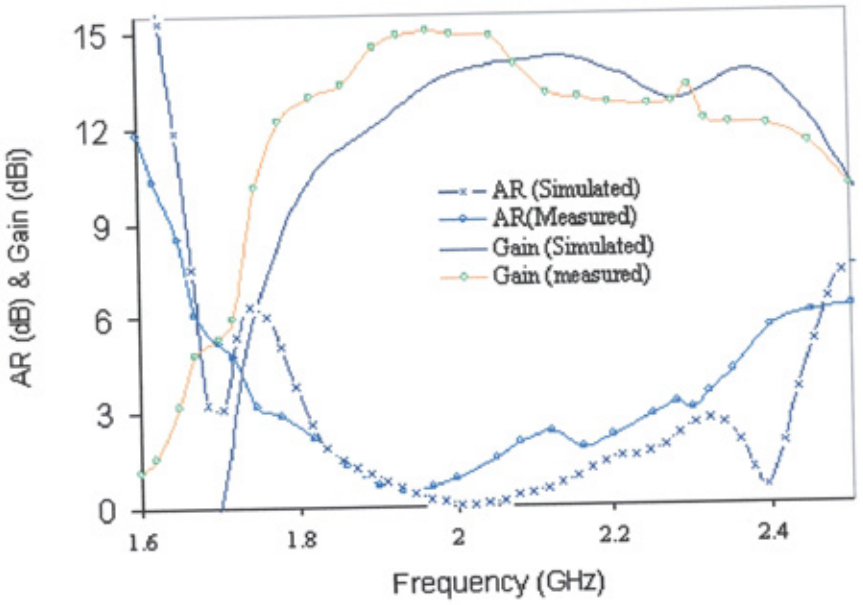

(c)

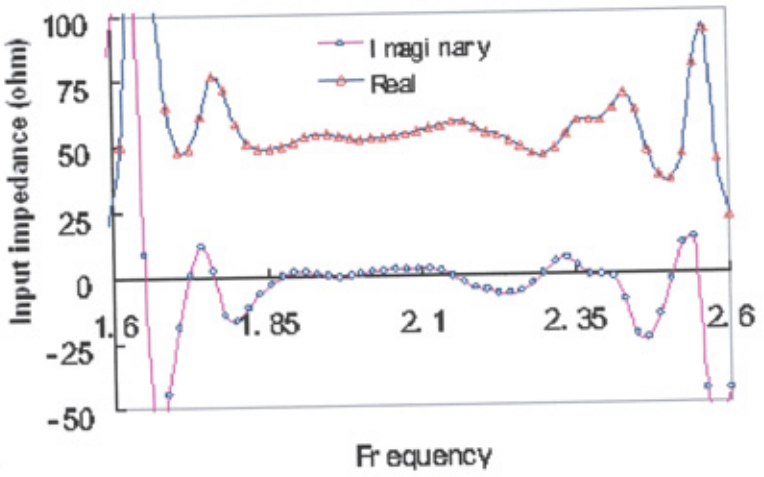

(d)

Figure 3.19: The comparisons of simulated and measured results (a) S11, (b) SWR, (c) axial ratio & gain, and (d) input impedance.

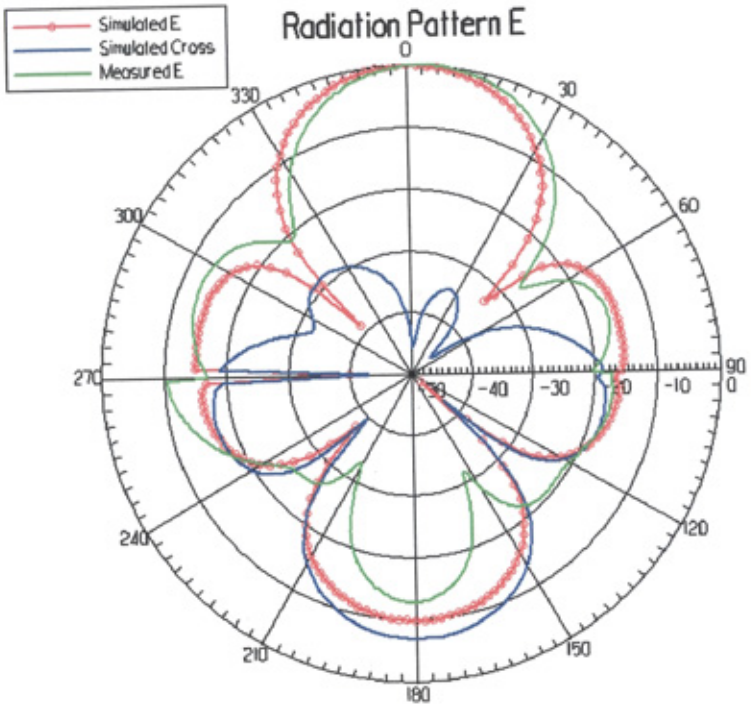

(a)

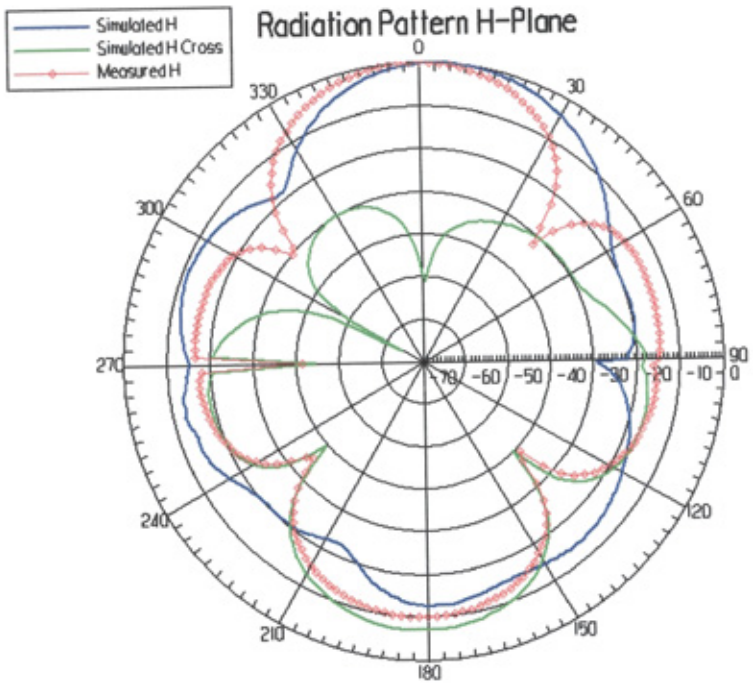

(b)

Figure 3.20: Measured and simulated radiation pattern of the designed antenna array

(a) E-plane, and (b) H-plane.

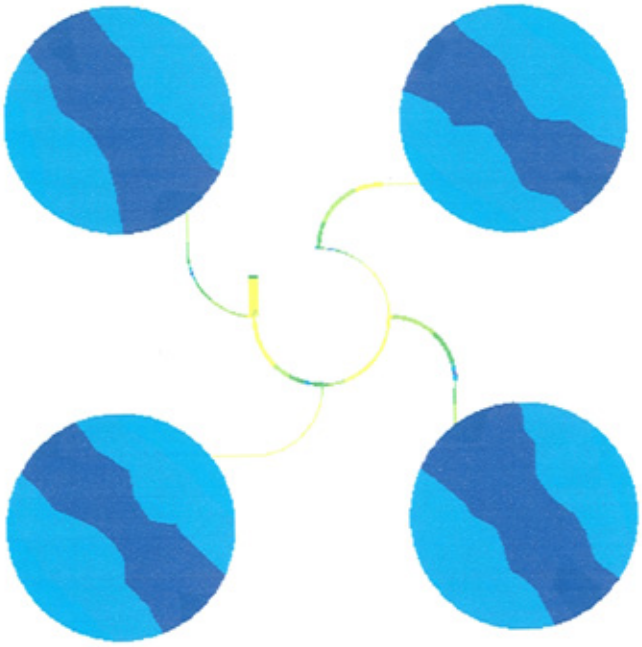

Figure 3.21 Current plot animation

	Frequency Band (GHz)	Bandwidth (%)
Axial Ratio<3dB (Single element)	1.88-2.07	9.6
Gain >6dB (Single element)	1.86-2.27	20
S11<10dB (Single element)	1.76-2.29	26
Axial Ratio<3dB (array)	1.75-2.3	27.2
Gain >10dB (array)	1.73-2.5	36
S11<10dB (array)	1.62-2.45	41

Table 3.4. Comparison of the bandwidth of axial ratio, gain and S11.

Figure. 3.21 shows the current animation plot of the current distribution on the array antenna. Each element has approximately the same current phase and magnitude distribution and when rotated follows the same direction and time. This verified the success of the sequentially rotated antenna array. Table 3.4 shows the comparison of the AR, Gain and S11 bandwidth. The bandwidths are well overlaid with each other.

3.6 SUMMARY

In summary, two broadband LP, one CP and one CP array slot-coupled microstrip antenna were presented in this chapter. The characteristic of ring slot was investigated. A ring slot-coupled broadband LP antenna achieved a -10 dB S11 bandwidth of 50 %. A -10 dB S11 bandwidth of 51 % was achieved by the square ring slot-coupled LP broadband antenna. An unequal length cross-slot coupled circular patch antenna had been analysed, fabricated and tested. The results of the antenna were accurately predicted by the commercial software Ensemble v8. The array antenna achieved a 3 dB AR bandwidth of 27.2 %, and a –10 dB S11 bandwidth of 41 % respectively. Compared with single element, a 9.6 % AR bandwidth and 26 % S11 bandwidth, significant improvements were achieved. Good broadside radiation and peak antenna gain had been achieved, whilst maintaining a low cross-polar level within the entire frequency band. The bandwidths were well overlaid with each other. To achieve compact, broadband, high efficiency RF front-end in radio transmitter, the broadband antenna will need to be further integrated with the RF/microwave power amplifier. In the next chapter, a literature review of class-E PA is presented together with an improved design technique.

CHAPTER 4

Class-E RF/Microwave Power Amplifier : A Review and Theoretical Analysis

4.1 Introduction

RF/microwave PAs are widely used in the applications of wireless communication, radar, and industrial, scientific, and medical (ISM) fields. Switching-mode PA has been proposed and developed [49-51] for applications requiring high efficiency. By operating the transistor as a switch rather than a current source and employing appropriate output harmonic terminations, the amplifiers can achieve 100% efficiency in principle.

In this chapter, the definitions of PA are firstly introduced. Followed by the classifications of conventional PAs, the analysis of the idealized class-E operation is presented. The essential current and voltage equations and the resultant class-E design

equations are derived. The effects of non-ideal characteristics of practical device and duty cycle will be analyzed and discussed accordingly.

4.2 Definitions Of Power Amplifier

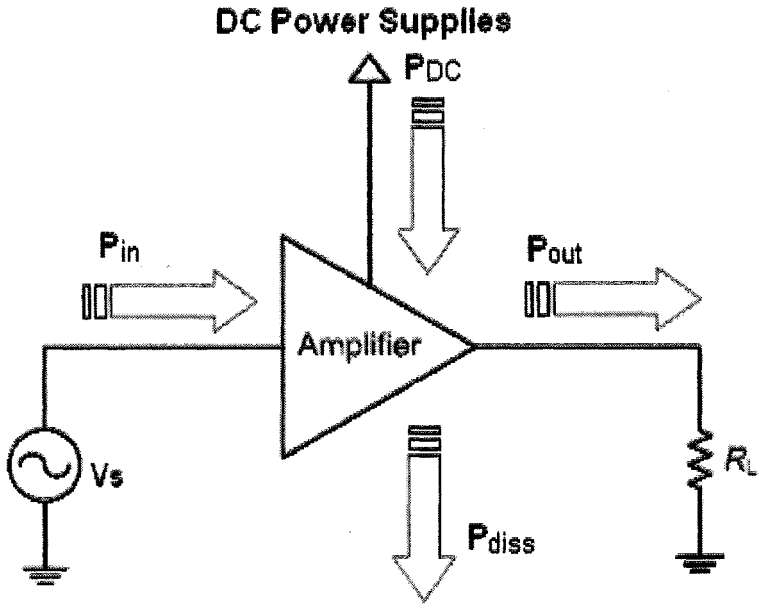

Figure 4.1: Typical power flows in a generalized power amplifier.

Figure.4.1 shows a diagram of typical power flow in a generalized PA. The function of the power amplifier is to convert DC power to RF power by amplifying an input RF signal. The efficiency at which this amplification takes place can be described in terms of the drain efficiency η_d (equation 4.1) and the power added efficiency (PAE) (equation 4.2).

Drain efficiency is a measure of how well the DC power is converting to output RF power. The most widely used definition of efficiency in all types of amplifiers however, is the power added efficiency, in which the produced power from an amplifier is defined as the RF power 'added' by an amplifier, i.e., the difference

between the RF input and output at f_0: while PAE is indicated by both drain efficiency and gain. These two types of efficiency are defined as:

$$\eta_D = \frac{P_{out}(f_0)}{P_{dc}}. \tag{4.1}$$

$$PAE = \frac{P_{out}(f_0) - P_{in}(f_0)}{P_{dc}}. \tag{4.2}$$

In terms of drain efficiency and gain, $G = P_{out}(f_0)/P_{in}(f_0)$, hence the equation 4.2 can be rewritten as:

$$PAE = \eta_D\left(1 - \frac{1}{G}\right). \tag{4.3}$$

4.3 Classes of Power Amplifiers

Amplifiers are classified into different classes such as A, B, C, D, E and F according to their circuit configurations and methods of operation. These classes range from entirely linear with low efficiency to entirely non-linear with high efficiency. The majority of this information is available in Solid State Radio Engineering by Krauss, Bostain, and Raab [49]. A short summary of the information given in this book is provided here for completeness.

4.3.1 Class-A

Class-A, in class A PA, the quiescent current is large enough that the transistor remains in the active region at all times and acts as a current source, controlled by the drive. Consequently, the drain voltage V_{DS} and current I_{DS}

waveforms are (ideally) both sinusoidal as shown in Figure 4.2. The class-A operation is where both devices conduct continuously for the entire cycle of signal swing, or the bias current flows in the output devices at all times. The key ingredient of class-A operation is that both devices are always on. There is no condition where one or the other is turned off. Due to this, class-A amplifiers are single-ended designs with only one type of polarity output device. Class A is the most inefficient of all power amplifier designs, averaging at around only 20 %. Thus, class-A amplifiers are large, heavy and run at very high temperatures. All this is due to the amplifier constantly operating at full power. The positive effect of all this is that class-A designs are inherently the most linear, with the least amount of distortion.

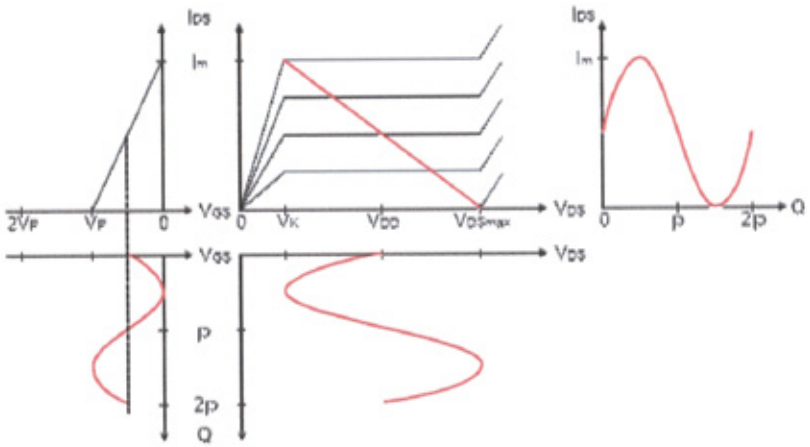

Figure 4.2: Load line and waveforms of class-A PA.

4.3.2 Class-B

Class-B operation is the opposite of class-A. Both output devices are never allowed to be on at the same time, or the bias is set so that current flow in a specific output device is zero when not stimulated with an input signal, i.e., the current I_{DS} in a specific output flows for one half cycle see Figure 4.3. Thus each output device is on

for exactly one half of a complete sinusoidal signal cycle. Due to this operation, class-B designs show high efficiency but poor linearity around the crossover region. This is due to the time it takes to turn one device off and the other device on, which translates into extreme crossover distortion. Thus restricting class B designs to power consumption critical applications, e.g., battery operated equipment, such as 2-way radio and other communications audio.

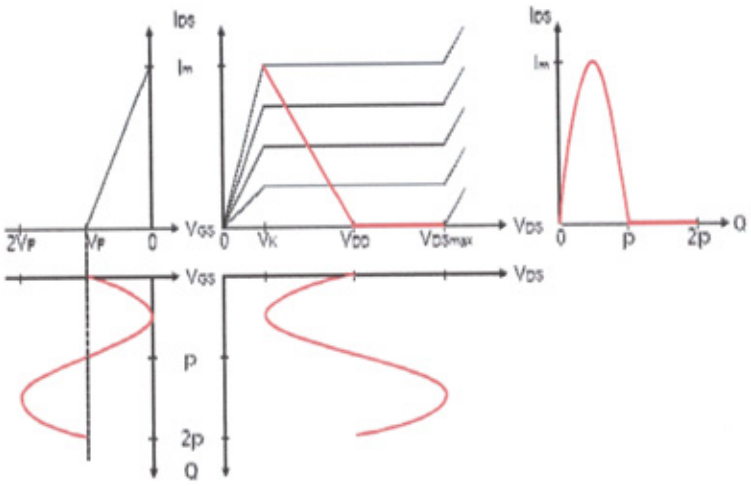

Figure 4.3: Load line and waveforms of class-A PA.

4.3.3 Class-AB

Class-AB operation allows both devices to be on at the same time (like in class A), but just barely. The output bias is set so that current flows in a specific output device appreciably more than a half cycle but less than the entire cycle. That is, only a small amount of current is allowed to flow through both devices, unlike the complete load current of class-A designs, but enough to keep each device operating so they respond instantly to input voltage demands. Thus the inherent non-linearity of class-B designs is eliminated, without the gross inefficiencies of the class-A design. It

is this combination of good efficiency (around 50 %) with excellent linearity that makes class-AB the most popular audio amplifier design. More detail of this class PA can be found in [43].

4.3.4 Class-C

Class-C, conducting less than half of the cycle, as shown in Figure 4.4, this PA sacrifices output power for efficiency as the conduction cycle gets smaller. It has an efficiency lager than class-B, approaching 100 % as the conduction cycle and output go to zero. Since it is a nonlinear PA, it only can be used in constant envelope applications. Class-C amplifiers, though usually used in the active and cut-off regions, are sometimes operating with large input signals such that the transistors enter saturation during a part of the conduction cycle.

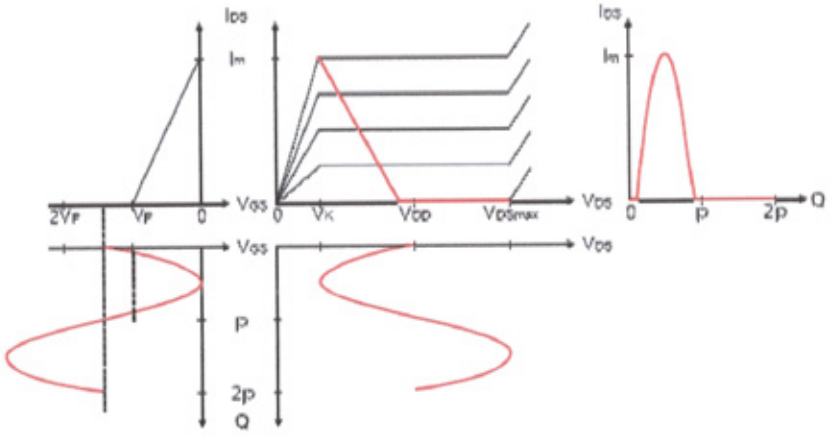

Figure 4.4: Load line and waveforms of class-C PA.

4.3.5 Class-D

Class-D uses two transistors that are usually drive in push-pull, so that they are alternatively switch on and off. By this two ports switching operation of

transistors, the drain voltage in voltage mode class-D or drain current in current mode class-D is shaped to a rectangular waveform. The output is connected with a bandpass filter that generates a sinusoidal output from the rectangular waveform from the drain terminal. Ideal drain voltage and current waveforms are shown in Figure.4.5. Since the output devices are either completely on or completely off they do not theoretically dissipate any power. However, practical class-D PAs suffer from discharge loss generated in the transistor output capacitance. The class-D PA designs do exist with true efficiencies approaching 90 %.

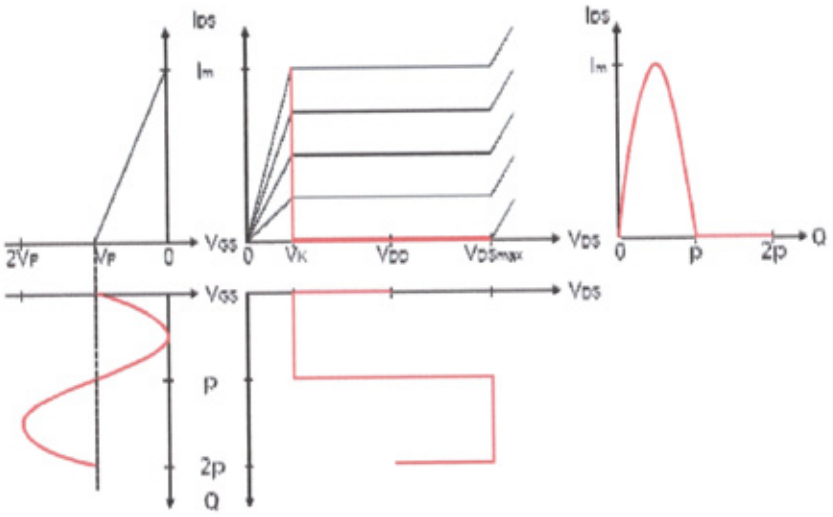

Figure 4.5: Load line and waveforms of switching-mode PA.

4.3.6 Class-E & F

Class-E and F, class-E is a very popular switching-mode PA due to its high efficiency characteristic with simple circuitry. It employs a single transistor act as a switch. Ideally it can achieve 100% efficiency. However, its small on resistance and a non-ideal filter at the output will degrade the efficiency. The theory behind the class-E

PA is detailed in the following sections. **Class-F** is basically derived from class-B with multiple harmonic resonant filters. The sinusoidal voltage is shaped to a rectangular waveform by output harmonic tuning: open circuit at all odd harmonics and short circuit for all even harmonics, where there is no overlap between voltage and current waveforms. Hence, an ideal 100 % efficiency can be achieved. However, in practical class-F PA, harmonic filters are imperfect due to unwanted harmonic tuning. Further more, the harmonic filters are usually employed up to the third harmonics although the efficiency is a little degraded.

4.4 Theoretical Analysis of Ideal Class-E Operation

The basic circuit topology for the class E power amplifier is shown in Figure 4.6 (a). The basic Class E power amplifier [51] consists of a transistor acting as a switch, an inductor L_{dc}, a shunt capacitor across the switch C_S and an ideal series filter L_2 and C_2 tuned to the fundamental frequency. When optimally configured, it operates with zero current at switch turn-off and zero voltage across the switch at switch turn-on. This allows high-efficiency operation with low power dissipation, low junction temperature, and high reliability. The idealized voltage and current waveforms is shown in Figure 4.6 (b).

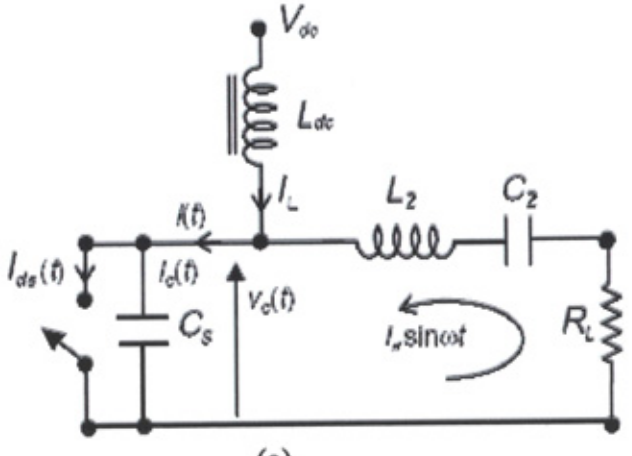

(a)

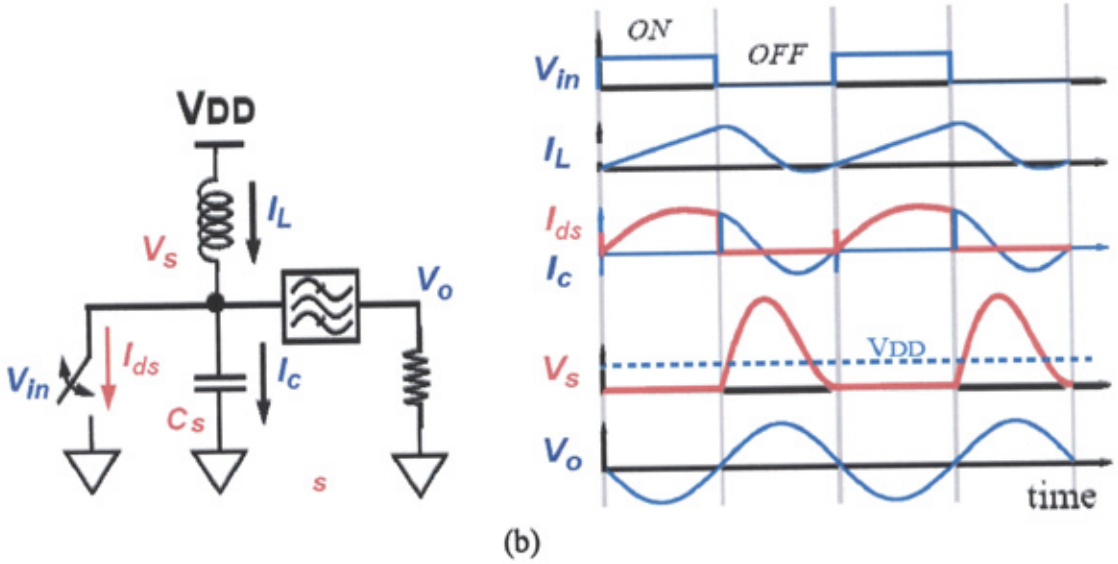

Figure 4.6 (a): Class-E PA circuit topology, and (b) voltage and current waveforms of class-E operation.

Since the introduction of the Class E amplifier, many analytical descriptions of this circuit have appeared [51–66, 70-71]. Early analyses have assumed an ideal switch, infinite output network which tune to a sinusoidal output current. A RF choke in the dc supply gives a constant current supply. Later works have investigated the effects of finite dc-feed inductance [58]–[60], finite output network [61]–[63] and nonzero active device ON-resistance [64]. The theoretical performance of a Class E amplifier with an infinite output network and a RF choke in the dc supply lead were described in [65].

In this section, the idealized operation of the class-E operation will be analyzed based on the early study done by Madder [70]. The current and voltage equations with the resultant design equations are derived.

The assumptions made in this analysis are:

1) The current flowing into the choke inductor L_{dc} is assumed to be constant

2) The current flowing into the filter load network is assumed to be sinusoidal at the switching frequency
3) An equivalent current is placed across the switched capacitor, which consists of constant (DC) and sinusoidal (RF) components
4) The current cross the transistor is $I_{dS}(1-\alpha\sin(\omega_s t+\phi))$
5) The transistor switch on and off for half of the period.

Based on these assumptions, the equivalent circuits for the OFF and the ON states of the switch are presented in Figure 4.6(b), respectively. The mathematical approach and the equations used to obtain the results given in this section are presented here.

When switch is on: The voltage is zero when a high current is flowing, that is, the transistor acts as a zero resistance closed switch during the "on" part of the RF period.

$$(\pi \le (\omega_S t) \le 2\pi) : i_S(t) = I_{ds}(1-\alpha\sin(\omega_S t+\phi)) \tag{4.4}$$

$$(\pi \le (\omega_S t) \le 2\pi) : V_S(t) = 0 \tag{4.5}$$

When switch is off: The current is zero when there is a high voltage, that is, the transistor acts as an open switch during the "off" part of the RF period

$$Cs\frac{dV_s}{dt} = I_{ds}(1-a\sin(\omega t+\phi)) \tag{4.6}$$

$$(0 \le (\omega_s t) \le \pi) : V_S(t) = \frac{I_{ds}}{\omega_S C_S}((\omega_S t)+\alpha(\cos((\omega_S t)+\phi)-\cos\phi)) \tag{4.7}$$

$$(0 \le (\omega_S t) \le \pi) : i_S(t) = 0 \tag{4.8}$$

Idealized voltage and current waveforms are plotted in Figure 4.7.

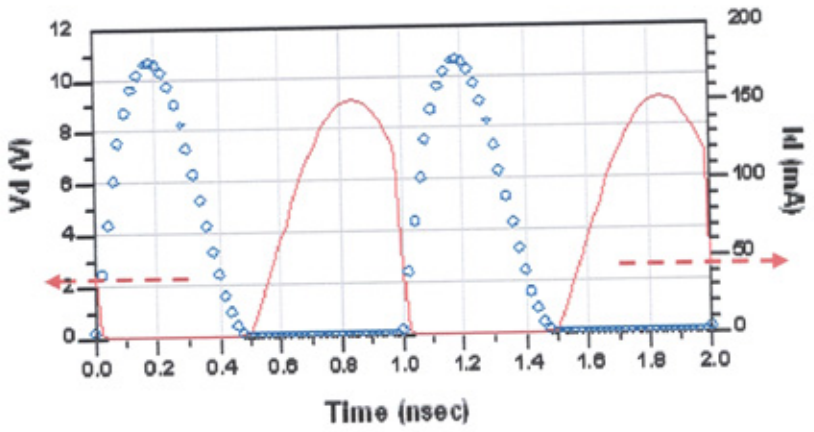

Figure 4.7: Ideal waveforms of switch voltage and current.

The mathematic expressions of the three conditions for class E operation are:

$$V_c(0) = 0 \tag{4.9}$$

$$V_s(0) = 0 \tag{4.10}$$

$$\frac{dV_s}{dt}\left(\frac{T_s}{2}\right) = 0 \tag{4.11}$$

The first condition avoids shorting the capacitor C_s when there is voltage across it during switching. The second condition ensures a "soft" turn on condition for the switching device. These two condition constraints determine the amplitude α and phase ϕ uniquely:

$$\alpha = \sqrt{1+\frac{\pi^2}{4}} \approx 1.862 \tag{4.12}$$

$$\phi = -\arctan\frac{2}{\pi} \approx -32.48^{o} \tag{4.13}$$

4.4.1 The Analysis Of Harmonics Contents of Drain Voltage

The simplified analysis of the class-E amplifier circuit given above assumes a sinusoidal output signal at the load resistor R. However, some higher harmonic components will present at the output load of the class-E PA in practice. The switch

voltage $V_s(t)$ is analysed using Fourier series in this section. The expressions for the magnitude and phase components of the switch voltage harmonics are given. The derived expressions then can be used to transform the load network to the optimum impedance. Thus, the design equations of a specified load network configuration can be obtained.

The switch voltage using the Fourier series is defined as:

$$V_S(t) = \sum_{n=-\infty}^{\infty} K_n e^{jn\omega_S t} \tag{4.14}$$

where,

$$K_n = \frac{1}{T_S}\int_0^{\frac{T_S}{2}} V_S(t) e^{-jn\omega_S t} dt \tag{4.15}$$

Now, the off state switch voltage equation 4.7 can be applied to equation 4.15. Thus, equation 4.15 can be rewritten as:

$$K_n = \frac{I_{ds}}{\omega_S C_S T_S}\int_0^{\frac{T_S}{2}} (\omega_S t + \alpha(\cos(\omega_S t + \phi) - \cos\phi)) e^{-jn\omega_S t} dt \tag{4.16}$$

The fundamental harmonic voltage V_{S1} can be obtained as:

$$V_{S1} = K_1 e^{j\omega t} \tag{4.17}$$

where K_1 is:

$$K_1 = \frac{1}{T_s}\int_0^{T_s} V_s(t) e^{-j\omega t} dt = \frac{I_{ds}}{\pi\omega_s C_s}\left(\frac{\pi^2}{8} - 1 - \frac{j\pi}{4}\right) \tag{4.18}$$

The amplitude factor can be solved by the equation:

$$\alpha_1 = \frac{2|K_1|}{I_{ds}} = \frac{1}{\omega_s C_s}\sqrt{\frac{\pi^2}{16} + \frac{4}{\pi^2} - \frac{3}{4}} \tag{4.19}$$

The phase factor can now be found by using the following equation:

$$\phi_1 = \frac{\pi}{2} + \angle K_1 = \frac{\pi}{2} + \arctan\left(\frac{2\pi}{8-\pi^2}\right) \tag{4.20}$$

Hence, the fundamental harmonic voltage can be written as

$$V_{s1} = \alpha_1 I_{ds} \sin(\omega t + \phi_1) = 22.495 \sin(\omega t + 49.051). \tag{4.21}$$

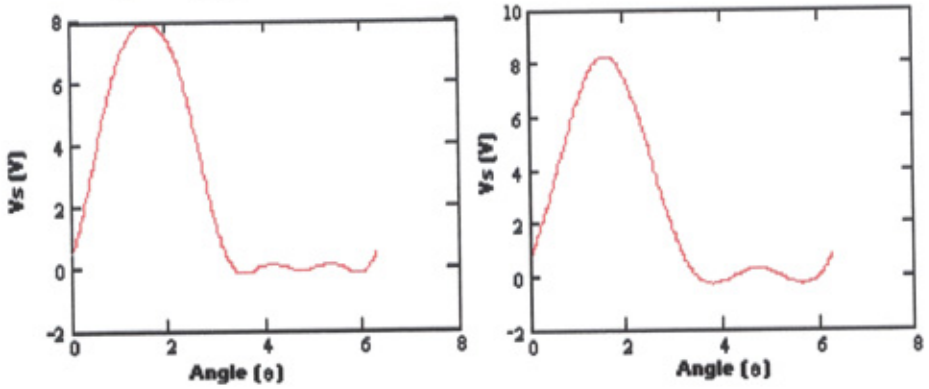

(a) (b)

Figure 4.8: Voltage waveforms which contains: (a) 1st ,2nd and 3rd harmonics, and (b) 1st and 2nd harmonics.

Using the same procedures the second harmonic voltage is obtained as:

$$V_{s2} = \alpha_2 I_{ds} \sin(\omega t + \phi_2) = 41.53 \sin(2\omega t - 19.374) \tag{4.22}$$

The switching voltage contains an infinite number of harmonics; however, it can be approximately represented by a limited number of harmonic components. The calculated switching voltage V_S is plotted with different harmonic contained in Figure 4.8. The comparison of Figure 4.8(a) and Figure 4.8(b) shows that the difference is made when the 3rd harmonic is not present.

4.4.2 Design Equations

In order to find out the information of the RF impedance seen by transistor output, the fundamental voltage and current have to be predetermined. The

fundamental current is founded using equation 4.6. The fundamental voltage has to be found using the Fourier-transform expansions introduced previously. The resultant expressions are presented here:

$$V_{S1} = \alpha_o I_{ds} \sin(\omega_S t + \phi_1) \tag{4.23}$$

$$i_{S1} = \alpha I_{ds} \sin(\omega_S t + \phi) \tag{4.24}$$

where the constants α and ϕ are designed in (4.12) and (4.13). Hence, the load impedance seen by transistor output can be determined by:

$$Z_{Load} = \frac{V_{S1}}{i_{S1}} = \frac{\alpha_o I_{ds} \sin(\omega_S t + \phi_1)}{\alpha I_{ds} \sin(\omega_S t + \phi)} = \frac{\alpha_o}{\alpha} e^{j(\phi_1 - \phi)} \approx \frac{0.28015 \times e^{j49.0524^o}}{\omega_S C_S}. \tag{4.25}$$

4.5 Analysis Of Effects Of Small Switch-On Resistance

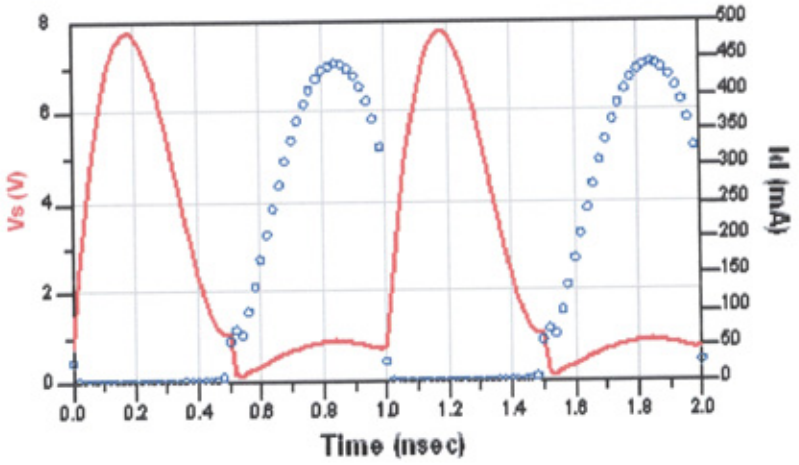

Figure 4.9: Voltage and current waveform in the switch (Ron=2).

The class-E circuit has a theoretical efficiency of 100%. However, microwave PA could never achieve such ideal performance in practice. The switch on resistance is the major cause for the losses in the microwave PA design. Mader has presented a

complete mathematical analysis of the voltage and current waveforms which take into account the effect of the switch-on resistance in [70]. In this section, a general analysis and review of this approach is presented. The detailed derivations can be found in [70].

A similar approach is applied into this analysis. The equations (4.26) and (4.27) can be rewritten as follow with the appearance of the switch-on resistance.

$$(0 \le t \le \frac{T_s}{2}) : V_s(t) = \frac{I_{ds}}{\omega_s C_s}(\omega_s t + \alpha_\tau(\cos(\omega_s t + \phi_t) - \cos\phi_\tau)) + 2R_s I_{ds} \tag{4.26}$$

$$(\frac{T_s}{2} \le t \le T_s) : V_s(t) = R_s I_{ds}(1 - \alpha_\tau \sin(\omega_s t + \phi_\tau)) \tag{4.27}$$

The calculated voltage and current waveforms in Figure 4.9 shows affect of the switch-on resistance on the current waveform. In this case, two boundary conditions are still remaining in order to find out the amplitude of the sinusoid current and the phase delay of the voltage as it crosses the switch.

$$\alpha_\tau = \sqrt{1 + (\frac{\pi}{2} + \omega_s C_s R_s)^2} \tag{4.28}$$

$$\phi_\tau = -\arctan(\frac{1}{\frac{\pi}{2} + \omega_s C_s R_s}) \tag{4.29}$$

Hence, DC to RF conversion efficiency is found:

$$\eta_d = \frac{1 + (\frac{\pi}{2} + \omega_s C_s R_s)^2}{(1 + \frac{\pi^2}{4})(1 + \pi\omega_s C_s R_s)^2} \tag{4.30}$$

The same as in the previous section, a Fourier-transform expansion is used to obtain the harmonic components of the switching voltage.

$$(0 \le t \le \frac{T_s}{2}) : V_s(t) = \frac{I_{ds}}{\omega_s C_s}(\omega_s t + \alpha_\tau(\cos(\omega_s t + \phi_t) - \cos\phi_\tau)) + 2R_s I_{ds} \tag{4.31}$$

$$(\frac{T_s}{2} \le t \le T_s) : V_s(t) = R_s I_{ds}(1 - \alpha_\tau \sin(\omega_s t + \phi_\tau)) \tag{4.32}$$

The fundamental voltage component can be obtained as the following equation.

$$V_{S1} = K_1 e^{j\omega t} \tag{4.33}$$

$$K_1 = \frac{1}{T_s}\int_0^{T_s} V_s(t) e^{-j\omega t} dt = \frac{1}{T_s}\int_0^{\frac{T_s}{2}} \frac{I_{ds}}{\omega_s C_s}(\omega_s t + \alpha_\tau(\cos(\omega_s t + \phi_t) - \cos\phi_\tau)) + 2R_S I_{ds} dt +$$

$$\frac{1}{T_s}\int_{\frac{T_s}{2}}^{T_s} R_s I_{ds}(1 - \alpha_\tau \sin(\omega_s t + \phi_\tau)) dt \tag{4.34}$$

$$K_1 = \frac{1}{T_s}((\frac{\pi^2 - 8}{4\omega} - j\frac{\pi}{2\omega} + \frac{4RI}{j\omega^2 CT}^2) + \frac{jRI\pi}{2\omega}(\frac{\pi}{2} + \omega CR) + \frac{\pi RI}{\omega}) \tag{4.35}$$

$$\alpha_1 = \frac{2|K_1|}{I_{ds}} = \frac{1}{\omega C_s}\left|(\frac{\pi^2 - 8 + 4\pi RI}{8\pi} - j(\frac{2 - \pi RI - 2CR^2 I\omega}{8} + \frac{RI^2}{C\pi^2})\right| \tag{4.36}$$

$$\phi_1 = \frac{\pi}{2} + \angle K_1 \tag{4.37}$$

4.6 Investigations Of Class E Power Amplifier In Frequency Domain

4.6.1 Modelling With Ideal Lumped Elements

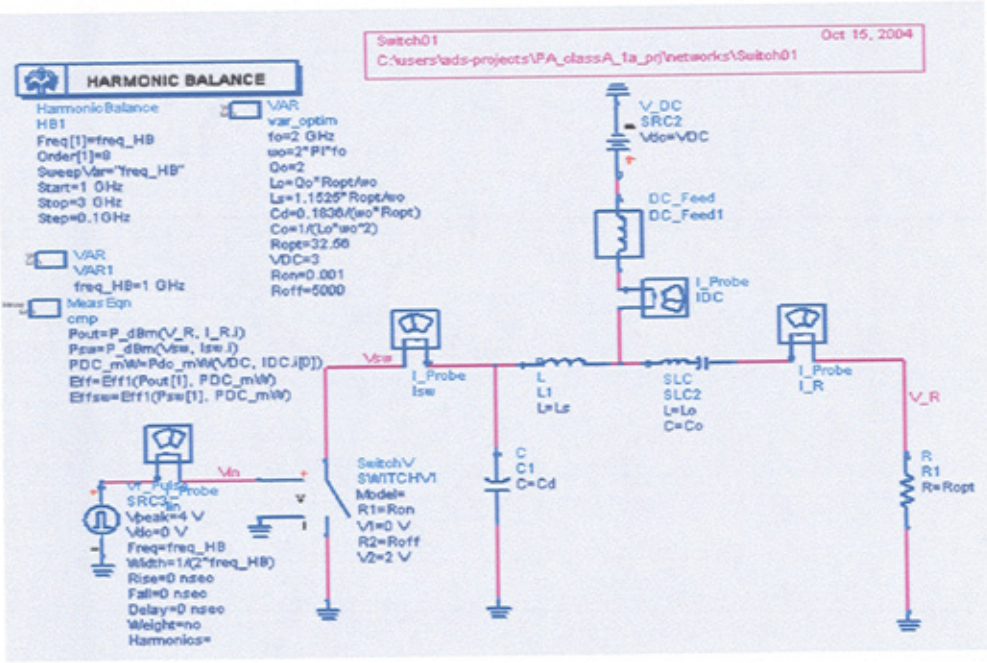

Figure 4.10: Idealize class-E PA modelling in ADS.

Frequency variation is a very important factor for the design of the broadband class-E PA. In order to have a visualized view of how each parameter affects the performance of the class-E PA, an ideal class-E PA is simulated in ADS® to investigate the switch on resistance effect, duty cycle effect and the quality factor of the load network effect. All the parameters are simulated in frequency domain. The results and discussions are presented in this section.

The simulation is done in ADS®. An ideal voltage controlled switch with a shunt capacitor is used to model the idealized class-E operation as shown in Figure.4.10. Two ideal RF chokes are used in the bias networks. The design equations from the previous section are used to define the lumped component values. The circuit allows ideal Class E operation with an efficiency of 100 percent when the Q factor of the load network is an infinite number.

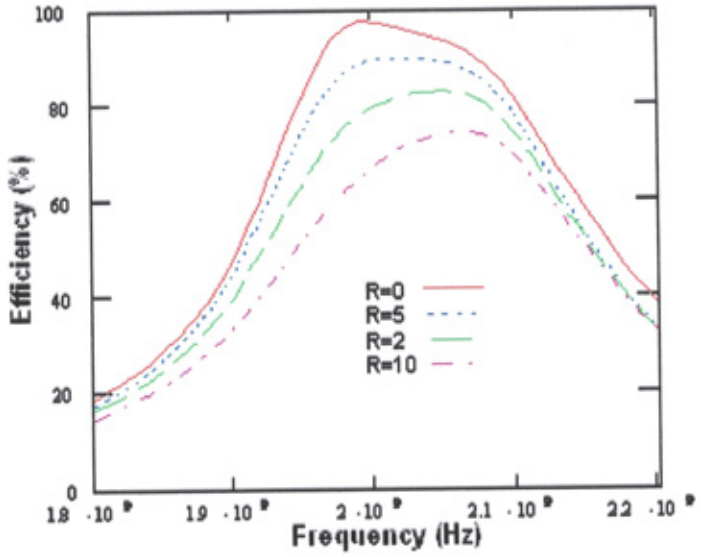

Figure 4.11: The efficiency against frequency when Switch on resistance R=0, 2, 5, 10.

Figure 4.11 shows the plot of the drain efficiency against the frequency with a selection of switch on resistance values. It shows that the bandwidth and efficiency both change when changing the value of the switch on resistance. Thus, the results confirm that the switch on resistance not only degrades the efficiency but also the frequency bandwidth.

Figure 4.12 shows how the quality factor of the load network affects the drain efficiency of the class-E PA. The assumption of the ideal class-E operation is that the load network has an infinite number of quality factors. However, this is not realizable in practice. The modelling of the class-E PA load network with a selection of a number of finite Q factors is carried out. The result show a well known fact which is that a higher quality factor will lead to a lower bandwidth. The efficiency does not change with the quality factor in this case. This is due to the switch-on resistance which is assumed to be zero. In practice, a lower quality factor means more loss in the circuit which means it will lead to a lower efficiency.

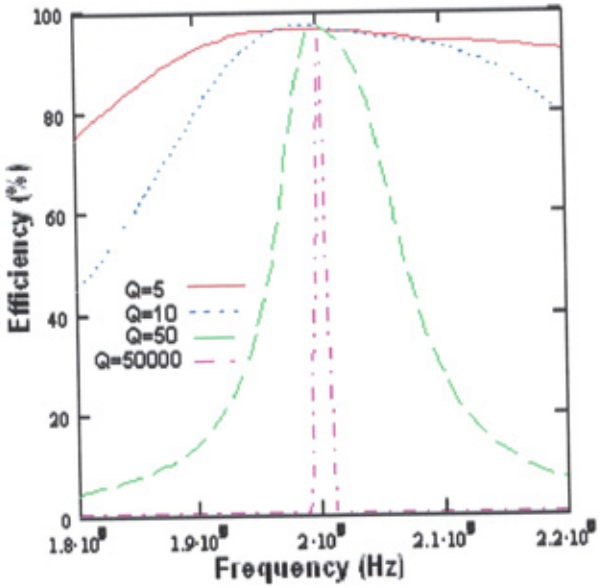

Figure 4.12: The efficiency against frequency when Q of the output load network Q =5, 10, 50, 50000.

Most of the investigations on the switch duty cycle effect are focused on the changes in the circuit parameters when the switch duty cycle varies. In this study, the circuit simulation is created with a tuneable switch duty cycle. The result in Figure 4.13 shows that the comparison of efficiency in the frequency domain with different duty cycles 50 %, 40 % and 30 %. Frequency shifts between every efficiency peak are found in Figure 4.13. This is due to the difference between switch duty cycles, which lead to the drifting of the class-E PA optimum frequency.

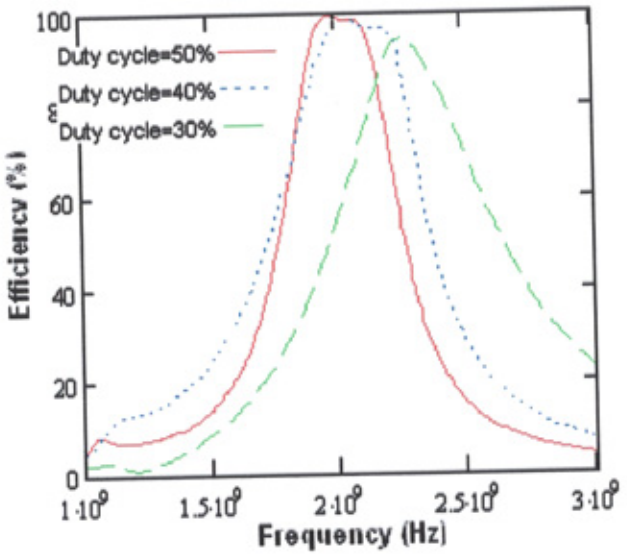

Figure 4.13: The efficiency against frequency when the duty cycle is 50 %, 40 % and 30 %.

4.6.2 Modelling With Transmission Lines

The transmission line takes an important part in high frequency microwave circuit design. The ideal lumped elements which are used in the load network are converted into a transmission line using the ideal transmission line theory. The simulation is carried out at centre frequency of 2 GHz. The simulation setup is shown in Figure 4.14. The circuit consists of a voltage control switch with a capacitor in parallel, which represents the total shunt capacitor in class-E PA. Once again, two ideal RF chokes are used as bias networks. An L-shaped transmission line network is connected with the output of the class-E PA, which is used as an output filter.

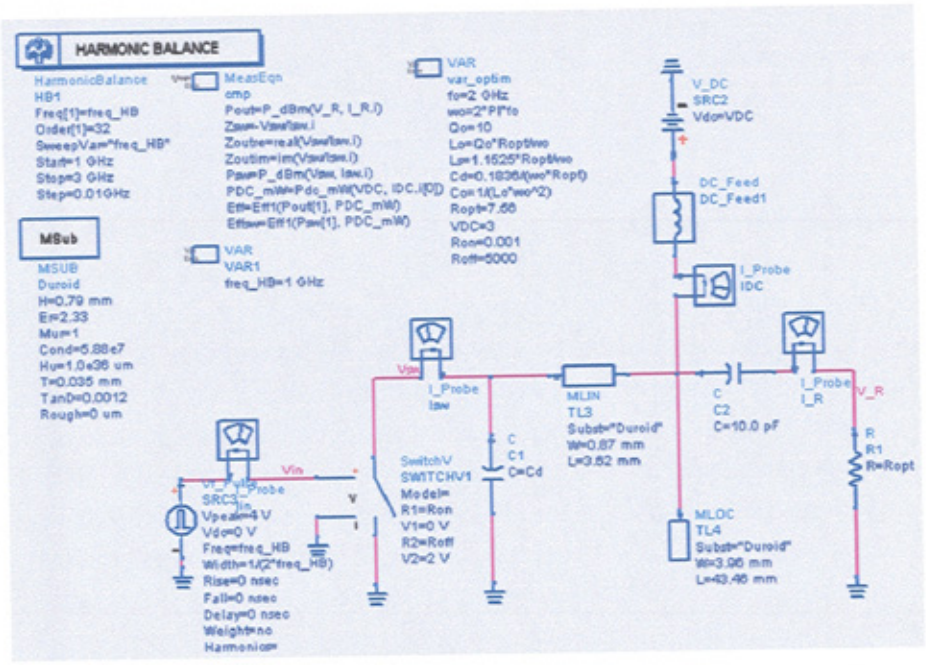

Figure 4.14: Idealize class-E PA (transmission line) modelling in ADS.

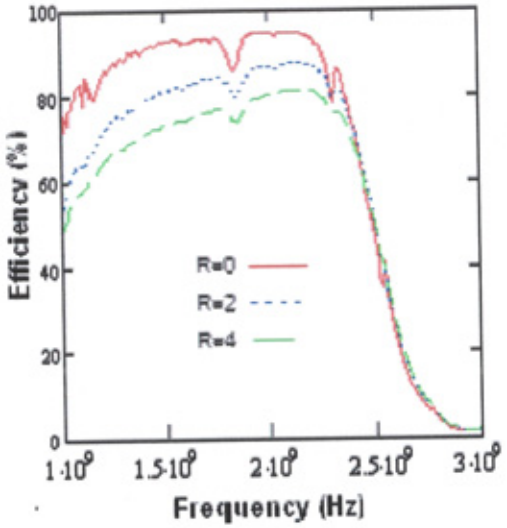

Figure 4.15: The efficiency against frequency when switch on resistance R = 0, 2, 4.

Figure 4.15 shows that the plot of the drain efficiency against the frequency with a selection of switch on resistance values. A much wider bandwidth is obtained compared with Figure 4.11. This is due to a much lower quality factor being used for

the transmission line load network. Thus, the peak efficiency can no longer achieve 100 % in this case. Once again, the simulation result shows that the bandwidth and efficiency both change with a changing switch on resistance value. Thus, the results confirm that the switch on resistance not only degrades the efficiency but also the frequency bandwidth.

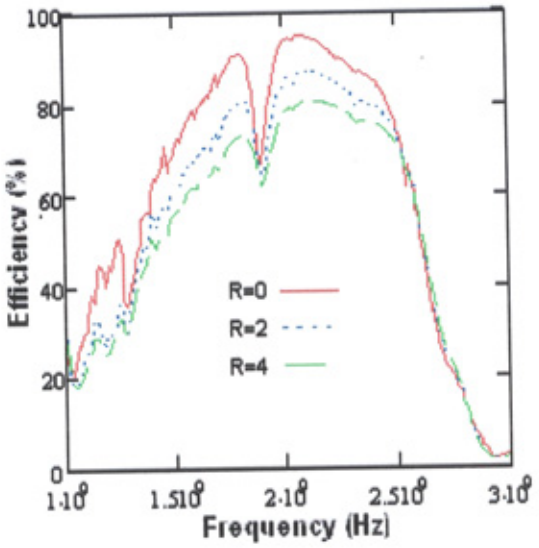

Figure 4.16 With the switch duty cycle of 40 %, the efficiency against frequency when switch on resistance $R = 0, 2, 4$.

Figure 4.16 shows that the simulated efficiency bandwidth when the switch duty cycle is set as 40 %. Three different values of switch-on resistance are simulated in this case. The efficiency bandwidth is narrower compared with Figure 4.15. The peak efficiency is shifting to a higher frequency band compare with the design frequency 2 GHz.

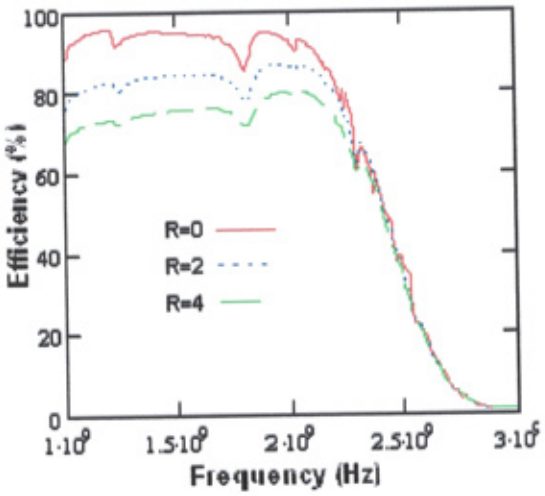

Figure 4.17: With the switch duty cycle of 60 %, the efficiency against frequency when Switch on resistance R = 0, 2, 4.

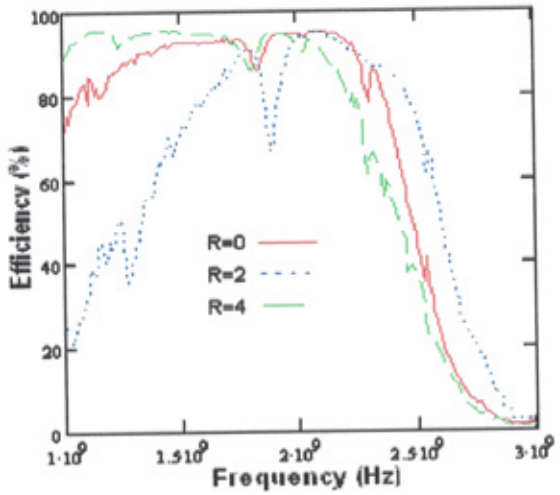

Figure 4.18: The efficiency against frequency when switch duty cycle is 40 %, 50 % and 60 %.

Figure. 4.17 shows how efficiency changes when the duty cycle is increased to 60 %. The high efficiency bands are shifted to a lower frequency compared with the previous case. This is due to the lower switch duty cycle meaning that it will perform at 50 % of the duty cycle at a lower frequency.

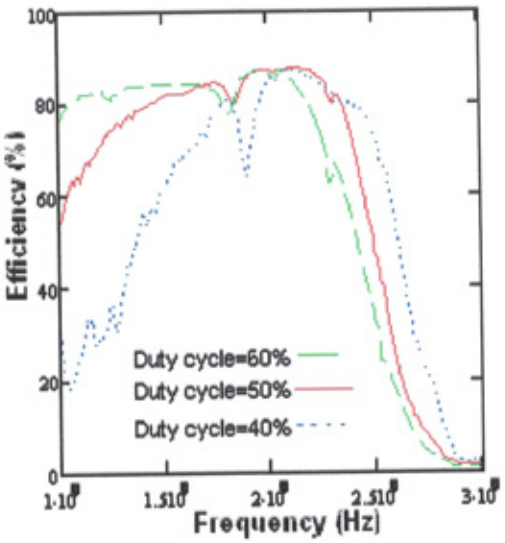

Figure 4.19 The efficiency against frequency when switch duty cycle is 40 %, 50 % and 60 %. (Switch-on resistance is 2 ohm).

Figure. 4.18 gives evidence of how the efficiency bandwidth shifts when the switch duty cycle changes. Further investigations on the effect of both duty cycle and switch-on resistance are carried out, with simulation results shown in Figures 4.19 and 4.20.

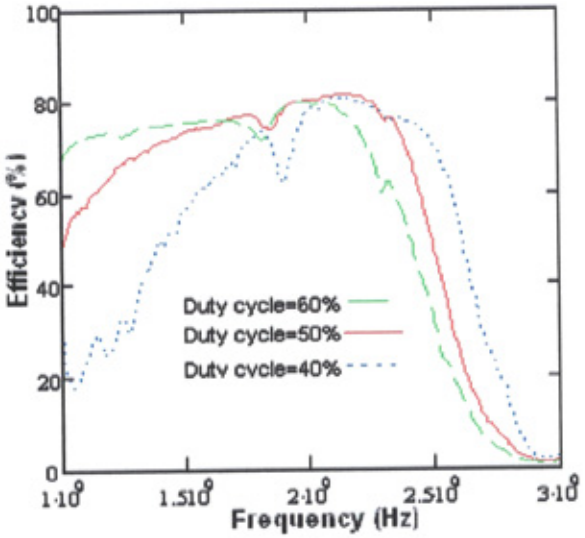

Figure 4.20 The efficiency against frequency when switch duty cycle is 40 %, 50 % and 60 %. (Switch-on resistance is 4 ohm).

4.7 Summary

A brief overview of the theoretical analysis of the class-E amplifier by Mader [70] was reported in section 4.3. In the overview, it was shown that the advantages of class-E amplifier are high efficiency and simple circuit configuration. However, the major part of these past works was focused on narrow operating bandwidth. As such, an investigation on the parametric analysis of class-E bandwidth was necessary and was shown in section 4.4 and 4.5. This investigation, performed in ADS® simulation includes parameters such as switch-on resistance, duty cycle and Q factor of the load network. In the next chapter, an experimental study of broadband class-E PA is described and an improved design technique for broadband class-E PA will be presented together with its implementations

CHAPTER 5

BROADBAND HIGH-EFFICIENCY CLASS-E POWER AMPLIFIER

5.1 INTRODUCTION

This chapter will present the simulation and measured data for three broadband class-E RF/microwave amplifier designs. Both of the designs in this chapter are using a PHEMT device in a frequency range from 500 MHz to 2.2 GHz. The chapter will begin with the characterization of the P-HEMT device ATF-34143. A harmonic balance simulation software ADS® is used to predict the DC performance and the bias condition of the device which will be used in the class-E PA design. Followed by the first design of a class-E PA at 800 MHz, the design procedures are described in detail. Also included in this chapter is the design of broadband class-E PA at 2 GHz frequency band. Practical results with simulation values are compared and discussed. Finally, a novel technique of load network design is implemented to a broadband class-E PA design at 2 GHz. The method described in this work is simple and straightforward and realizable. This chapter concludes with the presentation of the

measured power, gain, and other figures of merit for the class-E prototype. Where appropriate, the measured results are compared with the simulations values.

5.2 DEVICE CHARACTERIZATION

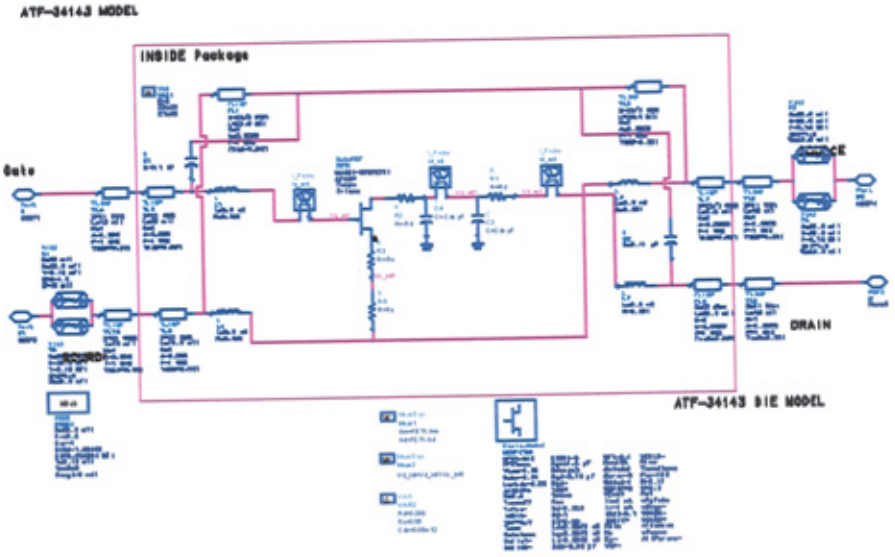

Figure 5.1: Large signal P-HEMT nonlinear device model (Agilent).

Transistor characterization is an important part of the power amplifier design process. An accurate transistor model provides a valuable resource for verification of the initial design and rapid design revision through computer simulation.

In this work, a nonlinear large signal model from Agilent, Figure 5.1, is used to characterize and model the small and large-signal behaviour of the packaged RF P-HEMT device. ADS® is used to perform DC and bias point simulations.

The complete simulation setup of the model with the ideal bias networks is shown in Figure 5.2. DC IV curves are simulated under the class-B bias condition. The simulated load line shown in Figure 5.3 confirms the correct bias condition.

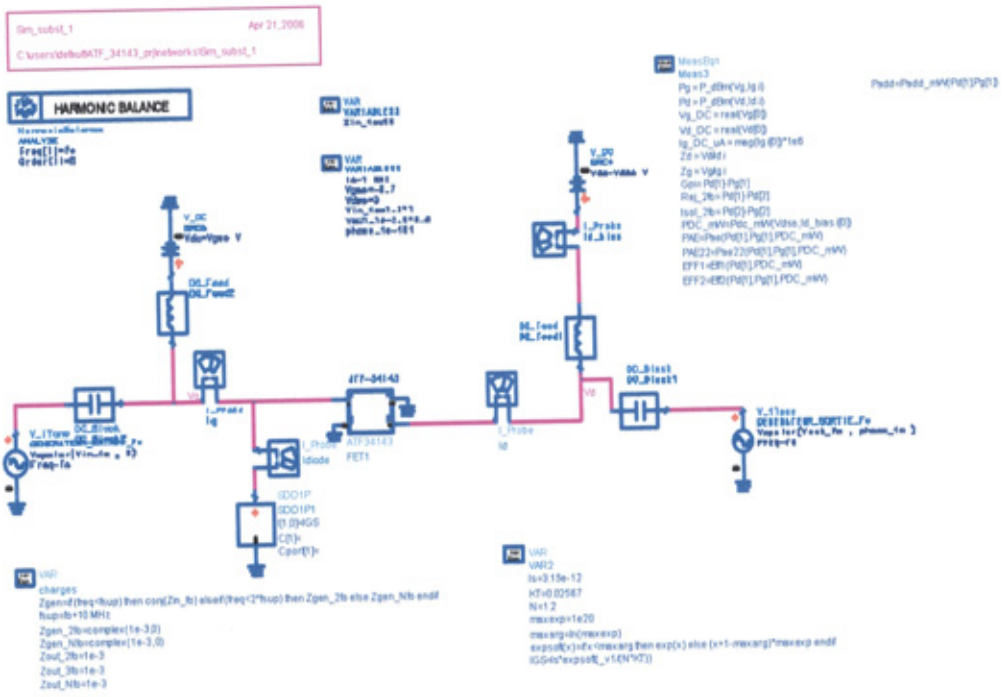

Figure 5.2: Simulation setup of the device characterization in ADS®. [68]

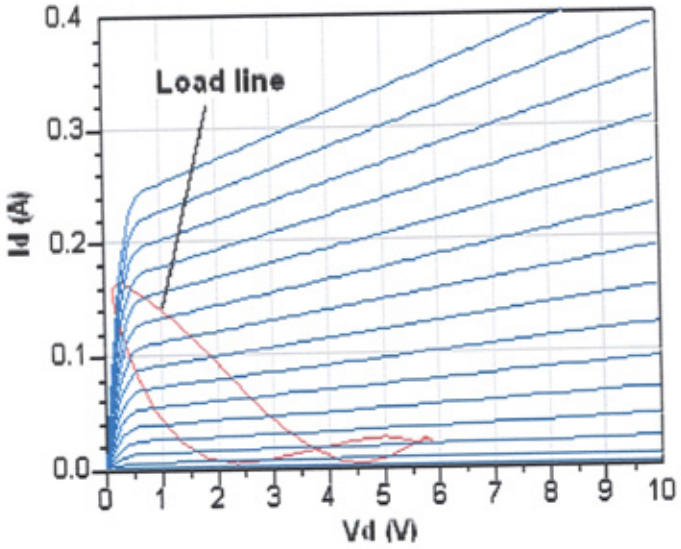

Figure 5.3: I V curves with intrinsic load lines (Class-B bias).

The simulated voltage and current waveforms are plotted in Figure 5.4. A high RF input power of 12 dBm is used to drive the transistor into saturation, which gives a 1 dB compression. The non-ideal displacement of the voltage and current waveforms verify the non-ideal class-E bias condition. The simulated results of both input and

output optimum impedance are shown in Table 5.1 together with the bias voltage.

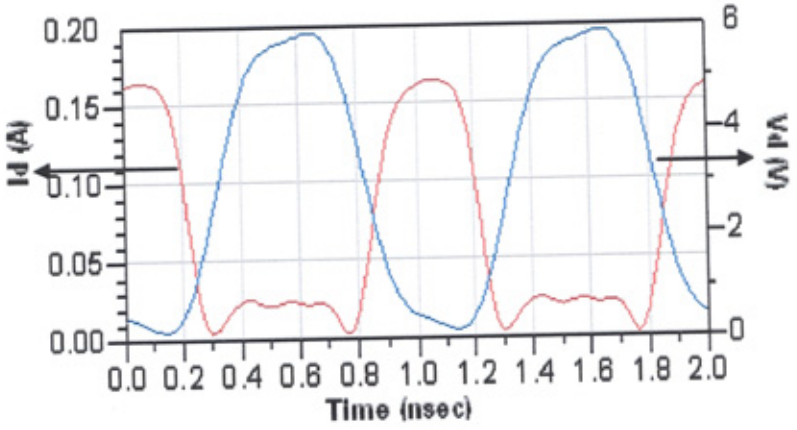

Figure 5.4: Drain current and voltage waveform with 1dB compression.

Both results are used as the initial values for the class-E PA designs in the following sections.

Parameters	Values
RF Frequency	1GHz
Gate Voltage Vg	-0.5V
DC Voltage Vd	3V
Zopt_load	4.2+16.8 j
Zopt_in	18-40.9j

Table 5.1 Simulated optimum input and output impedance of the device together with the bias voltage.

5.3 DESIGN OF BROADBAND CLASS-E PA AT 1 GHz

Most of the class E PAs use a series LC load network which results in limited

bandwidths. For example, a bandwidth of 10% over a 50% PAE is achieved in [71]. It has recently been reported that a T-transform circuit combined with an additional output-matching network can be used for an output load network in the class E PA design [72].

In this section, it will be shown that this T-transform circuit can also be used to achieve broadband operation. The study of class-E PA with a T-transform load network and practical implementation are then presented, together with the practical design.

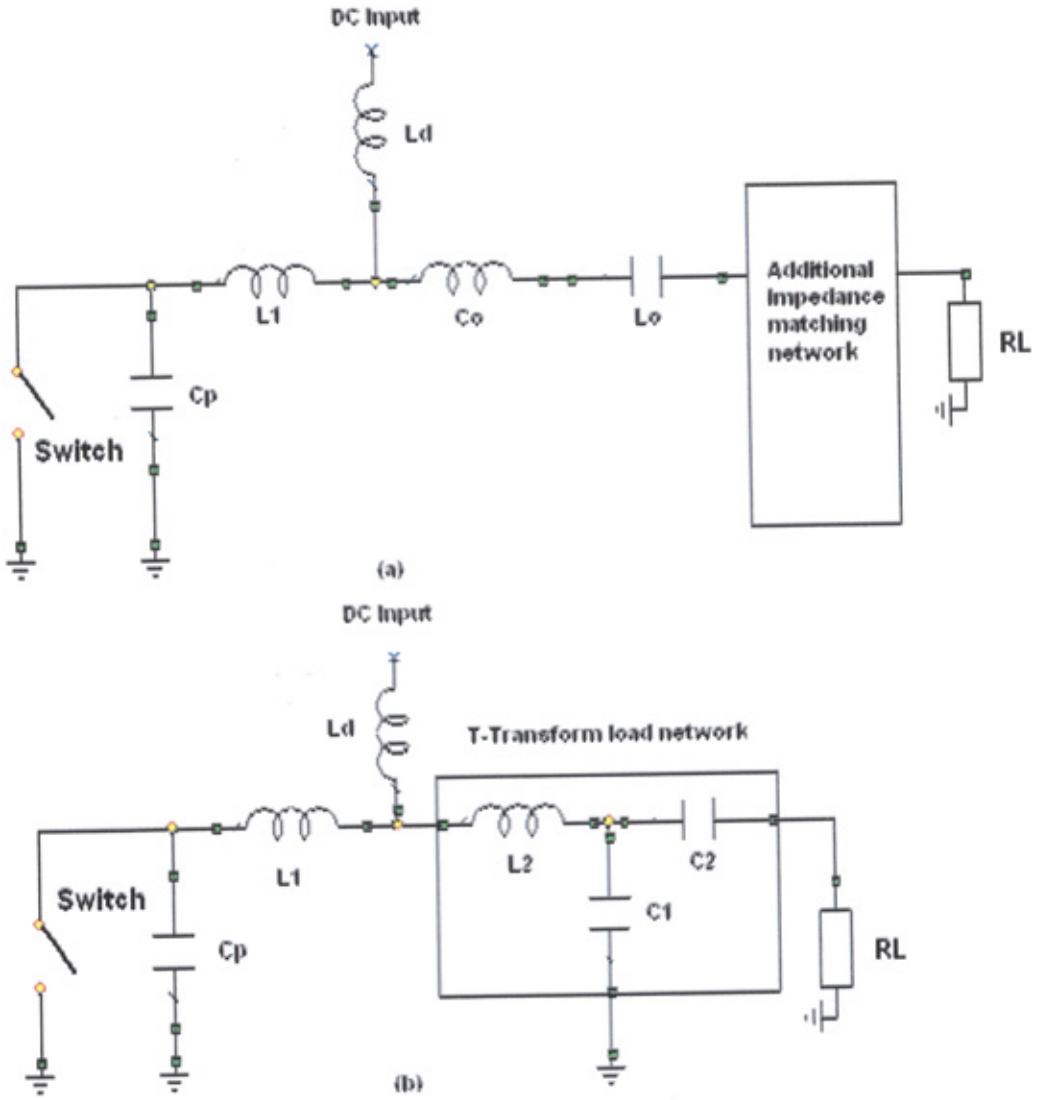

Figure 5.5 Class E switching PA with (a) series L-C load network, and (b) T-transform load network.

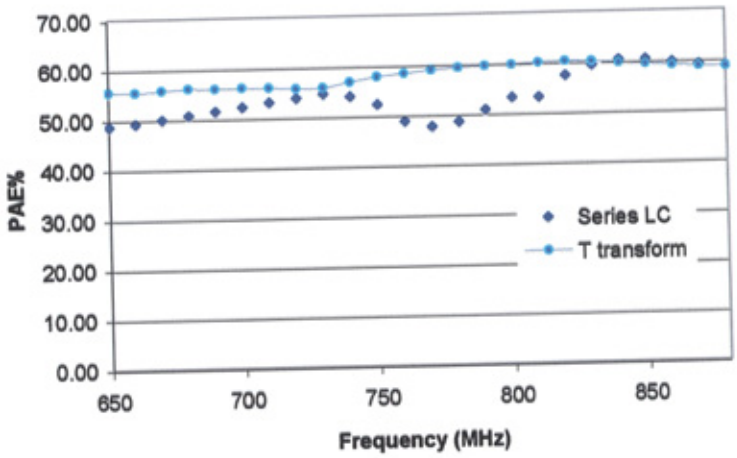

Figure 5.6 The comparison of simulated class E amplifier PAE versus frequency between series LC load and T-transform load network.

For class E amplifier, careful design of the load network is essential to maintain the switching performance of the amplifier. The original circuit topology of the class-E amplifier load network uses a series L-C combined with an additional impedance transformer as shown in Figure 5.5(a). It has been shown in [72] that this configuration has a limiting effect on the bandwidth. To overcome this, a three element T-transform load network, connected to the amplifier, as shown in Figure 5.5 (b) is used in this design. It consists of a series inductor L_2, a shunt capacitor C_1, and, a series blocking capacitor C_2. It is used for harmonic suppression, optimal impedance transform and DC blocking. Two class E amplifiers, one using the conventional series LC load and the other using T-transform load network, are simulated and compared. The initial values of the T transform are given by the following equations:

$$L_2 = \frac{k}{\omega^2 C_p}(\sin\theta + \cos\theta\sqrt{\frac{\omega C_p R_L}{k\cos\theta} - 1}) \qquad 5.1$$

$$C_1 = \frac{1}{\omega R_L}\sqrt{\frac{\omega C_p R_L}{k\cos\theta} - 1} \qquad 5.2$$

where, θ is the phase angle between input and output current.

Figure 5.6 shows the PAE frequency response of the two class E amplifiers, one is using a series *LC* load network and another one is using a T-transform circuit. The results demonstrate that using a T-transform circuit produces a much wider bandwidth of more than 45 %, with bandwidth defined as greater than a 50 % PAE. This is a significant improvement over the conventional series LC circuit with the bandwidth of less than 25 %.

5.3.1 DESIGN PROCEDURES

PA design requires accurate predictions of the device characteristics in order to achieve the best performance. The design procedures using an Advance Design System ADS® are given below:

1. DC operation point testing and bias network design: The bypass capacitors are shown in Figure 5.7. The values of capacitors are chosen to avoid oscillations at low frequencies, and are given in Table 5.2. In the practical design, due to the switching time effect the gate bias point has to be slightly moved from class B to class C.
2. Design input matching network and output matching network: The complex conjugate matching technique is using for designing the input matching network. Load pull simulation is used to transform the 50 Ω load to the optimal impedance value which can maximize the output power from this amplifier design. It gives the optimal load impedance value with which the device output should be terminated in order to give maximum PAE. The

parameters of the T-transform are optimized by this method.

3. Amplifier performance testing: The class-E amplifier has been simulated by using the harmonic balance method in ADS. Several parameters have been monitored, such as power added efficiency, power output, gain, and switching waveforms. The results in the next section demonstrate the accuracy of the simulation predictions. Instability, a major concern in the amplifier design, is caused by the positive feedback from the output port. This was tested in ADS to determine if unwanted oscillation occurs across the wide frequency range. The results show that this device is unstable at low frequencies such as below 1.5 GHz. Two resistors were used in the design and are shown in Figure 5.7. The optimal values and locations of the resistors have been carefully chosen in order to minimize the power losses in the resistors.
4. Conversion to transmission lines: To minimize the loss in the circuit, most of the passive lumped elements are replaced by low loss transmission lines. Two high-impedance quarter wave transmission lines are used as RF chokes, as shown in Figure 5.7. The dimensions of the transmission lines are given in Table 5.2.
5. Whole circuit simulation and optimization: This simulation takes into account the loss in the substrate and effect of grounding and via holes. Figure 5.8 shows the simulation results of the drain voltage and current waveforms.

The final circuit was fabricated using Duroid Rogers 5880 with a dielectric constant of 2.33 and thickness of 0.79 mm.

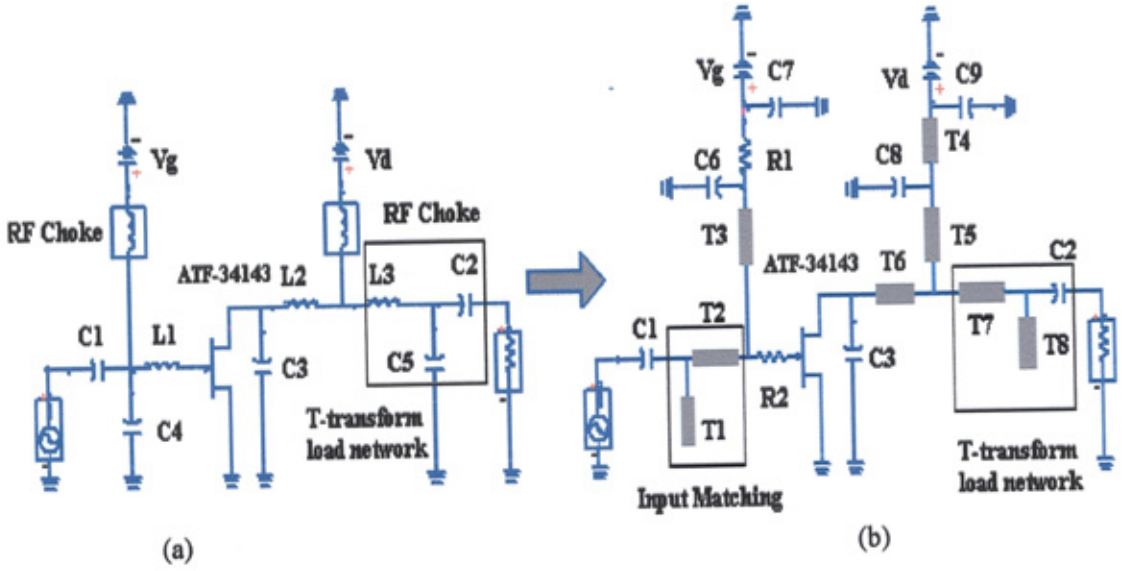

Figure 5.7 Schematic of the class E amplifier with (a) lumped elements, and (b) transmission line.

Parameters	Values	Parameters	Values
C_1	100 pF	L_3	3.3 nH
C_2	100 pF	R_1	20 Ω
C_3	3.9 pF	R_2	30 Ω
C_4	100 pF	$T_{1(mm)}$	L=6.4, W=4.77
C_5	10 pF	$T_{2(mm)}$	L=21.89, W=0.98
C_6	22 pF	$T_{3(mm)}$	L=67.1, W=0.67
C_7	100 pF	$T_{4(mm)}$	L=3, W=0.67
C_8	0.5 pF	$T_{5(mm)}$	L=67.1, W=0.67
C_9	0.23 pF	$T_{6(mm)}$	L=15, W=0.8
L_1	12 nH	$T_{7(mm)}$	L=8.05, W=1.37
L_2	4.7 nH	$T_{8(mm)}$	L=21.67, W=4.39

Table 5.2 Component values and the transmission line dimensions of the class E amplifier

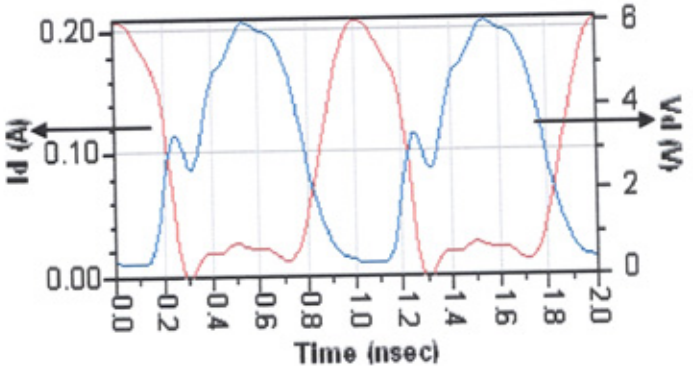

Figure 5.8 Simulated drain voltage and current waveforms for the class E operation.

5.3.2 EXPERIMENTAL RESULTS AND DISCUSSIONS

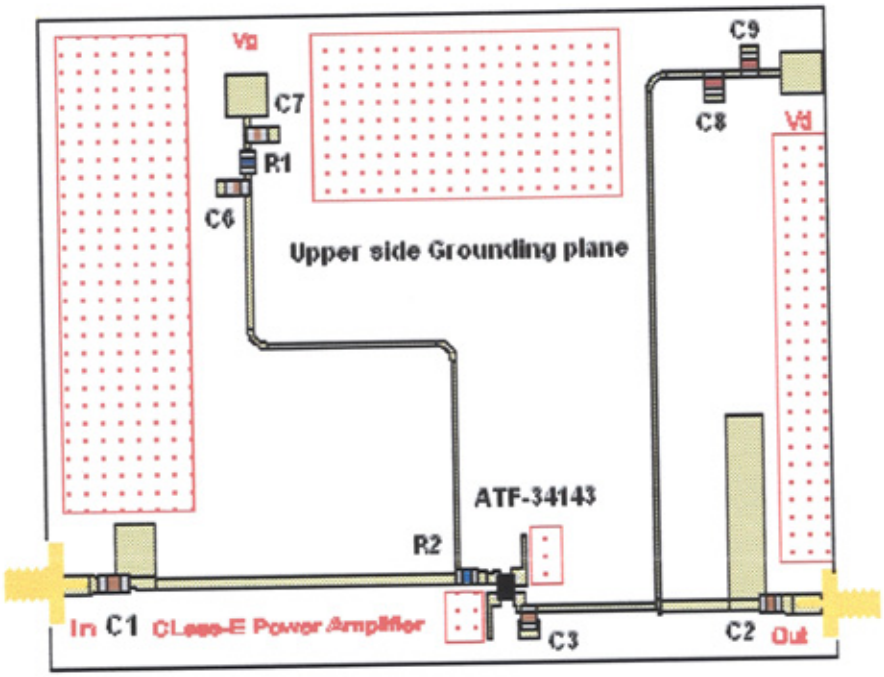

(a)

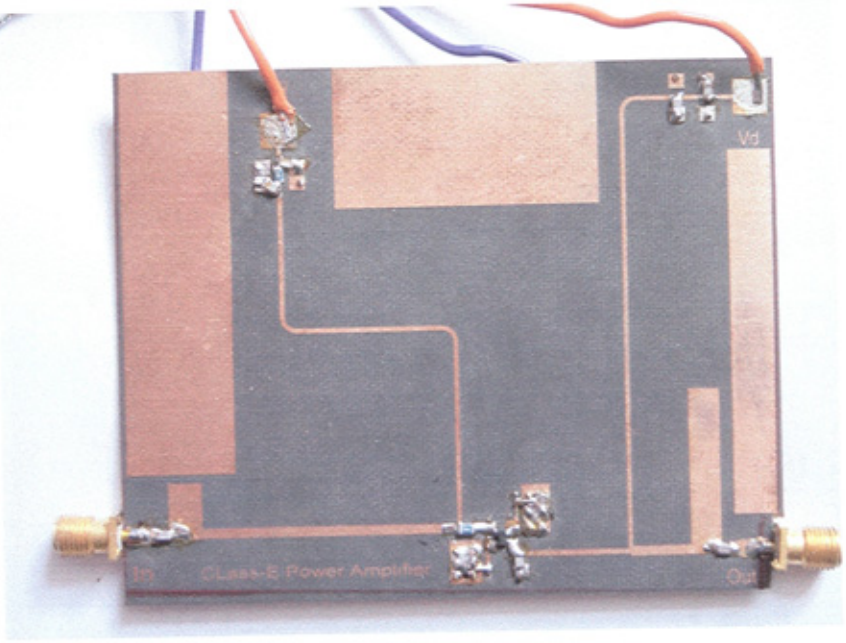

(b)

Figure 5.9 (a) Broadband class-E amplifier circuit layout, and (b) photograph of class-E PA design.

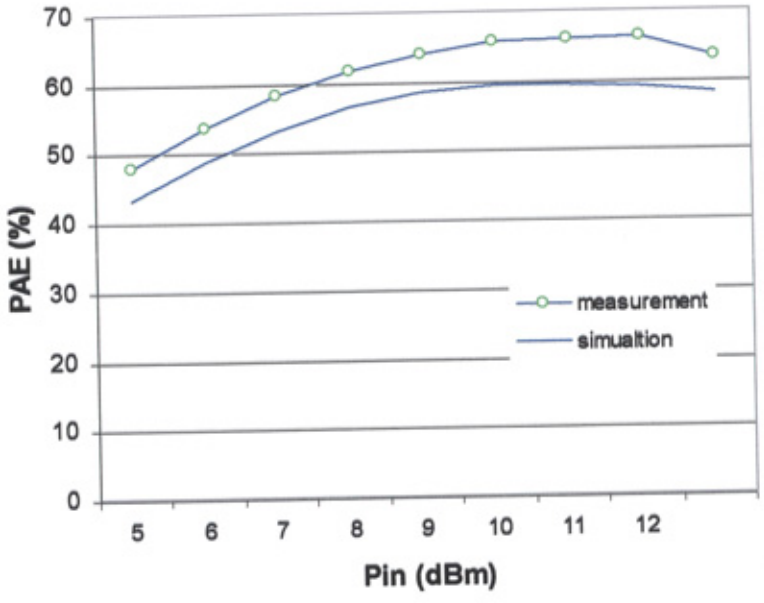

Figure 5.10 The comparison of simulated and measured PAE as function of input power

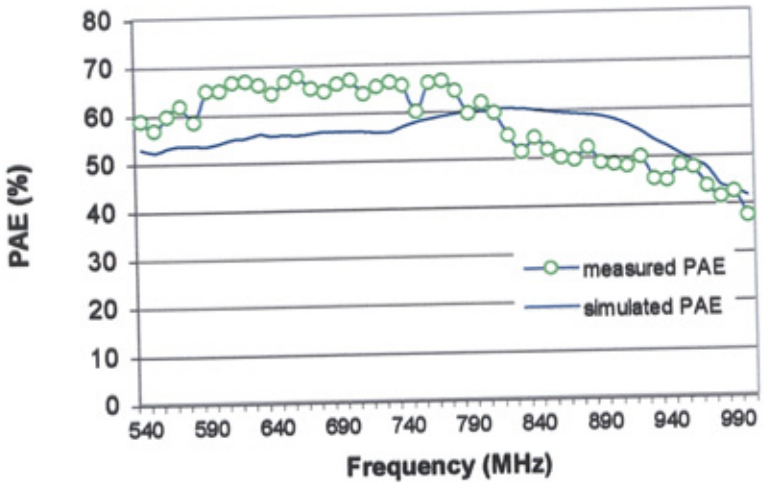

Figure 5.11 The comparison of simulated and measured PAE as function of frequency.

The layout and photograph of the design is shown in Figures 5.9 (a) & (b). The device is biased at V_d= 3 V and V_g= -0.7 V. Figure 5.10 shows the comparison between simulated and measured PAE against the RF input power. Good agreement is achieved. The small difference is mainly due to less drain current being drawn in the practical measurement. The simulated and measured PAE for this design are plotted in Figure 5.11 as a function of frequency. Good agreement is observed. The maximum PAE of 66.5 % is measured at 750 MHz with 22.7 dBm output power at RF input power of 12 dBm. The results show that T-transform circuit design gives an operational performance with a wide bandwidth coupled with a high efficiency for a class E amplifier.

5.3.3 DISCUSSION

A broadband high efficiency class-E PA is designed. It uses both transmission lines and lumped elements. The design methodology is described. A low cost PHEMT device is used and the simulation is complete using software ADS®. Design equations are applied to the design of the class-E power amplifier with a T-transform

output load network. The amplifier achieves a PAE above 50 %, within a frequency range between 540 MHz and 890 MHz. A peak PAE of 66.5 % is obtained at 740 MHz with an output power of 22.7 dBm.

5.4 DESIGN OF CLASS-E PA AT 2 GHz

The design of a broadband high efficiency class-E PA for use in wireless communication systems is presented in this section. The same P-HEMT device is employed to enhance both efficiency and bandwidth performance. The design has been investigated experimentally and simulated using the harmonic balance method in the Advance Design System (ADS®). Figure 5.12 shows the circuit diagram of designed class-E PA.

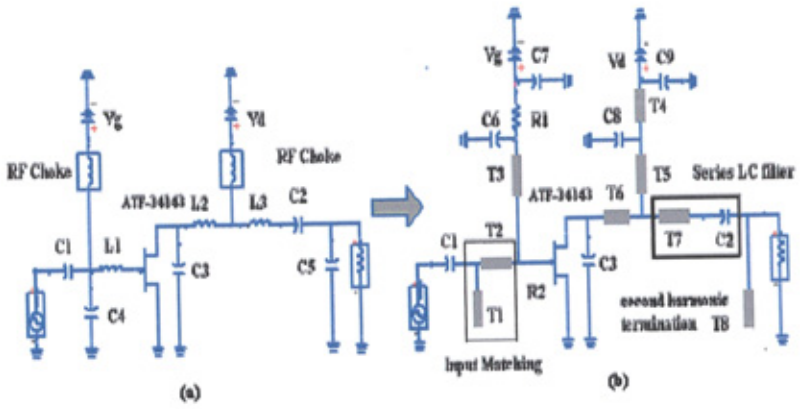

Figure 5.12 Schematic of the class E amplifier with (a) lumped elements, and (b) transmission line

5.4.1 EXPERIMENTAL RESULTS AND DISCUSSIONS

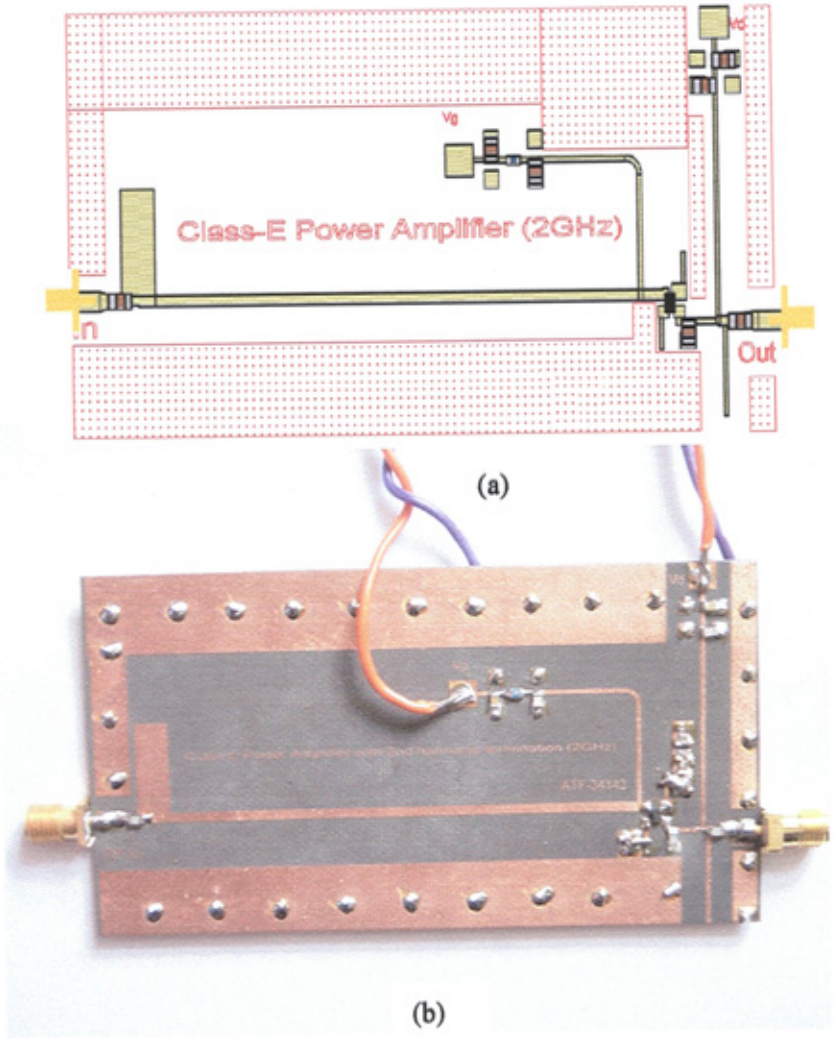

Figure 5.13 (a) Broadband class-E amplifier circuit layout, and (b) photograph.

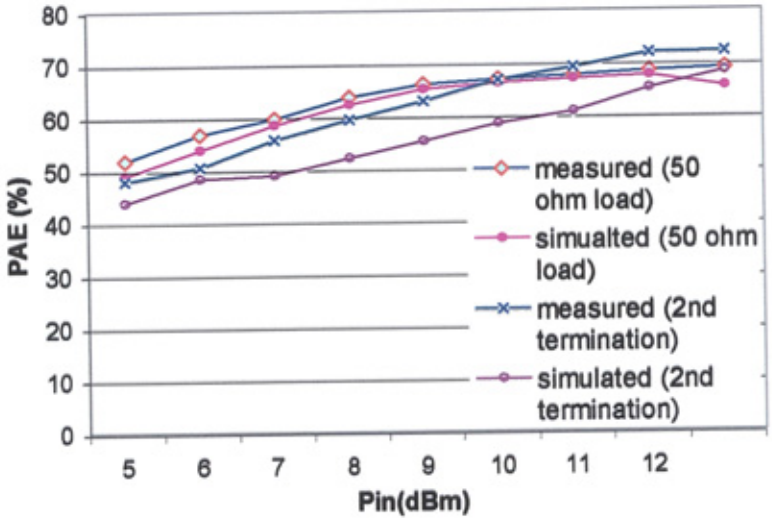
80
70
60
50
40
30
20
10
0
PAE (%)
5
6
7
8
9
10
11
12
Pin(dBm)
measured (50 ohm load)
simualted (50 ohm load)
measured (2nd termination)
simulated (2nd termination)

(a)

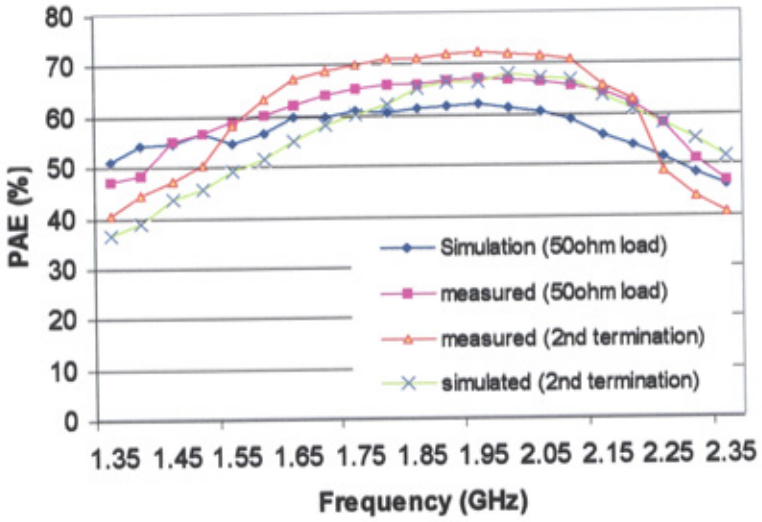
80
70
60
50
40
30
20
10
0
PAE (%)
1.35 1.45 1.55 1.65 1.75 1.85 1.95 2.05 2.15 2.25 2.35
Frequency (GHz)
Simulation (50ohm load)
measured (50ohm load)
measured (2nd termination)
simulated (2nd termination)

(b)

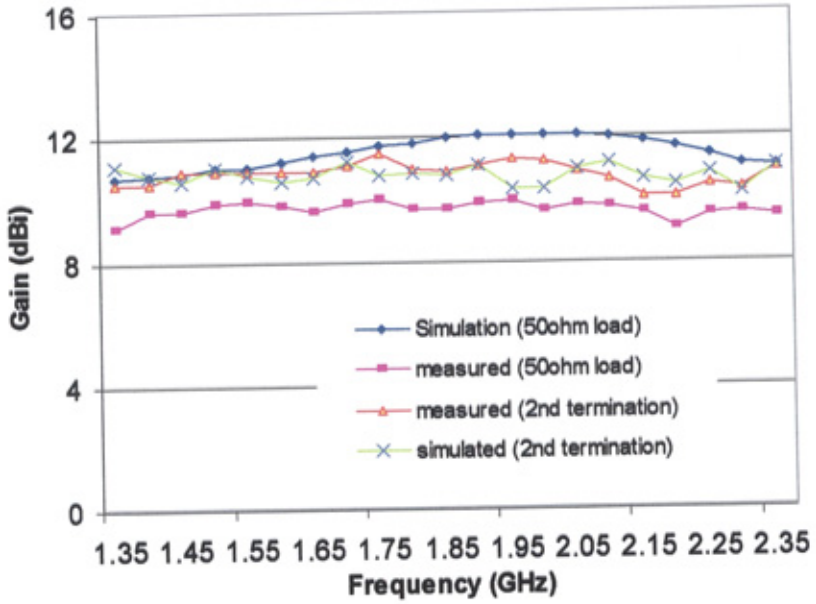

(c)

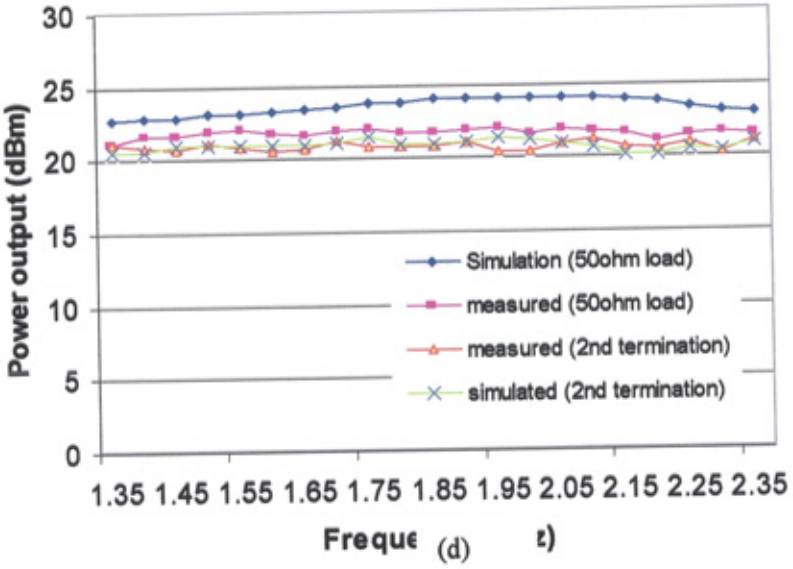

(d)

Figure 5.14 The comparison of simulated and measured results for both designs with and without 2nd harmonic termination circuit.
(a)PAE as function of RF input power.
(b) PAE as function of frequency (12 dBm RF input).
(c) Gain as function of frequency (12 dBm RF input).
(d) Power output as function of frequency (12 dBm RF input).

The layout and photograph of the enhanced design is shown in Figure 5.13 (a) and (b). The device is biased at V_d= 3 V and V_g= -0.7 V. The results for both designs are shown in Figure 5.14. Figure 5.14 (a) shows the comparison between the simulated and measured PAE against the RF input power. Close agreement is achieved. The small difference is mainly due to less drain current being drawn in the practical measurement. The simulated and measured PAE for this design are plotted in Figure 5.14 (b) as function of frequency. Good agreement is observed. The peak PAE of 72.1 % is measured at 1.95 GHz with 22.8 dBm output power and with an RF input power of 12 dBm. This result is obtained using the design with a 2^{nd} harmonic termination load. Figures 5.14 (c) and 5.14 (d) shows good agreement between the measured and simulated output power and gain versus frequency from 1.52 GHz to 2.16 GHz, where the bandwidth produced was as wide as 37 %. The results show that the design gives an operational performance with a wide bandwidth coupled with high efficiency for a class E amplifier

5.4.2. DISCUSSION

A broadband high efficiency class-E PA is designed. It uses both transmission lines and lumped elements. The design methodology is described. A low cost PHEMT device is used and the simulation is done by software ADS®. Design equations are applied to the design of the class-E power amplifier. A second harmonic termination circuit is used in the enhanced design. This amplifier achieved a PAE above 50 %, within a frequency range between 1.52 GHz and 2.16 GHz. A peak PAE of 72.1 % is obtained at 1.95 GHz with an output power of 22.8 dBm.

5.5 IMPROVED DESIGN TECHNIQUE OF A BROADBAND CLASS-E POWER AMPLIFIER AT 2 GHz

5.5.1 INTRODUCTION

In class-E PA design, a high Q resonator is required to terminate all the unwanted harmonics in order to achieve a high efficiency. Unfortunately, it is extremely hard to find such high Q resonator in a high frequency band practically. The load network design for class-E PA is crucial and important since it maintains the switching voltage and current waveforms and terminates unwanted harmonics. Furthermore, RF design engineers need to compromise high efficiency and broadband width performance in order to suit new generation mobile communication.

Recent works of broadband class-E PA have been reported in [71] and [72]. In this section, we propose and demonstrate an improved design method. To obtain optimized class-E operation in a reasonable frequency bandwidth, a computational CAD method for output matching network is established first time. Unlike the conventional CAD method optimization techniques, this method takes into account the unwanted harmonics rejection and utilizes the simulated data from large signal simulation software in order to give the optimized practical design solution. The improved design technique gives the optimum circuit parameters for the class E power amplifier matching networks in order to maximize the PAE within a wide frequency bandwidth. To obtain optimized class-E operation in a reasonable frequency bandwidth, a numerical method to calculate the optimum values of the output matching network elements is established. Non-linear simulations using the harmonic balance analysis confirm the validity of the approach.

5.5.2 THEORETICAL DESIGN TECHNIQUE

From the analysis done by T. Mader [70], the optimum impedance at the output capacitance is found to be:

$$Z_{opt} = \frac{V_{S1}}{i_{S1}} = \frac{0.28015}{\omega_s C_S} e^{j49.0524°} \qquad 5.3$$

The real and imaginary parts of optimum impedance obtained from equation 5.3 are plotted in Fig. 5.15 over a broad frequency range from 1 GHz to 3 GHz. In order to achieve broadband class-E operation, the input impedance of the load network should agree with the optimum impedance.

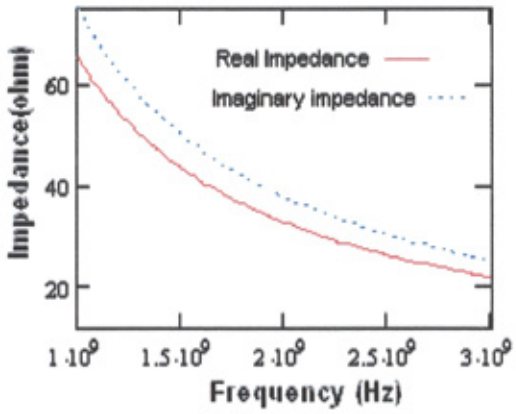

Figure 5.15 Optimum fundamental output impedance of Class-E power amplifier vs. frequency

An improved design technique for the class-E PA is shown in the following section. A CAD method in MathCAD is developed to verify this analytical approach. Excellent agreements are obtained.

5.5.3 IMPROVED DESIGN METHODOLOGY FOR CLASS-E PA

In order to achieve a broad bandwidth Class-E mode operation, a load network

providing the correct load impedance over the bandwidth of operation is required (Fig. 5.15). The proposed load network configuration using lumped elements is shown Fig. 5.16(a). It consists of a series DC blocking capacitor C_2 followed by a series inductor L_2. A parallel tuned circuit is attached at the node connecting with the 50Ω load R_L.

In order to obtain the optimized solution from the given circuit configuration, we need to find out the minimum difference between the calculated optimum impedance Z_{OPT} and the actual impedance obtained Z_{IN} over the frequency bandwidth f_1 to f_2. This is performed by minimizing the error function given by:

$$\int_{f1}^{f2} |Z_{OPT}(f) - Z_{IN}(f)| df = I(L_2, f_o) \qquad 5.4$$

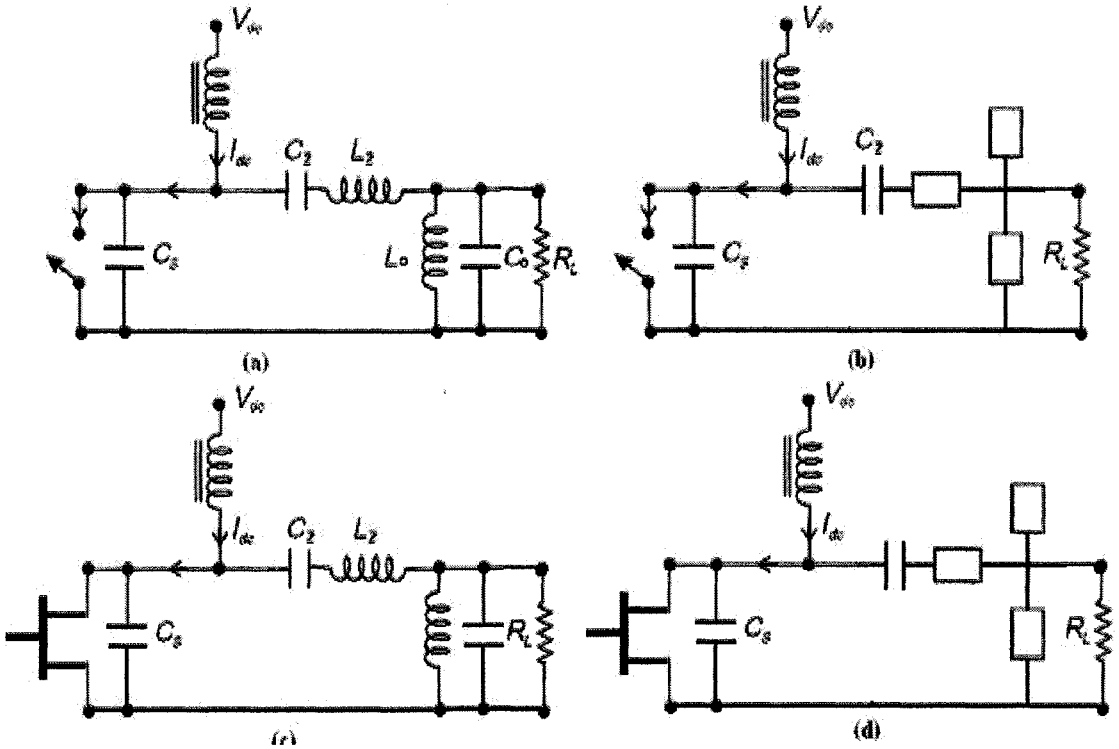

Figure 5.16 Proposed circuit diagram of Class-E PA (a) switch model with lumped elements, (b) switch model with transmission lines, (c) transistor model with lumped elements, and (d) transistor model with transmission lines.

$$Z_{OPT}(f) = a(f) + jb(f) = \frac{0.28015}{2\pi f C_S} e^{j49.0524^o} \qquad 5.5$$

$$Z_{IN}(f) = c(f) + jd(f) = \frac{1}{\frac{1}{R_L} + \frac{1}{R_L} Q^2 (\frac{2\pi f}{2\pi f_o} - \frac{2\pi f_o}{2\pi f})^2} + j(2\pi f L_2 - \frac{Q(\frac{2\pi f}{2\pi f_o} - \frac{2\pi f_o}{2\pi f})}{\frac{1}{R_L} + Q^2 \frac{1}{R_L} (\frac{2\pi f}{2\pi f_o} - \frac{2\pi f_o}{2\pi f})^2})$$

5.6

f_o is defined as the resonant frequency of the parallel tuned circuit. Q is defined as the quality factor of the load network.

At a frequency $f = f_1$ we measure the difference between Z_{IN} and Z_{OPT} by using $|Z_{OPT} - Z_{IN}|$.

Measuring this difference over the bandwidth $f_1 \le f \le f_2$ and summing the results given by the integral expression:

$$\int_{f1}^{f2} |Z_{OPT}(f) - Z_{IN}(f)| df = I(L_2, f_o) \qquad 5.7$$

In order to integrate this equation, the composite trapezoidal rule is used to solve it numerically

$$f(L_a, f_o) = \int_{f1}^{fn} |Z_{in}(f) - Z_{opt}(f)| df = \frac{h}{2} \times$$

$$\left[|Z_{in}(f_1) - Z_{opt}(f_1)| + |Z_{in}(f_n) - Z_{opt}(f_n)| + 2\sum_{j=1}^{n-1} |Z_{in}(f_j) - Z_{opt}(f_j)| \right]$$

$$- \frac{(f_n - f_1)h^2}{12} f''(\mu) \qquad 5.8$$

Where $Z_{in}(f)$ can be simplified as equation 5.9 since Q, Cs and R_L are given.

$$Zin(f) = \frac{1}{0.02 + 0.08(\frac{f}{f_o} - \frac{f_o}{f})^2} + j(6.28fL_2 - \frac{2(\frac{f}{f_o} - \frac{f_o}{f})}{0.02 + 0.08(\frac{f}{f_o} - \frac{f_o}{f})^2}) \quad 5.9$$

$$Zopt(f) = \frac{7.3\times10^{10}}{f} + j\frac{8.4\times10^{10}}{f} \quad 5.10$$

Evaluating this integral will give us a function $I(L_2, f_o)$ of the parameters L_2 and f_o. $I(L_2, f_o)$ is a measure of the difference between Z_{in} and Z_{opt}. We want the value of L_2 and f_o for this is a minimum. The minima occur at:

$$\begin{cases} \frac{\partial I(L_2, f_o)}{\partial L_2} = 0 \\ \frac{\partial I(L_2, f_o)}{\partial f_o} = 0 \end{cases} \Rightarrow \begin{Bmatrix} L_2 \\ f_o \end{Bmatrix} \quad 5.11$$

$$L_o = \frac{1}{2\pi f_o QG} \quad 5.12$$

$$C_o = \frac{QG}{2\pi f_o} \quad 5.13$$

The problem is solved numerically using the composite trapezoidal rule. After the minimum of the error function is determined, the optimum load network component values are calculated. For a centre frequency of 2GHz, the following values were obtained: L_2=4.17 nH, L_0=2.92 nH, C_0=2.42 pF and a value of 10 pF was chosen for C_2.

The results are verified by using a CAD method in MathCAD® by plotting a matrix of error function. The matrix of error is obtained by the absolute value of the error function (5.14). This CAD method can generate the error function showing the optimum and actual value of each data point for function with two independent

variables, L_2 and f_o.

$$|error(L_2, f_o)| = |Z_{in}(L_2, f_o) - Z_{opt}(L_2, f_o)| \qquad 5.14$$

There are m steps of f_o over the frequency range from 1.5 to 10 GHz and n steps of L_2 from 0.01 nH to 100 nH.

$$f_{o\_1} \quad f_{o\_2} \quad \cdots\cdots\cdots\cdots \quad f_{o\_m}$$

$$\begin{matrix} L_{2\_1} \\ L_{2\_2} \\ \cdot \\ L_{2\_n} \end{matrix}$$

$$|error(L_2, f_o)|_{m,n} = \begin{Bmatrix} |error|_{1,1} & \cdots\cdots & |error|_{m,1} \\ \cdot & \cdots\cdots & \cdot \\ |error|_{1,n} & \cdots\cdots & |error|_{m,n} \end{Bmatrix} \qquad 5.15$$

The optimum solutions of L_2 and f_o can be obtained by finding the minimum result of the error function contour plot as shown in Figure 5.17. Very similar results are obtained by this CAD method: L_2 = 4.4 nH, L_0 = 2.67 nH, C_0 = 3.47 pF with a same value of C_2 = 10 pF. Figure 5.18 shows the input impedance curves resulted by this CAD method is compared with the previously described numerical method.

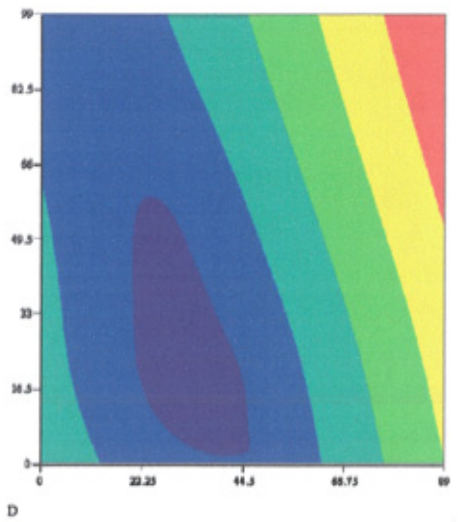

Figure 5.17 Contour plot of error function (5.14) in MathCAD®.

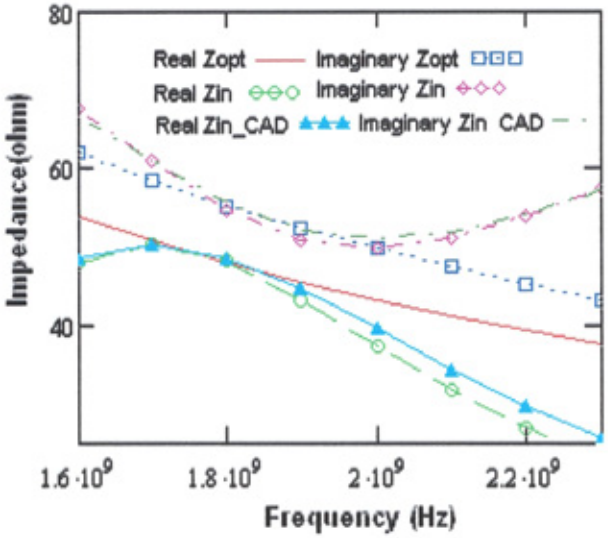

Figure 5.18 Comparison between Zopt and Calculated Zin

Figure 5.18 shows the comparison between calculated Zin and Zopt. A very good agreement between the input impedance of the designed load network and the desired optimum impedance over a wide bandwidth is obtained by this improved design method and CAD method. The difference between improved numerical method and CAD method is due to the approximation of the composite trapezoidal rule.

Based on these optimum values, the output network is then converted to the microstrip equivalent represented in Figures 5.16 (c) & (d). The drain efficiencies obtained for the circuits Figures5.16 (a) and (b) are plotted Figure 5.19 (a).

To validate this result, load-pull simulations including the output networks of circuits Figure 5.16(a) and (b) and a switch model for the transistor were performed

using the harmonic balance method to determine the optimum output impedances over the frequency band. Excellent agreement is obtained with the previously determined optimum impedances (Figure 5.19(b)). Moreover, the results remain in reasonable agreement when the ideal switch model is replaced by a full non-linear transistor model.

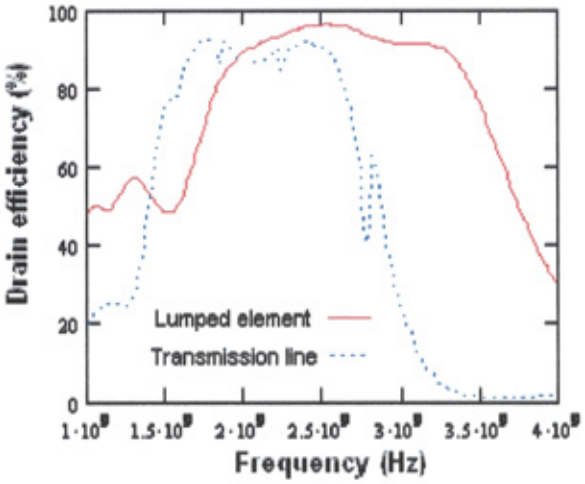

(a)

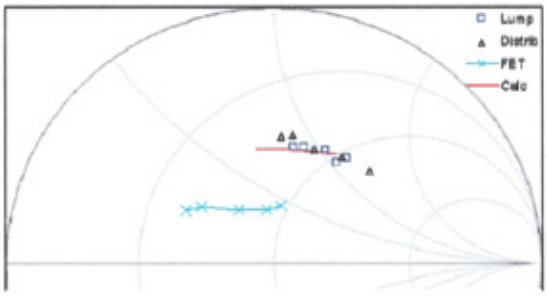

(b)

Figure 5.19 (a) Calculated drain efficiencies using lumped elements and microstrip line configurations (b) Representation of calculated and simulated optimum impedances.

5.5.4 PRACTICAL IMPLEMENTATION

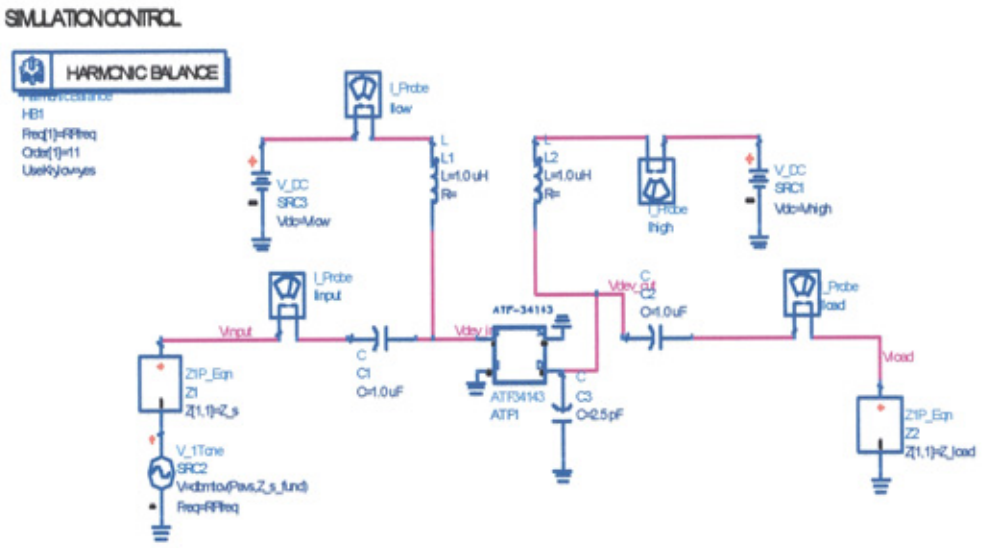

Figure 5.20 Harmonic simulation setup in ADS for load-pull and source-pull.

In the practical design of class-E PA, due to the intrinsic active device behaviour, the large signal simulation is used to obtain the optimum source and load impedance under class-E mode operation. In this design a medium power PHEMT device ATF-34143 from Agilent Technologies® is chosen to achieve object frequency and output power as well as high efficiency and broad bandwidth. A nonlinear modelling of the transistor is simulated using Harmonics balance simulation software and ADS is used to determine the optimum source and load impedance under the Class-E operation condition.

The setup of this simulation is shown in Figure 5.20. The principle of this simulation is to obtain the optimum source and load impedance at the fundamental design frequency for a maximum PAE with the class-E operation condition, which is an open circuit for higher harmonics at the load. Two impedance tuners are placed at the source and load of the device. During the simulation process, two impedance tuners are simultaneously tuning the fundamental source and load impedance which is

defined in ADS.

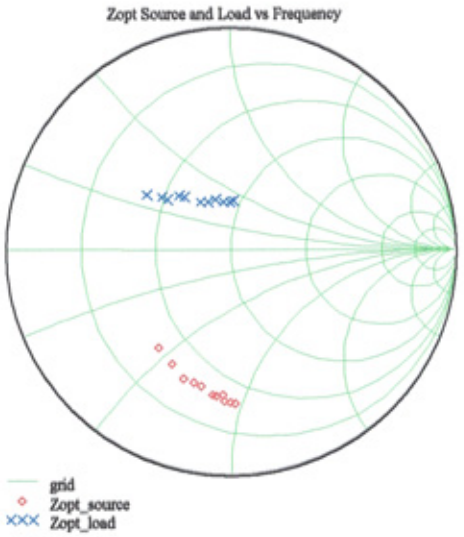

Figure 5.21 Simulated contours of source and load impedance.

Frequency (GHz)	Optimum Zsource	Optimum Zload	Drain efficiency(%)
1.5	18.2-22.6j	46.66+21.46j	50.1
1.6	18.3-27.7j	45.36+20.37j	57.6
1.7	17.6-32.2j	43.0+19.5j	63.52
1.8	18.1-34.7j	39.9+18.9j	68.91
1.9	19.56-36.8j	37.56+17.2j	73.2
2	18-40.9j	35.2+16.1j	75.6
2.1	18.1-41.8j	30.1+15.8j	72.97
2.2	19.5-43.2j	28.5+15.3j	67.26
2.3	18.0-44.5j	26.0+13.5j	62.37
2.4	18.5-16.4j	24.15+13.48	60.83
2.5	18.4-47.9j	20.62+12.62j	52.1

Table 5.3 Simulated source and load impedance

Optimum source and load impedance contours from the simulation are shown in Figure 5.21. Sample values from these results are given in Table 5.3. The load impedance values were then used to obtain the values of the matching network elements.

As is seen in Table 5.3, Zsource nearly independent of the frequency and consequently a simple L-C matching network was used at the source.

Using the previously calculated component values as a starting point for the output network, a broadband Class-E PA was designed using a low-cost medium power packaged PHEMT transistor. The design was further optimized using the methodologies presented in previous section.

The circuit diagram is shown Figure 5.22(a) and the photo of the fabricated circuit in PCB technology is shown Figure 5.22(b). Excellent results are observed. A peak PAE of 82.1 % is measured at 1.99 GHz (Figure 5.22(c)) with 22.8 dBm output power for 12 dBm RF input power (Figure 5.22(d)). Figure 5.22(c) shows that the resulting bandwidth for PAE greater than 60 % is more than 12 %. The bandwidth could be further improved by decreasing the input matching losses, as the PAE performance is limited by the relatively low gain of the device used. The results nevertheless show an operational high-efficiency performance coupled with a wide bandwidth for a Class-E amplifier.

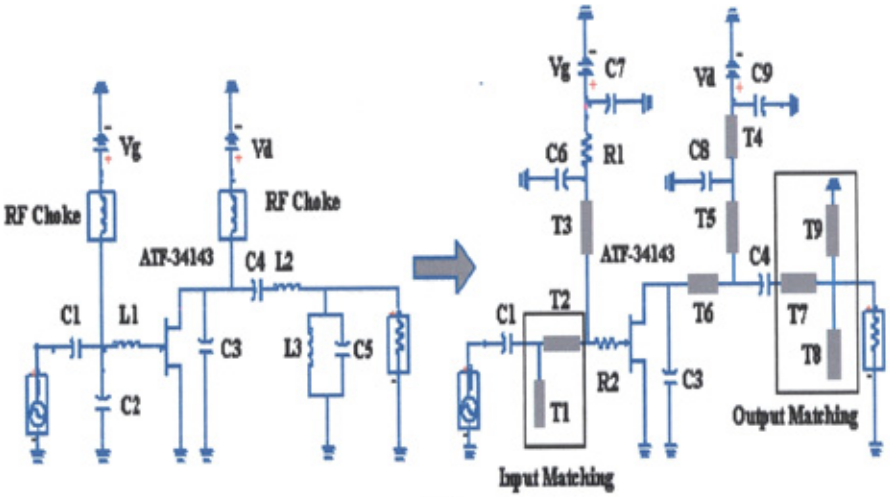
Vg
Vd
RF Choke
RF Choke
ATF-34143
C4 L2
C1
L1
C3
L3
C5
C2
Vg
C7
Vd
C9
C6
R1
C8
T4
T3
T5
T9
ATF-34143
C4
T2
C1
T6
T7
T8
R2
C3
T1
Output Matching
Input Matching

(a)

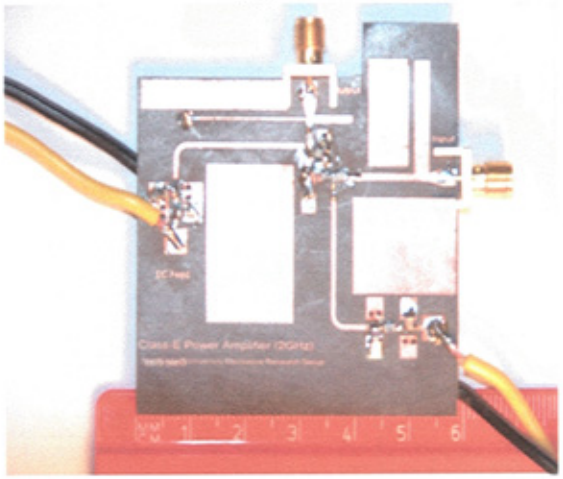

(b)

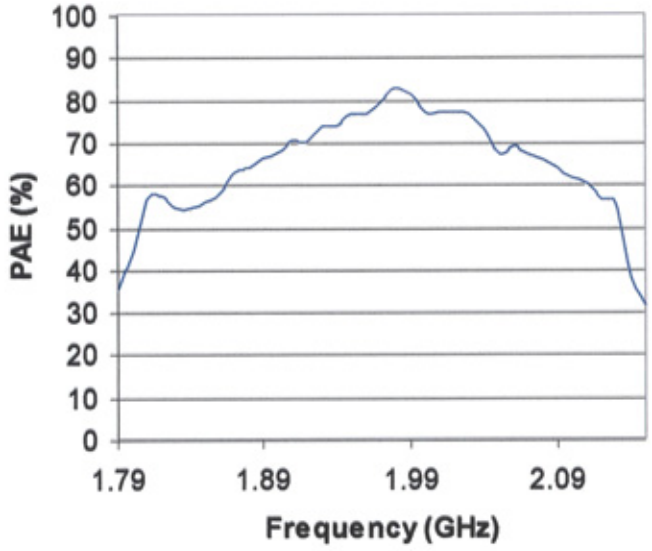
100
90
80
70
60
50
40
30
20
10
0
PAE (%)
1.79
1.89
1.99
2.09
Frequency (GHz)

(c)

(d)

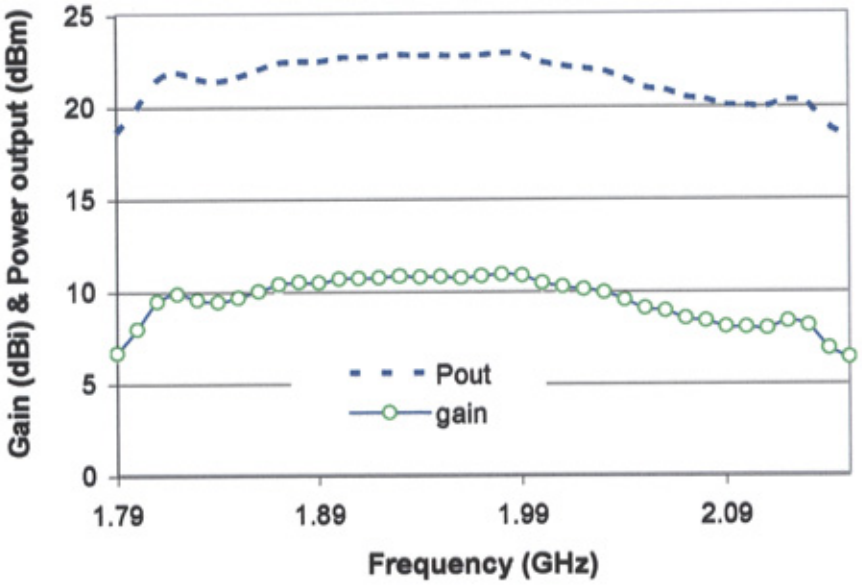

Figure 5.22 (a) Proposed circuit diagram of Class-E PA, and (b) the photo of broadband Class-E PA design.

(c) Measured result of PAE vs. frequency. (d) Measured gain and output power.

5.5.5 DISCUSSION

The analysis and design methodology of a broadband, high-efficiency class-E power amplifier has been presented. The method is based on the determination of the optimum output network component's values for broadband Class-E operation. The optimum output impedance results obtained were confirmed by load-pull simulations at different frequencies taking into account the output network. A practical amplifier designed using the presented methodology was fabricated achieving a PAE above 60% between 1.73 GHz and 2.16 GHz. A peak PAE of 82.1 % is obtained at 1.99 GHz with an output power of 22.8dBm, thus demonstrating the validity of this approach.

5.6 SUMMARY

Previous chapters had highlighted a lack of significant work on the broadband high efficiency class-E PA design. In this chapter, two experimental studies were performed to compromise the trade-off between efficiency and bandwidth at different frequencies. A PAE greater than 50% was achieved by the first design within the frequency range between 540 MHz and 890 MHz. The second design achieved a PAE above 50%, within a frequency range between 1.52 GHz and 2.16 GHz. In the following section, this knowledge gap was fully addressed by an improved design technique of broadband class-E PA load network. A practical amplifier designed using this methodology was fabricated achieving a PAE above 60% between 1.73GHz and 2.16GHz. To realize compact broadband high efficiency RF Front-End, AIA will be needed, where high efficiency class-E RF PA will be integrated with broadband antenna. The present and previous works on AIA are reviewed in the next chapter, followed by the designs of broadband high efficiency AIA and array.

CHAPTER 6

A Review of Active Integrated Antennas

6.1 Introduction

The terms "active antenna" or "integrated antenna" are known as a radiation structure with an active device embedded in or located close by [6-9]. This means the radiating element can be integrated very closely with the power source or head amplifier. It is most appropriate when the active component is coupled directly to the element without any internal matching circuit or connection cables. AIA has become an area of growing interested in recent years due to the rapid developments in microwave integrated circuit technology. The idea of using active antennas can be traced back to as early as 1928 [4]. A small antenna with electron tube was commonly used in radio broadcast receivers using frequencies around 1 MHz at that time. In 1960's and 1970's, due to the invention of high frequency transistors, the study of active antennas received much attention and several pioneering works were reported

[1, 2]. The implementation of active devices in passive radiating elements shows several advantages:

- Increasing the over all efficiency
- Reduce the over all size
- Increasing the bandwidth
- Decreasing the mutual coupling between array elements
- Improving the noise factor.

These advantages helped improve the antenna performance and made the research of active antennas popular at that time.

In this chapter, a general review of AIA is carried out. Starting from the classification of AIA, the structures and functions of different AIA types are reviewed. In addition to experimental achievements, recent developments in the high efficiency active integrated antenna are reviewed.

6.2 Classifications of Active Antennas

The active integrated antenna can be classified by the function of the active device into which the antenna is integrated. A general definition covering a variety of semiconductors is used here. By this definition, the active component is the device which can be used for amplification, rectification, or to change energy from one to another. Therefore, the active integrated antenna can be classified into three different types, named as the oscillator type, amplifier type, and the frequency converting type. The previous works of these three types of AIA are discussed in the next section.

6.2.1 Oscillator Type

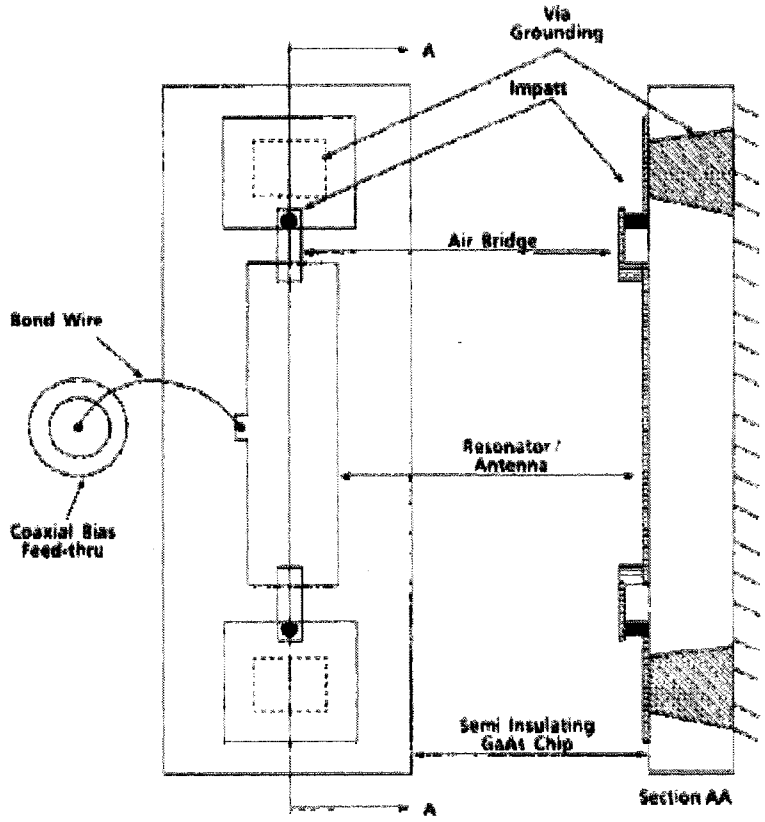

Figure 6.1: A schematic drawing of the monolithic resonator/antenna structure [74].

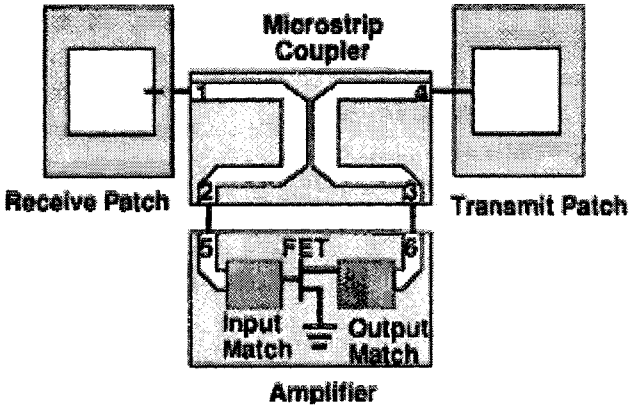

Figure 6.2: Schematic of a two-port quasi-optical oscillator [75].

An oscillator type of AIA uses an active device function as an oscillator and a passive radiating element at its output port. It is also named as a quasi-optical

oscillator since the generated RF power radiates into free space. This type of AIA attracted great attention recently due to its potential to fulfil many applications needs [74-79].

Microstrip patch antenna and slot antenna are two popular candidates use in AIA design. They are not only the output loads of oscillators, but also serve as the resonators determining oscillation frequencies. The input impedance of the antenna element is therefore important information for designing oscillator type active integrated antennas. Two examples of oscillator type active integrated antennas are shown in Figures 6.1 and 6.2. Example one [74], GaAs IMPATT diodes are monolithically integrated with a microstrip resonator and a loop antenna to produce a single chip millimetre-wave transmitter module. The device operates at 43.3 GHz and produces 27 mW CW output power with only 7.2 % conversion efficiency. Linear arrays of such radiating elements were produced and radiation patterns were determined as a function of imperilment spacing and element number. A study of the effect of substrate thickness of oscillation frequency and efficiency is conducted. It is concluded that the monolithic millimetre-wave IMPATT diodes can be used in more complex circuits than has hitherto been possible.

The other example is the integration of an FET and a slot antenna [75]. This design consists of an FET oscillator equipped with two patch antennas: one for the reception of the injection signal and the other for radiating the oscillator output power. The design provides a separate receive antenna for reception of the injection signal. This design method is used to overcome the synchronising of the oscillator elements in large quasi-optical power combining arrays, which is usually accomplished by relying on the weak interactions between the elements to cause phase locking.

Therefore, using this approach, broadband locking bandwidth could be achieved with a relatively low injected signal level.

6.2.2 Amplifier Type

The amplifier type active integrated antenna integrates an amplifier and passive antenna elements at its input or output port. The active integrated antenna works as a receiver when the antenna is at the input port only. [89]-[90]. Thus, the LNA is commonly used in this case due to its great low noise performance. When the antenna is at the output port only, the active integrated antenna works as a transmitter [86].

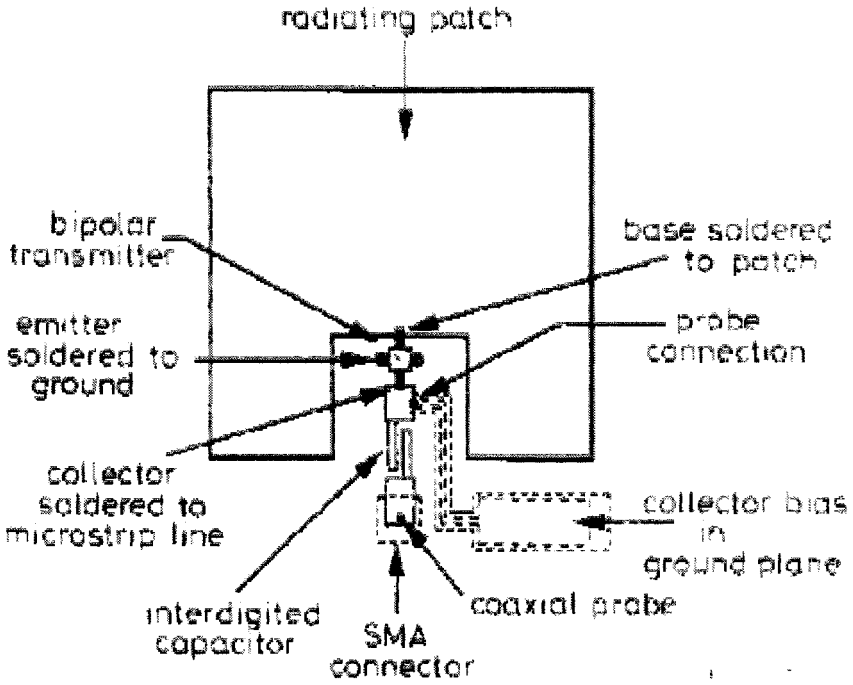

Figure 6.3: Structure of receiving active antenna

When antenna elements are integrated at the input and output ports, the circuit becomes a quasi-optical amplifier where it receives and transmits signals spatially with amplification [87]. The implementation of amplifiers in a passive antenna

structure increases the antenna gain and bandwidth, and improves the noise performance. The amplifier type active integrated antenna modules can be integrated in an array structure to increase the power handling capability.

An example is shown in Figure 6.3; a HP MA-0211 bipolar transistor is embedded in a square microstrip patch. A quarter wave transformer is used to match the active device and antenna. The active antenna uses a small number of components and takes the same place as a passive antenna. An extra gain of 8dB is obtained at 1.68GHz.

6.2.3 Frequency Conversion Type

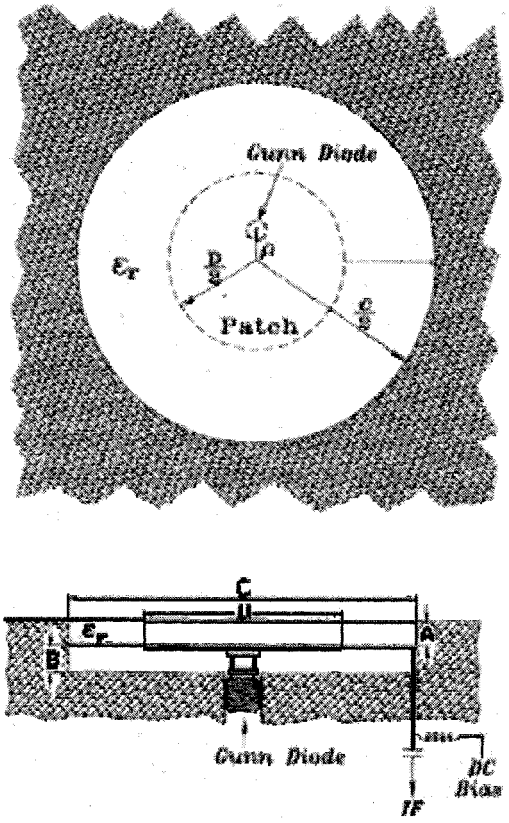

Figure 6.4: Configuration of self-mixing active antenna

The development of frequency conversion type active integrated antennas can be traced back as early as 1977 [92]. This concept of quasi-optical approach initialized the development of frequency conversion type active integrated antennas [92]-[96]. Most of the effort was concentrated on the quasi-optical mixer, but some of the works on quasi-optical multipliers were also reported [97]. Recently, with interests in simple and low-cost components for intelligent highway systems and non-contact ID'S, quasi-optical transponders using self-oscillating mixers or subharmonically pumped causing mixers to become an interesting research subject [94], [96]. A quasi-optical mixer integrates a receiving antenna and a mixer together, and functions as a receiver front end. A practical example of cavity-backed, Gunn-diode-driven, self-mixing active inverted stripline circular patch antenna is shown in Figure 6.4. The antenna provides good radiation performance with cross-polarization levels 18 dB below co-polarization at boresight. The self-mixing performance shows that the circuit has a -2 dB conversion gain for IF'S up to 450 MHz and a single side band noise figure of 12 dB at 200 MHz. The self-mixing antenna is also capable to mix signals with its second-harmonic, providing a conversion loss of 3.7 dB. Also, a varactor diode has been incorporated with an inverted stripline circular patch active antenna to allow for electronic tuning. A 13 % tuning bandwidth with a power variation of ±1.0 dB was achieved.

6.3 Advantages and Disadvantages

Generally the active circuits are placed either directly within the physical structure of the antenna or in its very close proximity. In order to avoided losses, such as non-radiating energy storage and unwanted impedance transformations, the

connection transmission line or wires between the antenna and the active device should be minimized. When the active element is placed in the immediate vicinity of the radiator, the radiator itself acts as a matching network. Therefore, a possible solution used to improve AIA efficiency is to remove the interconnection completely. Further more, removing the interconnections will lead to a potential broadening of the bandwidth since there is only a single impedance matching operation performed. The integrated structure makes it possible to use one impedance transformation instead of two stages of matching involved where transformation is made to and from intermediate impedance.

The active microstrip antenna, in which an amplifier or oscillator is integrated with a patch radiator, and is used to convert dc energy to RF power, has recently received a great deal of attention. Besides small size, low production cost and avoidance of impedance matching networks with attendant losses, there are possibilities for improved efficiency as well as bandwidth [1, 2].

For AIA the following advantages are identified as following:

1. Easy integration with a transceiver's RF circuitry
2. They are amenable to monolithic implementation due to their planar nature
3. An array antenna can be implemented in where a large power output is required
4. The active device can be used to improve the passive microstrip antenna gain bandwidth

5. When the active device and antenna are mounted on the same side of the circuit, the conformal nature of the structure can be preserved, and in array applications the inter-patch mutual coupling can also be reduced
6. In active microstrip array antennas where amplifiers and phase shifters are integrated behind the ground plane, spurious radiation from matching networks and feed lines can be avoided
7. High power can be achieved by combining the outputs of a number of devices which are integrated directly into an antenna array. By synchronising the oscillations of a large number of such oscillators, a high power source maybe achieved and radiate directly into free space, where propagation losses are low. Using free space, the losses of combining networks can be avoided
8. They are attractive for future applications, such as short range personal communication, sensors, and transport control and monitoring, where low cost will be the ultimate system requirement and fully monolithic construction will be used. In addition, reduction in device size to allow conventional element spacing for phase array action will be important. The microstrip active antenna is one example of such size reduction in which the patch is used as a frequency control element in microwave oscillators
9. The amalgamation of active devices with radiating patches makes it possible to obtain large bandwidth and extra power gain, so the results are very attractive for broadband MIC active array design.

However, AIA also have some disadvantages such as the following:

1. Most of the existing AIA suffer from low overall efficiency

2. Narrow bandwidth. This is due to the difficulty of impedance matching between the active device and antenna over the wide bandwidth
3. The solid state devices are integrated or located next to patch antennas, which in practice might increase their inherently high cross-polarised field
4. Efforts to integrate a number of devices have sometimes been unsuccessful because low DC to RF efficiencies of active devices lead to overheating problems. However efforts were made to design patch antennas in which the ground plane serves as the heat sink

The following comments can be made on the many existing or potential applications for AIA:

1. There are many potential applications in radar and satellite communications/applications where active integrated array antennas can be used
2. The AIA has the potential for use in low cost transmitters, active arrays, spatial power combiners, and quasi-optical combiners.
3. Active microstrip antennas are likely to find a wide variety of applications in either discrete or monolithic form due to their planar nature
4. The active antenna array concept is an efficient and lightweight method for generating high RF power for communication and radar systems
5. The primary application areas of such devices have been in low-power element cable of self-sustained oscillation for use in spatial power combining networks, radar array, or as stand-alone transmitters for vehicle tolling applications

6. Future applications such as in short range personnel sensors and transport control and monitoring, where the requirement and fully monolithic construction will be used
7. Active antennas are inherently good Doppler sensors because radiating sources are sensitive to Doppler return from moving objects.

6.4 High Efficiency Amplifying Transmitting AIA

Advanced communication systems require both a broad bandwidth and a high efficiency. Broad bandwidth offers the capacity to carry voice, data and video simultaneously, thus being attractive for broadband multimedia communications. High efficiency in a power amplifier can increase the battery life, reduce the power dissipation, relax the cooling requirement, and lower the cost. High efficiency active integrated antenna (AIA) has been a popular research topic in recent years [1, 2]. Using this approach the antenna can be integrated directly with the PA, hence the losses in the connecting cables, matching networks and connectors can be eliminated. The integration of a highly efficient RF/microwave power amplifier with an antenna will further reduce the size of the radio frequency front-end, improve the efficiency and lower the cost. Very few papers have been reported base on this approach. Some pioneering work on high efficiency active antenna designs have been reported in [2] with class-E PA and [1] with class-F PA.

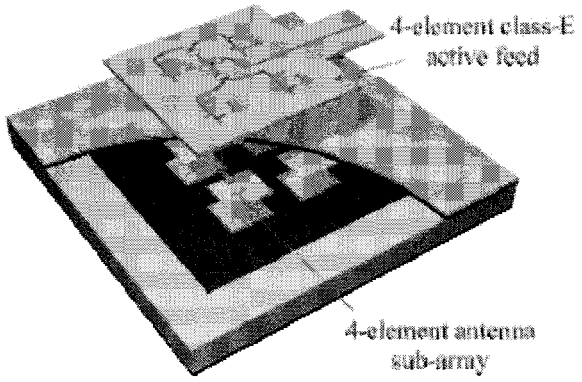

Figure 6.5: High efficiency AIA sub array [2].

A class-E PA is directly connected with a slot-coupled microstrip patch radiator [2] as shown in Figure 6.5. For the class-E PA used in the AIA design, a low cost GaAs MESFET is used to produce 20 dBm power output with drain efficiency on the order of 60 % to 70 %. A short matching network section is used in between the PA and radiating element. The design is implemented into a 16 element AIA array to maximize the power output. The paper shows that 70 % average drain efficiency is achieved by using 16 active antenna elements. It exhibits an output EIRP (Effective isotropically-radiated power) of 162 W at 10.2 GHz. However, the design concentrates on a narrow frequency band high efficiency AIA design. A bandwidth of 6 % of PAE greater than 50 % is achieved by the class-E PA used in the AIA design.

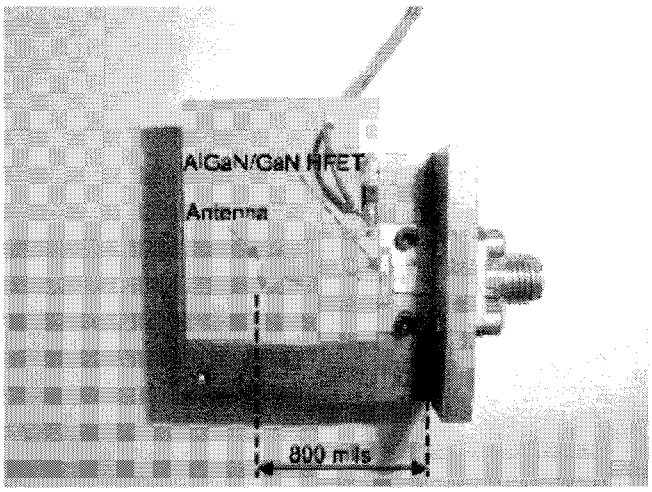

Figure 6.6: Photo of the prototype Class-F PA with a circular segment microstrip antenna [1].

The single-ended AIA amplifier design employed a modified circular segment microstrip antenna, which is capable of reactively terminating both the second and the third harmonics [1]. In this design, a compact ALGAN/GaN Heterohuction field-effect transistor (HFET) PA is integrated with this circular segment microstrip antenna at 7.25 GHz. The antenna is employed as both a radiator and frequency dependent output load. Higher order harmonics can be reactively terminated because of the harmonic termination characteristics of the antenna. The input impedance of the antenna is directly transformed to the optimum output impedance of the amplifier. Thus, there is no physical matching circuit between the radiating element and amplifier. Figure 6.6 shows the photo of this class-F AIA design. A high PAE of 42 % is achieved at 7.25 GHz with the output power of 30.3 dBm. In addition, there is no major degradation in the antenna radiation patterns with the cross-polarization level below – 16 dB at all directions in both the E- and H-planes. Once again, the design is concentrated on designing high efficiency AIA in a narrow frequency bandwidth.

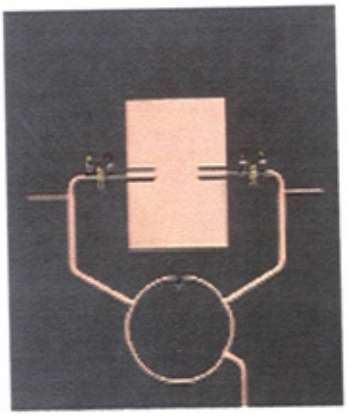

Figure 6.7: Push-pull power amplifier integrated with a patch antenna.

As reported in [98], the AIA concept is applied into the push-pull power amplifier designs, where the power of two anti-phase driven class-B power amplifiers are directly connected with a dual feed planar antenna Figure 6.7. in this case, the microstrip antenna has microstrip feed placed at opposite radiating edges to excite the proper radiating mode. A peak PAE of 55 % is measured at output power of 25 dBm. Additionally, second harmonic power suppression is found to be about 17 dBm lower than the fundamental frequency. However, the loss associated with the output hybrid limits the practical efficiency of this type of power amplifier at microwave frequencies. The bandwidth of this design is limited by the antenna and feeding network, and therefore it is a rather narrow band.

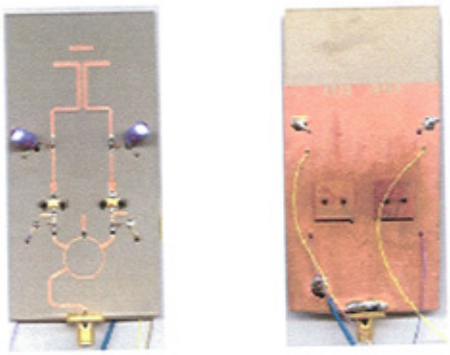

Figure 6.8: Push-pull PA with a Quasi-Yagi antenna.

In the most recent push-pull PA design [98], the amplifier is integrated with a modified Quasi-Yagi antenna Figure 6.8. The antenna is use as the harmonic termination circuit. The second harmonic suppression of about -30dB has been measured in both E and H plane. A peak PAE of 60.9 % with an output power of 28.2 dBm is achieved at 4.15 GHz. A measured PAE which is better than 50 % from 4.08 GHz to 4.29 GHz is achieved.

6.5 Summary

A general overview of AIA was discussed in this chapter. The AIA is classified into three different types; these are the oscillator type, amplifier type and frequency conversion type. The functionalities of each type of AIA were outlined. Ideally, AIA is capable of achieving a broad bandwidth with high efficiency due to the elimination of the matching network and harmonic tuning network. In reality, there are practical limitations on the efficiency and bandwidth that depend on the characteristics of the active device and radiating element. Thus, most of the existing works on AIA suffer with low efficiency and narrow bandwidth. A summarization of the advantages and disadvantages of AIA were presented followed by a selection of some pioneering work on highly efficient AIA designs. In the next chapter, the broadband antenna and broadband high efficiency class-E PA presented in previous chapters are integrated together. The improved design technique is extended and applied to the design of broadband high efficiency AIA. A number of LP and CP AIAs are designed, fabricated and measured.

CHAPTER 7

Broadband High Efficiency AIA Design and Fabrication

7.1 Introduction

This chapter contains the design, fabrication and measurements of broadband high efficiency AIA operating in LP and CP, respectively. The use of new design methodology presented in Chapter 5 allows a high PAE to be achieved over a broad bandwidth. In this chapter, the antenna is designed to serve the functions of both a radiator and a harmonics-terminated load for class-E high-efficiency PA integration over the wide bandwidth. The LP AIA is realized by integrating the broadband class-E PA with a broadband LP antenna, which uses a ring-slot coupled icrostrip patch antenna. Then, the CP AIA is realized by integrating the broadband class-E PA with a broadband CP antenna, which uses a single-feed cross-slot-coupled icrostrip patch antenna. Measurement results are discussed. Finally, the novel design of 2×2 CP AIA array at 2 GHz is presented. To realize the broadband CP antenna, a circular

patch is aperture coupled by crossed slots in the ground plane, which are fed by an L-shaped icrostrip feed line below the ground. Measured results are discussed.

7.2 Broadband High Efficiency AIA Element (LP) and (CP)

High efficiency active antenna designs have been reported in [98] with push-pull PA, [2] class-E PA and [1] with class-F PA. In this section, a novel design of broadband high efficiency LP AIA is presented. The design procedures are described in the following sections.

7.2.1 Broadband Antenna Design for The Load Of Class-E PA

The antenna is connected directly to the output of the PA forming the load network in the AIA. It not only has to provide the optimum impedance for the first resonant frequency, but also has to exhibit open circuit characteristics for higher order harmonics of the fundamental resonant frequency. The slot coupled antenna is carefully designed to suppress the higher harmonics. The structure of the LP antenna design is shown in Figure 7.1. The characteristics of the ring-slot coupled patch antenna have been reported in Chapter 3. The dimension of the patch is predetermined by the standard equation 7.1 for rectangular patch antenna operation at the fundamental frequency, given by:

$$f_o \approx \frac{c}{2L\sqrt{\varepsilon_r}} \tag{7.1}$$

where c is the speed of light, L is the patch length and ε_r is the substrate permittivity.

The dimensions of the ring slot can be determined by the equation from reference [42].

$$f \approx \frac{c}{2(R_1 + R_2)} \times \left(\frac{1+\varepsilon_r}{2\varepsilon_r} \right)^{\frac{1}{2}} \tag{7.2}$$

where R_1 is the outer slot width, R_2 is the inner slot width, f is the resonant frequency of the slot and ε_r is the permittivity of the substrate.

To achieve broadband LP operation, circular ring-slot coupling and low Q value substrate (air) an H-shaped patch on the top are employed. There is a 10 mm air gap between the ground plane and patch.

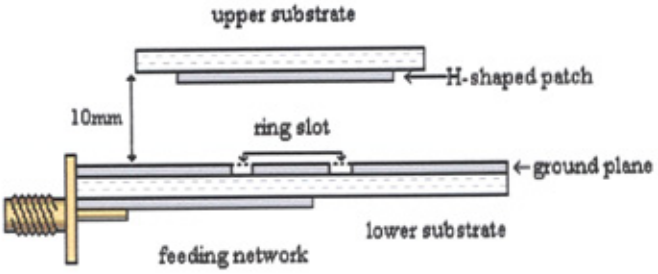

(a)

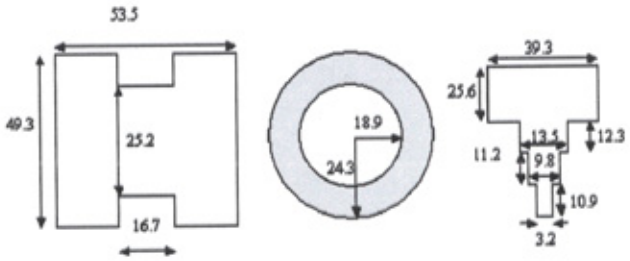

(b)

Figure 7.1: (a) Side view of the cross-slot coupled patch antenna, and (b) detailed dimensions of the proposed design (mm).

In Figure 7.1(a) the metallic H-shaped patch is attached to the underside of the upper supporting substrate, which is held in position by vertical supporting rods. Figure 7.1(b) shows the top view, where the relative positions and dimensions of the

feed, circular ring-slot, and, H-shaped patch are shown. A 0.79 mm thick duroid (5870) substrate is used to attach the feed line.

FREQUENCY (GHZ)	OPTIMUM SOURCE IMPEDANCE	OPTIMUM LOAD IMPEDANCE	MAXIMUM PAE (%)
1.8	18.1-34.7j	5.2+24.4 j	68.91
1.9	19.56-36.8j	5.3+19.3 j	73.2
2	18-40.9j	4.2+16.8 j	75.6
2.1	18.1-41.8j	5.1+12.3 j	72.97
2.2	19.5-43.2j	5.56+10.2 j	67.26

Table 7.1: Simulated optimum impedances over the frequency bandwidth from 1.8 GHz to 2.2 GHz

The geometry of the antenna feed line is obtained by first examining experimental results using a rectangular microstrip line. Due to the low output impedance required at the fundamental frequency for class-E PA operation, stepped-width transmission lines are formed to give the approximate optimum load impedances over a wide bandwidth, as shown in Table 7.1. Furthermore, approximately open circuit conditions for both the 2^{nd} and 3^{rd} harmonics were provided by the antenna design. The antenna was fabricated and measured. The measured input harmonic impedances of the antenna and the optimum load impedance obtained are shown in Table 7.1 and are compared in Figure 7.2 Close agreements between the optimum load impedance and the fundamental input impedance of the designed antenna are obtained. High reactive terminations for higher order harmonics are given by the input impedance of the design at 2^{nd} and 3^{rd} harmonic frequencies. Hence, the measured input impedance of the designed

antenna is directly transformed to the optimum impedance for high efficiency at the fundamental frequency. The measured harmonic input impedances are used in the simulation of PA.

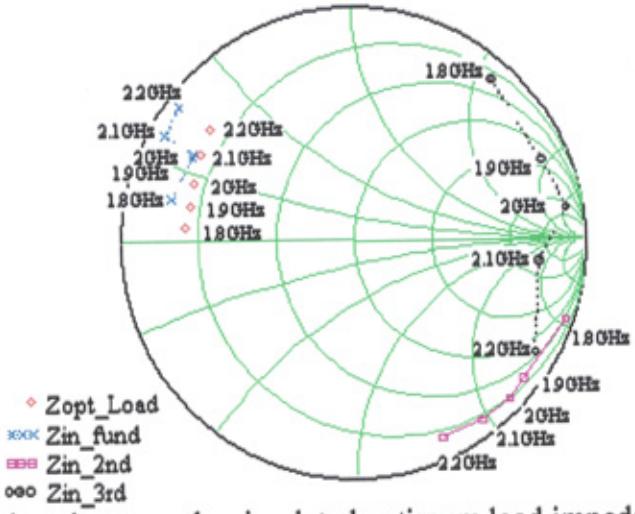

Figure 7.2: Comparison between the simulated optimum load impedance with the measured input impedance of the antenna (fundamental, $2P^{ndP}$ harmonic, and $3P^{rdP}$ harmonic impedance).

7.2.2 Broadband Linearly Polarized Active Antenna

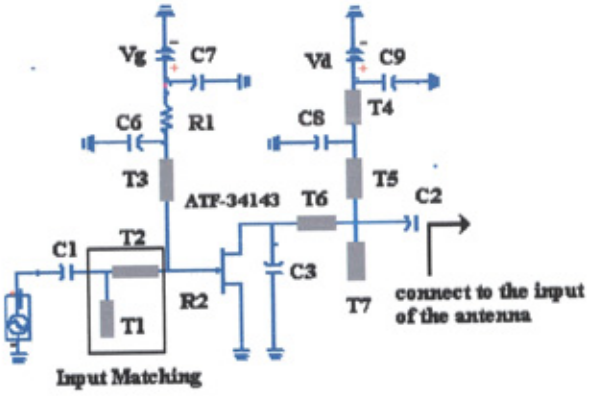

Figure 7.3: Schematic of AIA with class-E amplifier integration.

In order to reduce the size and improve the efficiency of the RF front end, the antenna is to be integrated directly to the class-E PA output without using a 50 Ω

interface, as shown in Figure 7.3. The class-E PA is re-designed in Figure7.3, without the output load network. A shunt (1.12mm (W) ×7.6mm (L)) open circuit stub T7 is connected to the DC bias line. The detailed design methodology can be found in Chapter 5.

Based on the class-E amplifier design and broadband LP antenna design, a LP AIA is fabricated and measured. The photos of the LP AIA are given in Figure 7.4. The voltage and current waveforms in the time domain confirm the non-ideal class-E mode of operation is resulted.

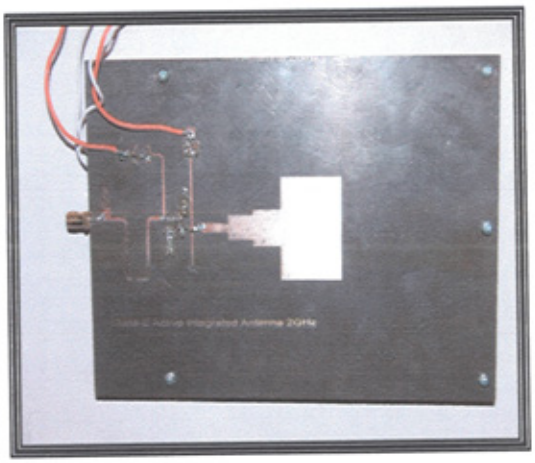

(a)

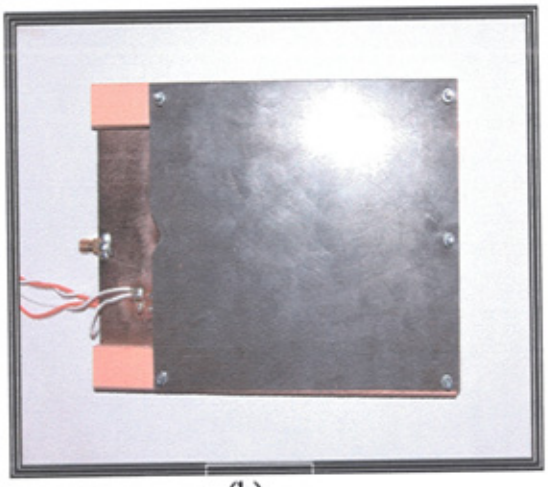

(b)

Figure 7.4: Photos of broadband LP active integrated antenna: (a) Back view, and (b) top view.

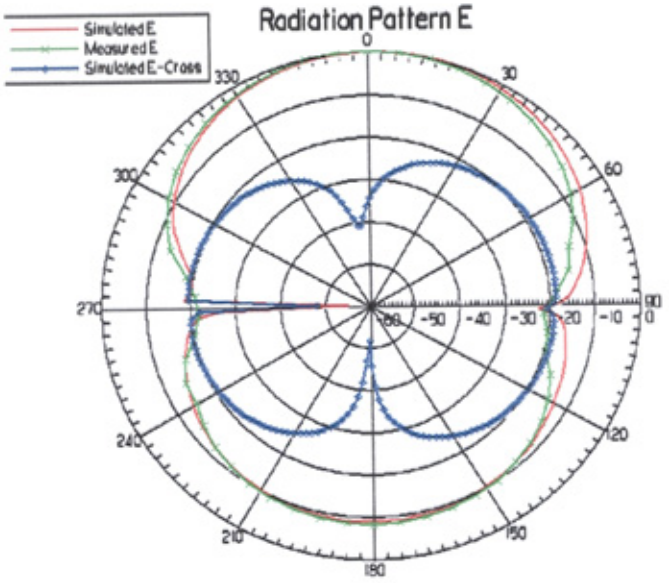

(a)

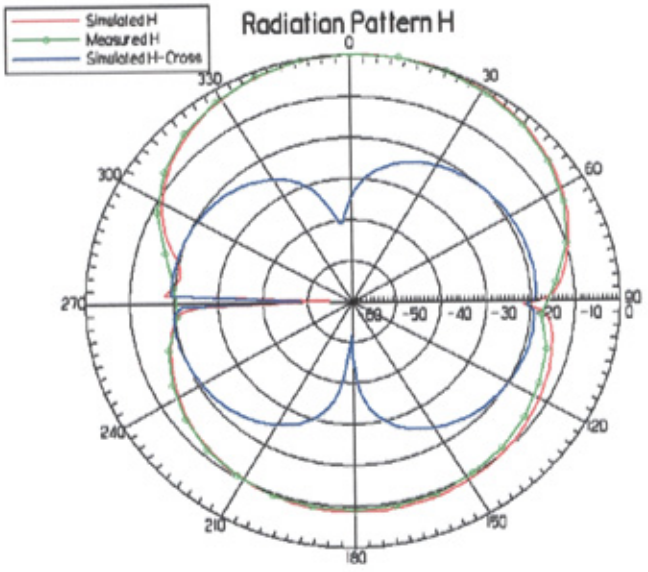

(b)

Figure 7.5: Measured and simulated radiation pattern of the designed active antenna:

(a) E-plane. (b) H-plane.

The LP AIA was measured at the central frequency 2 GHz in an anechoic chamber. Figure 7.5 shows a good agreement is obtained between the measured and simulated results of the radiation pattern. The antenna radiation pattern simulation is completed using *Ensemble*, from Ansoft. Practical measurements show that symmetric radiation patterns are obtained in both the E & H plane, and, cross polarizations are well below -20 dB in the broadside direction. The simulated voltage and current waveforms in Figure. 7.6(a) show the non-ideal class-E operation.

The PAE of this LP AIA amplifier module is determined by using the standard definition of PAE and the Friis transmission equation shown as follows:

$$P_{out} = \frac{P_{\mathrm{Re}}}{G_A G_{Sd}} \left(\frac{4\pi r}{\lambda} \right)^2 L_{Cable} \tag{7.3}$$

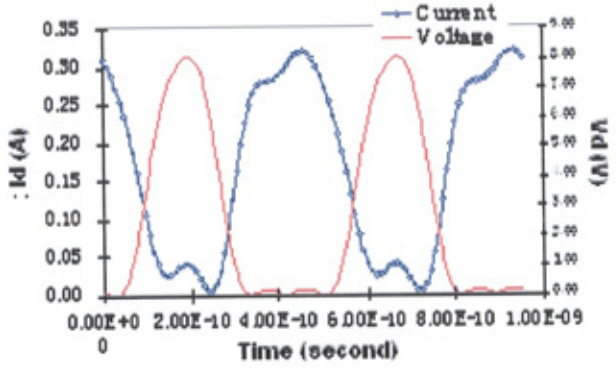

(a)

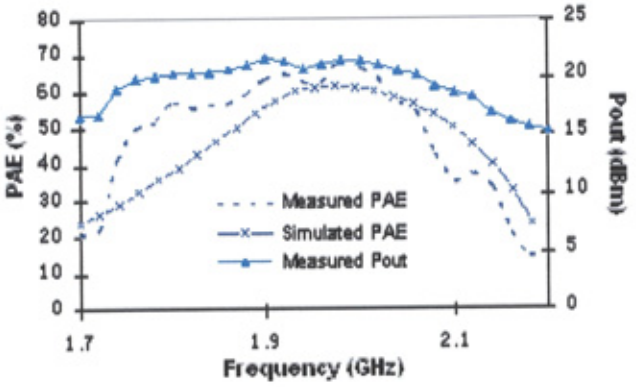

(b)

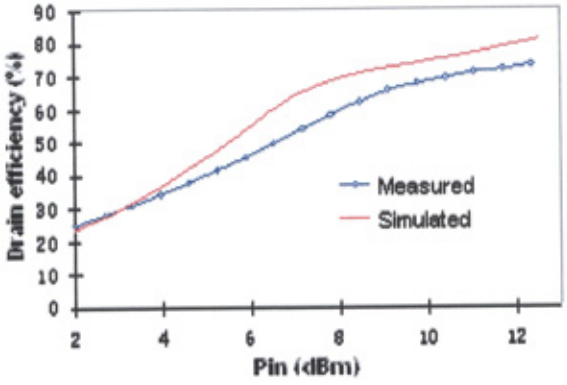

(c)

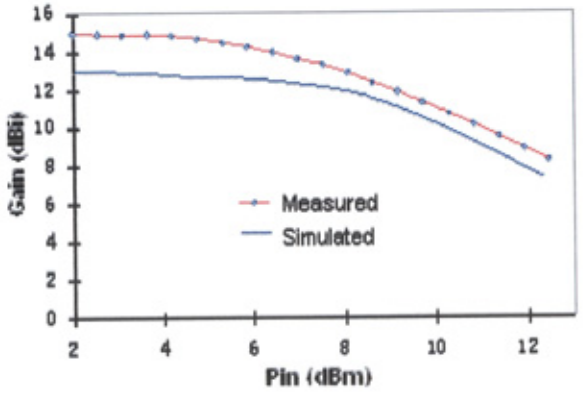

(d)

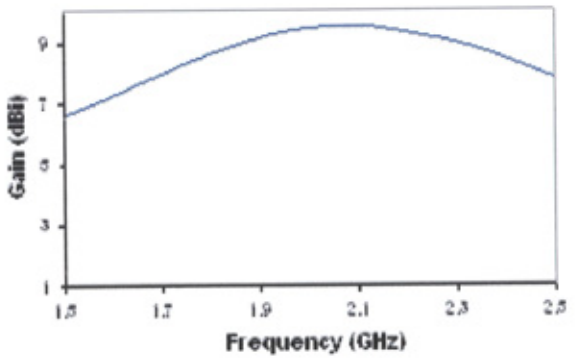

(e)

Figure 7.6: (a) Simulated voltage and current waveform, (b) measured power output against frequency and the comparison of measured and simulated PAE vs frequency, (c) the comparison of measured and simulated drain efficiency, (d) the comparison of measured and simulated gain at 2 GHz, and (e) simulated passive antenna gain.

where P_{Re} is the received power measured by the standard horn antenna, G_{sd} is the gain of the standard horn, L_{cable} is the power loss in the cable, and G_A is

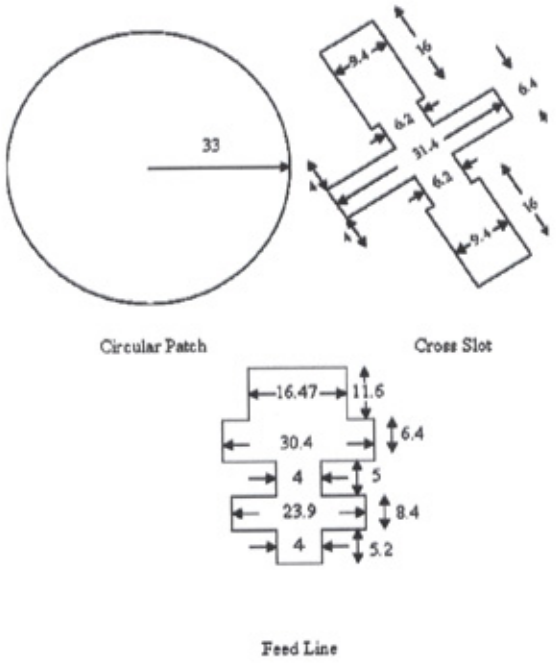

(b)

Figure 7.7: (a) Side view of the cross-slot coupled patch antenna, and (b) detailed dimensions of the proposed design (mm)

The same considerations for suppressing higher harmonics which were described in previous section are applied to this design. The characteristics of cross-slot coupled patch antenna have been reported in [10, 11]. By using a cross slot for coupling the electromagnetic energy from the microstrip feed to the radiating element, circular polarization can be obtained. The proposed design can achieve a right-hand circularly polarized antenna with a centre frequency of 2 GHz. The structure is shown in Figure 7.7. It consists of a stepped fed line, a cross-slot with unequal length and width and a simple circular patch as a radiator. Tuning the width and length of two crossed slots mainly controls two near degenerate resonant modes. Two orthogonal slots are used to excite the two equal amplitude fields with 90 °-phases. There is a 10 mm high air layer between the ground plane and patch.

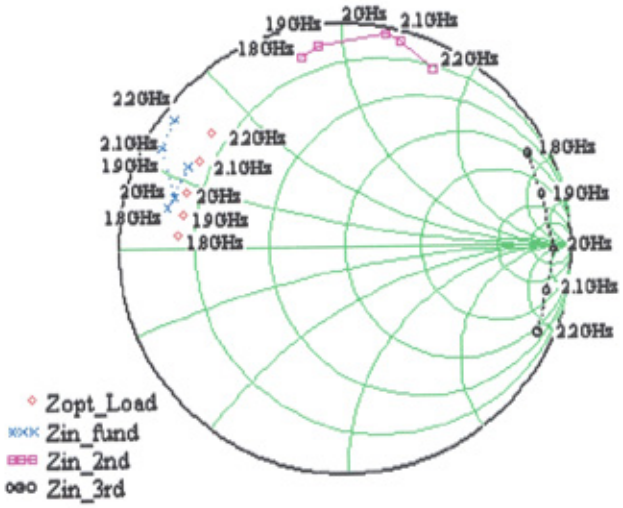

Figure 7.8: Comparison between the simulated optimum load impedance with the measured input impedance of the antenna (fundamental, $2P^{ndP}$ harmonic, and $3P^{rdP}$ harmonic impedance).

Once again, stepped-width transmission lines are formed to give approximate optimum input impedances over a wide bandwidth. The antenna was fabricated on Duroid (5870) with a thickness of 0.79 mm. The measured harmonic impedances of the antenna and the optimum load impedance obtained are shown in table 1 and are compared in Figure 7.8. The harmonics impedances of the antenna design show that the antenna can be used to replace the output load network of class-E PA.

7.3.1.2 Broadband Circularly Polarized Active Antenna

The broadband CP AIA is realized by integrating the broadband class-E PA with the broadband CP antenna. The photos of the fabricated CP AIA are shown in Figure 7.9. The CP AIA was then measured at the central frequency 2GHz in anechoic chamber. A standard LP Horn is used to measured the total radiation

pattern at $\phi = 0^\circ$ and $\phi = 90^\circ$. The measured radiation patterns of the active antenna at 2 GHz are given in Figure 7.10(a). It shows that symmetric radiation patterns are obtained at $\phi = 0^\circ$ and $\phi = 90^\circ$. The antenna pattern simulation (passive) is done by using *Ensemble*, from Ansoft. Simulation results in Figure 7.10(b) show that symmetric radiation patterns are obtained at both Phi $\phi = 0^\circ$ and $\phi = 90^\circ$ and cross polarizations are well below –20 dB in the broadside direction.

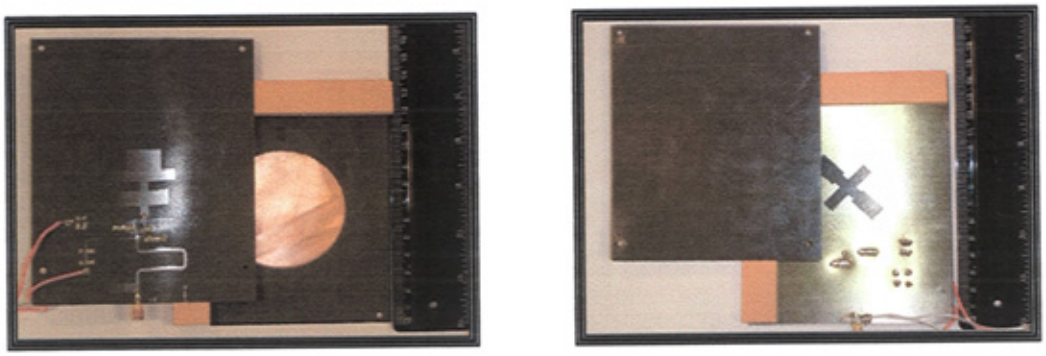

(a) (b)

Figure 7.9: Photos of CP active antenna: (a) back view, and (b) top view.

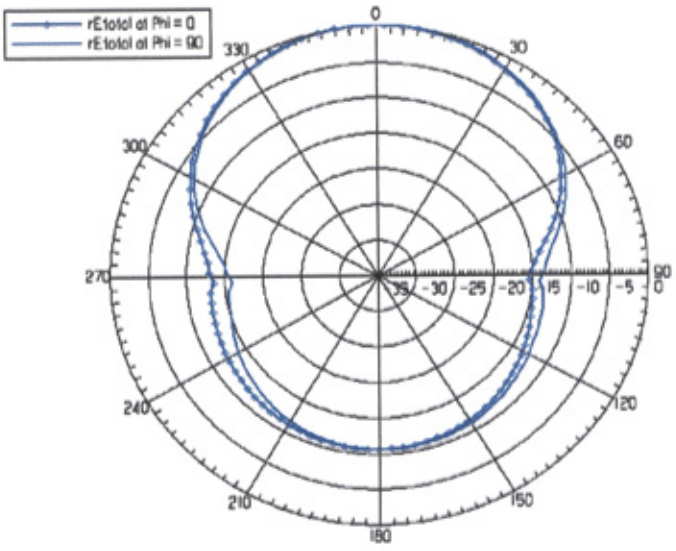

(a)

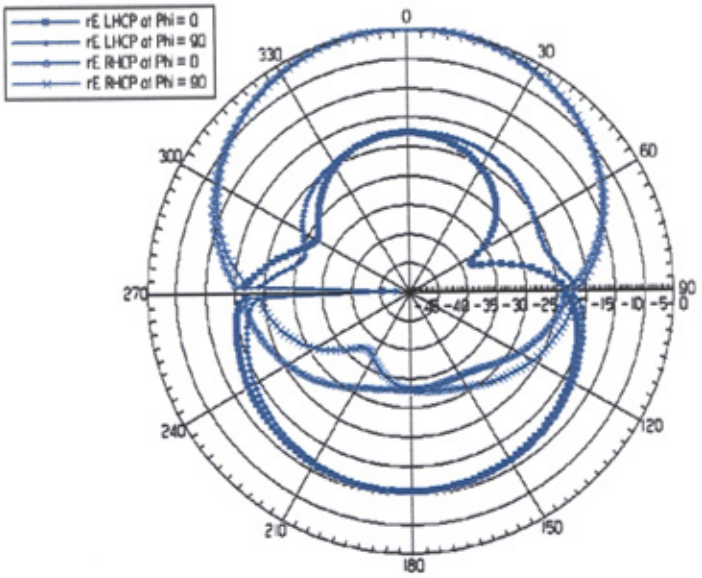

(b)

Figure 7.10: (a) Measured (AIA) total radiation pattern, and (b) simulated (passive) radiation patterns of the broadband active antenna, measured and simulated radiation pattern of the designed active antenna.

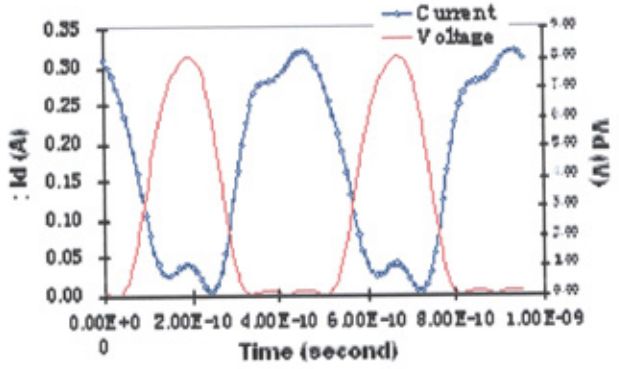

(a)

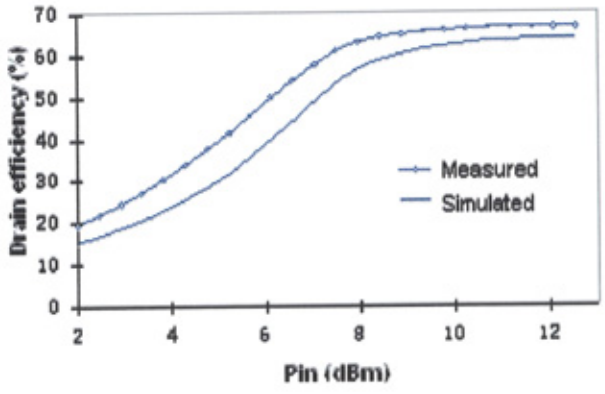

(b)

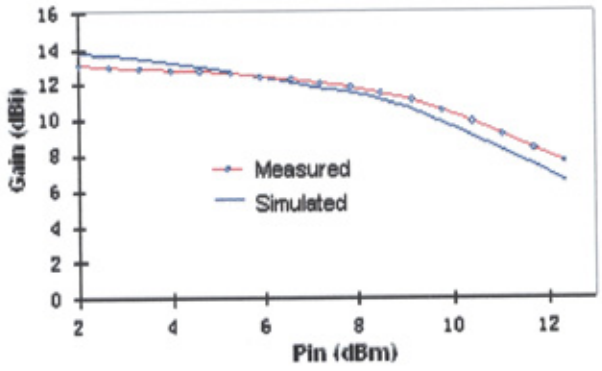

(c)

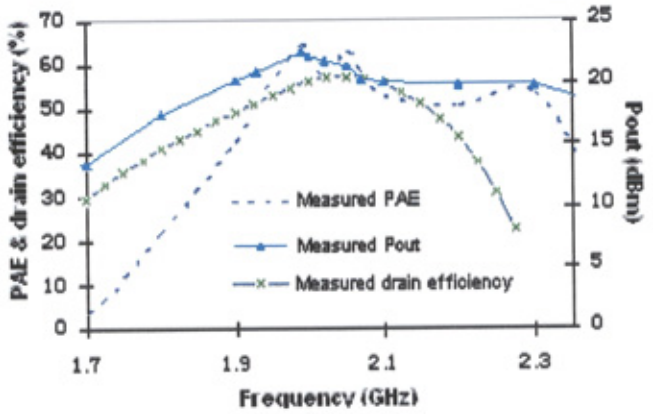

(d)

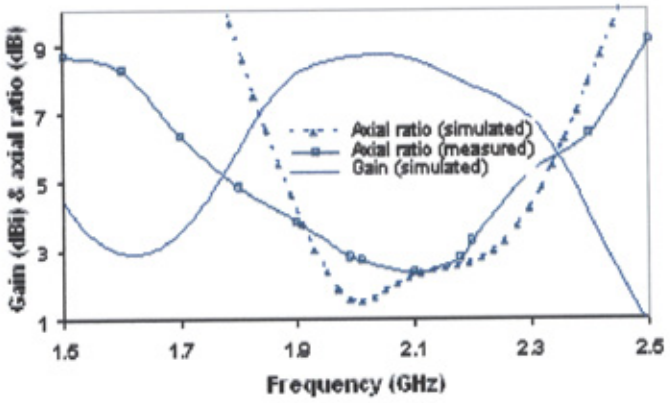

(e)

Figure 7.11: (a) Simulated voltage and current waveform, (b) measured power output against frequency and the comparison of measured and simulated PAE vs frequency, (c) the comparison of measured and simulated gain at 2 GHz, (d) the comparison of measured and simulated drain efficiency, and (e) The comparison of measured and simulated AR vs Frequency.

Figure 7.11 shows the measured and simulated results of PAE, drain efficiency and gain versus frequency. The measured PAE is above 50 % over a 14 % bandwidth from 1.92 GHz to 2.21 GHz. A peak output power of 22.3 dBm is obtained at the output of class-E PA. Figure 7.11(e) shows that the comparison between measured and simulated AR results versus frequency together with simulated passive antenna gain. A closed agreement is shown. The axial ratio of the CP AIA is below 3 dB over a 9 % bandwidth from 1.99 GHz to 2.18 GHz.

7.3.1.3 Discussion

This work presented novel designs of two broadband high efficiency active integrated antennas, *i.e.*, a LP AIA and a CP AIA. First, an improved design technique is proposed for designing broadband class-E PAs, so that a high PAE can be achieved over a broad frequency range instead of a single frequency point. A broadband LP antenna and also a broadband CP antenna are designed, to function as both a harmonics-terminated load and a broadband radiator. Broadband high-efficiency LP AIA and CP AIA at 2 GHz are then realized by integrating the above two broadband antennas with broadband class-E PA, respectively, without using a 50Ω interface between them. A low cost PCB technology is employed in the fabrication and a low cost PHEMT transistor is used. The LP AIA achieves a PAE over 50 % within a 14.6 % bandwidth from 1.78 GHz to 2.06 GHz. The CP AIA achieves a PAE over 50 % within a 14 % bandwidth from 1.92 GHz to 2.21 GHz. The axial ratio of the CP AIA is below 3 dB over a 9 % bandwidth from 1.99 GHz to 2.18GHz.

7.3.2 Novel Design of High Efficiency CP AIA and Array.

This section presents a broadband high efficiency CP AIA, and a broadband CP active array at 2 GHz. To realize the broadband CP antenna, a circular patch is aperture coupled by crossed slots in the ground plane, which are fed by an L-shaped microstrip feed line below the ground. The antenna is designed to serve the functions of both a radiator and a harmonics-terminated load for class-E high-efficiency power amplifier (PA) integration.

7.3.2.1 Broadband CP Active Antenna Element

The characteristics of cross-slot coupled patch antenna have been reported in [44, 45]. By using crossed slots to couple the electromagnetic energy from the microstrip feed to the radiating element, CP radiation can be obtained.

The detail design methodology is reported in Chapter 3. The configuration of the proposed broadband CP antenna is shown in Figure 7.12. It consists of an L-shaped microstrip feed line below the ground plane, crossed-slots with unequal lengths cut in the ground plane, and a circular patch above the ground plane. To reduce the cost, a single patch is used, instead of stacked patches. The circular microstrip patch is printed on the underside of the top substrate, which is held in position by vertical supporting plastic rods. In the top view shown in Figure 7.12(b), the relative positions of the feed, crossed-slots, and, circular patch are shown. Both substrates are 0.79 mm thick duroid (5870). There is a 10mm-thick air gap inserted between the slot and the patch. The crossed slots excite two orthogonal modes in the antenna; the length of the L-shaped microstrip feed line between two slots is

adjusted to be approximately a quarter of the wavelength, so as to introduce a 90° phase shift between two orthogonal modes.

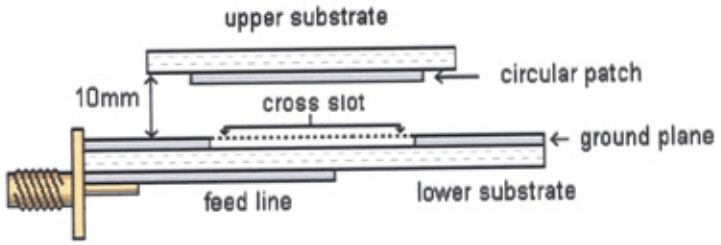

(a)

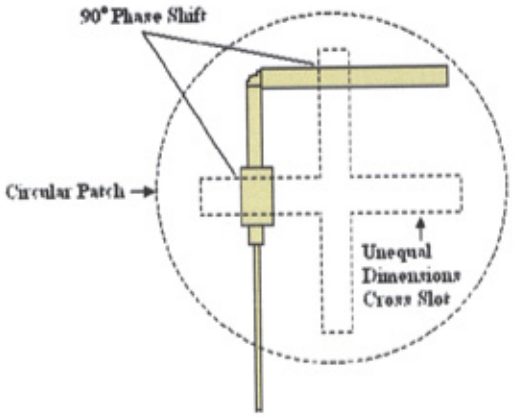

(b)

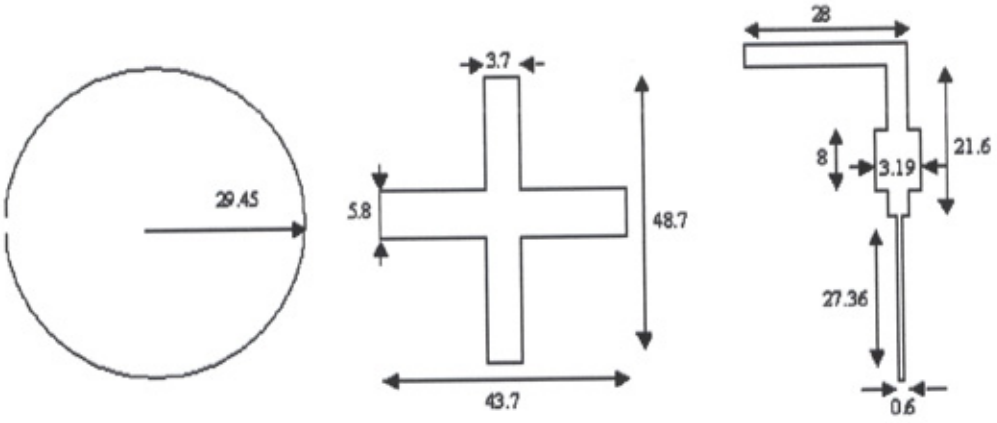

(c)

Figure 7.12: (a) Side view, (b) Top view of the broadband CP antenna, and (c) detailed dimensions (mm) of the proposed design.

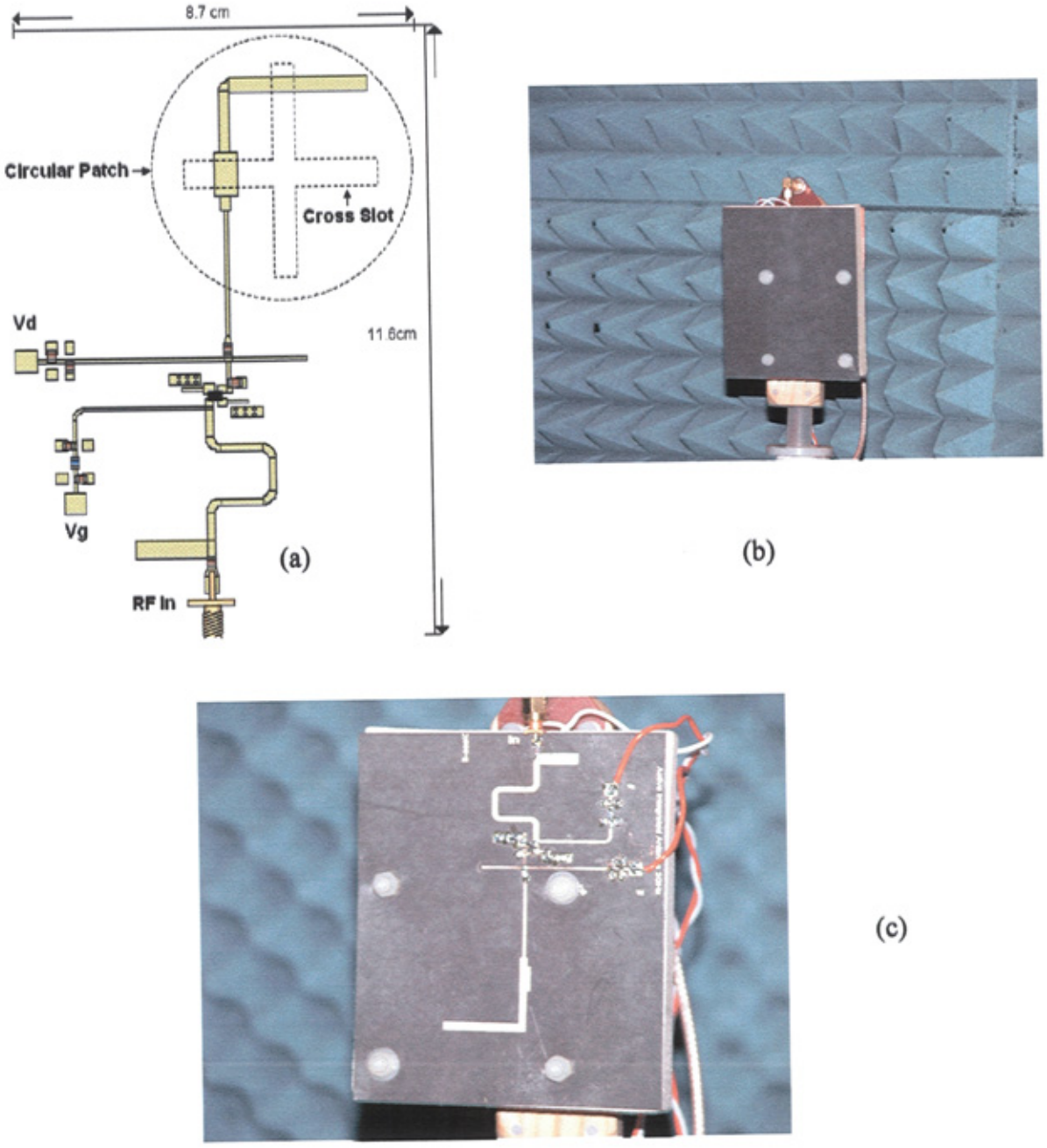

Figure 7.13: (a) Design layout of the broadband CP active antenna, (b) photo of the antenna viewed from the front, and (c) photo of the antenna viewed from the back.

To form the broadband CP active antenna, the broadband CP antenna is integrated with the broadband class-E amplifier, which has been reported in Chapter 5. It is then fabricated using PCB technology, and the practical results are measured. The layout of the active antenna is given in Figure 7.13(a), which has a size of 8.7

cm by 11.6 cm. The photos of the active antenna viewing from the front and the back are shown in Figure 7.13(b), and Figure 7.13 (c), respectively.

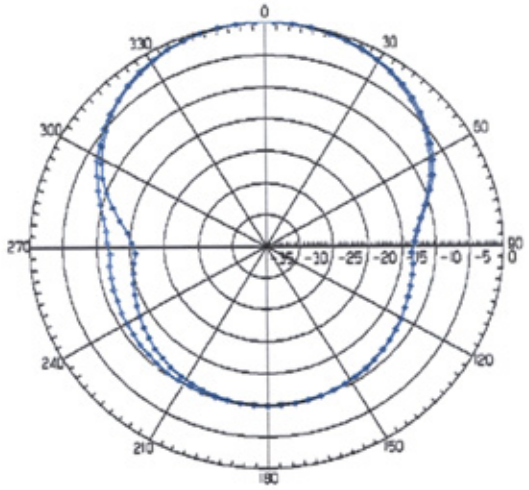

(a)

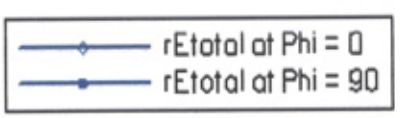

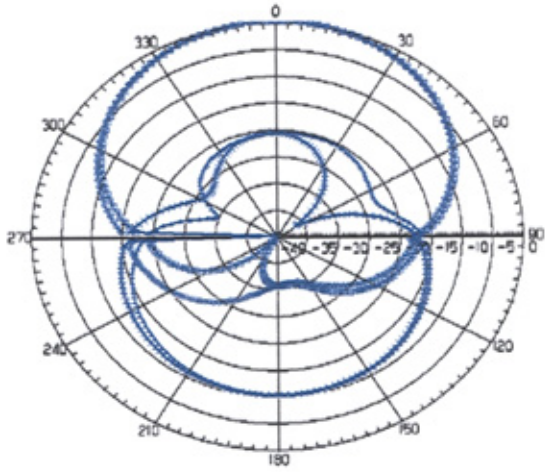

(b)

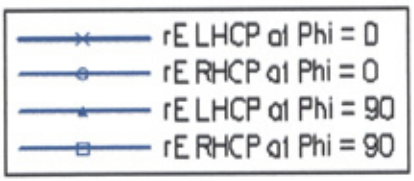

Figure 7.14: (a) Measured (AIA) total radiation pattern, and (b) simulated (passive) radiation patterns of the broadband active antenna.

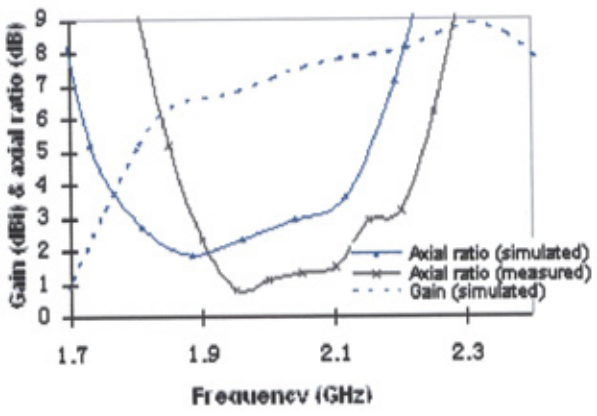

(a)

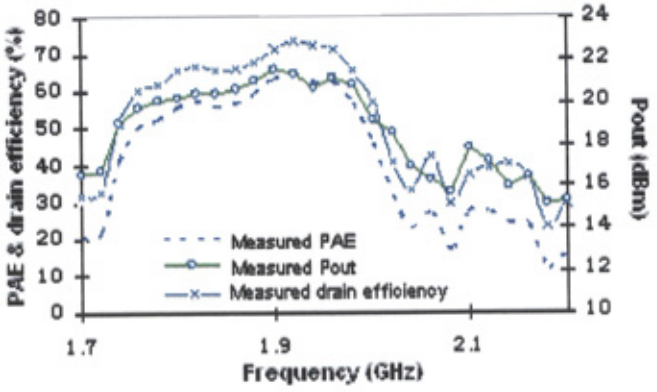

(b)

Figure 7.15: (a) The comparison of measured and simulated AR vs Frequency, and (b) measured PAE, (c) drain efficiency and Power output, and (d) measured power output against frequency and the comparison of measured and simulated PAE vs frequency.

This broadband CP active antenna was measured at the centre frequency 2GHz in anechoic chamber with an input power of 12 dBm. A standard LP Horn is used to measured the total radiation pattern at ϕ = 0° and ϕ =90°. The measured radiation patterns of the active antenna at 2 GHz are given in Figure 7.14(a). It shows that symmetric radiation patterns are obtained at ϕ = 0° and ϕ =90°. The antenna pattern simulation (passive) is complete by using Ensemble from Ansoft. Simulation results in Figure 7.14 (b) show that symmetric radiation patterns are

obtained at both $\phi = 0^{\circ}$ and $\phi = 90^{\circ}$ and cross polarizations are well below -20 dB in the broadside direction.

The PAE of this AIA amplifier module is determined by using the standard definition of PAE and using the Friis transmission equation shown as followed:

$$P_{out} = \frac{P_{\mathrm{Re}}}{G_A G_{Sd}} \left(\frac{4\pi r}{\lambda} \right)^2 L_{Cable} \tag{7.4}$$

where P_{Re} is the received power measured by the standard horn antenna, G_{Sd} is the gain of the standard horn, L_{Cable} is the power loss in the cable, and G_A is the predetermined passive antenna gain. The active antenna achieves an AR value below 3 dB within a 9 % bandwidth, i.e., from 1.84 GHz to 2.01 GHz, as shown in Figure 8(a). Figure 7.15(a) also shows that the antenna gain is above 6.5 dBi within this frequency range. The measured power output, PAE and drain efficiency are shown in Figure 7.15(b). Practical measurements show an output power flatness of 1dBm and drain efficiency above 60 % over a 15 % bandwidth. A peak drain efficiency of 73.3 % is achieved. A 12 % bandwidth for PAE over 60 % is obtained, with a peak output power of 21.7 dBm.

7.3.3 Broadband CP High Efficiency Active Array

Sequential rotation in the feed network can improve the axial-ratio bandwidth of CP antennas, and many designs using this technique have been reported for passive arrays [46-47].

The passive broadband CP antenna array in chapter 3 is applied into the design of high-efficiency active arrays in this section. Detailed design methodology can be found in Chapter 3. In order to further improve the axial ratio bandwidth and produce greater power output, four broadband CP active antennas, described in previous sections, are employed in a sequential-rotation arrangement. The important issue of designing the sequential feeding network for deeply saturated class-E PA is of highly important. This is because an unequal input power level will lead to a different compression level. The feed network is designed for right hand circular polarization, which is the same with the single CP active antenna element.

The configuration and layout of the proposed broadband CP active array are shown in Figure 7.16(a). Based on the single element broadband CP active antenna design, a 2×2 array is designed. The feed network consists of seven quarter-wave transformers, which are designed to produce an impedance match for 50 Ω at the input feed point, produce a 90° phase difference between adjacent antenna elements and ensure that each element is fed with equal input power.

Four identical class-E PA, which has been reported in Chapter 5, are used in this AIA array design. The active array is fabricated by using the PCB technology, and measured. Figure 7.16(b) shows the back view of the fabricated active array, while Figure 7.16(c) shows its side view and Figure 7.16(d) shows the crossed slots in the ground plane and the circular patches.

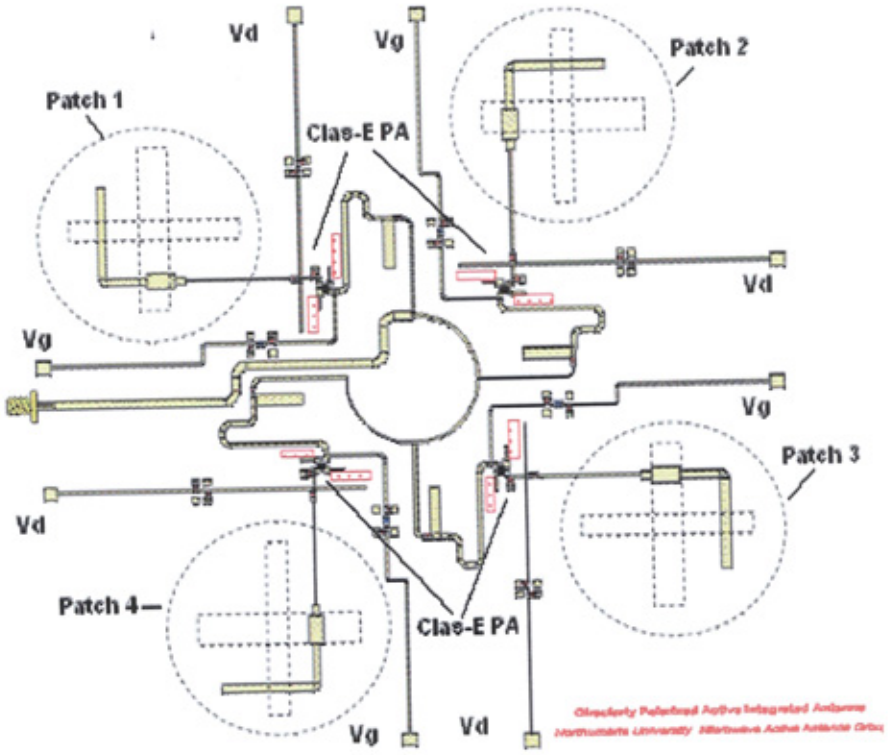
Vd
Vg
Patch 2
Patch 1
Class-E PA
Vd
Vg
Vg
Patch 3
Vd
Patch 4
Class-E PA
Vg
Vd

(a)

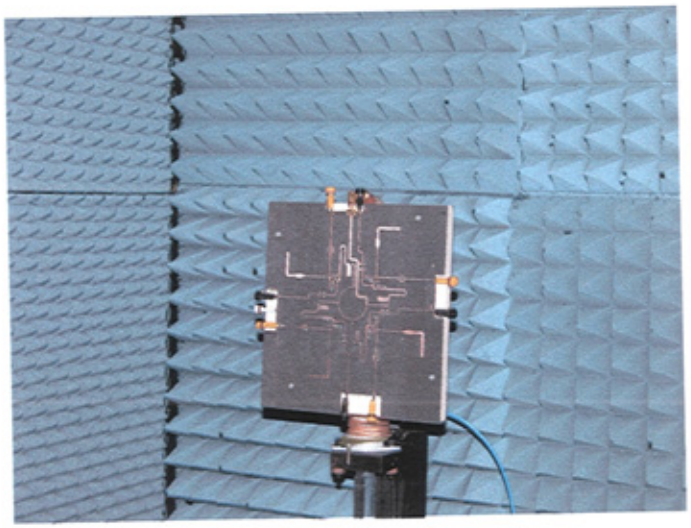

(b)

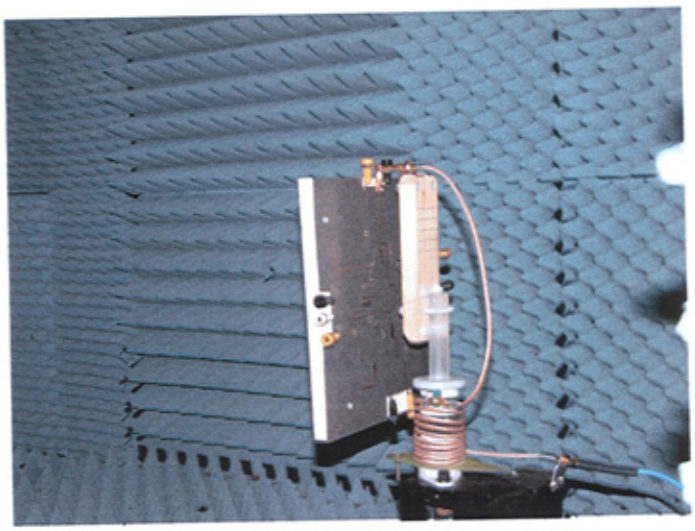

(c)

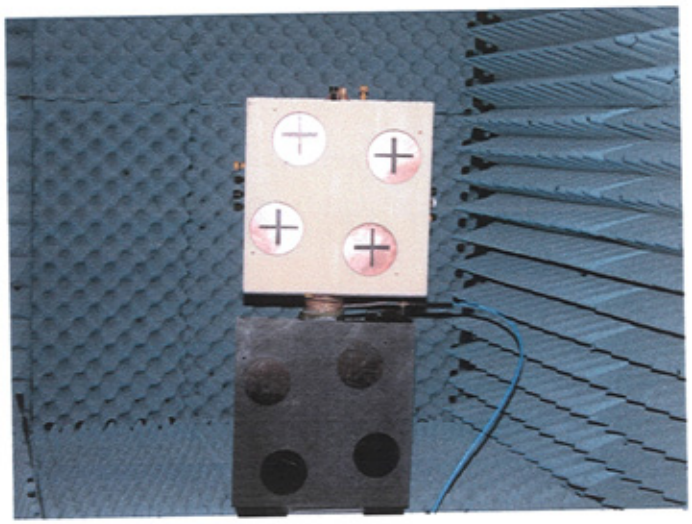

(d)

Figure 7.16: Broadband CP active array (a) layout, (b) photo of back view, (c) photo of side view, and (d) photos of the crossed slots and patched.

7.3.3.1 Performances

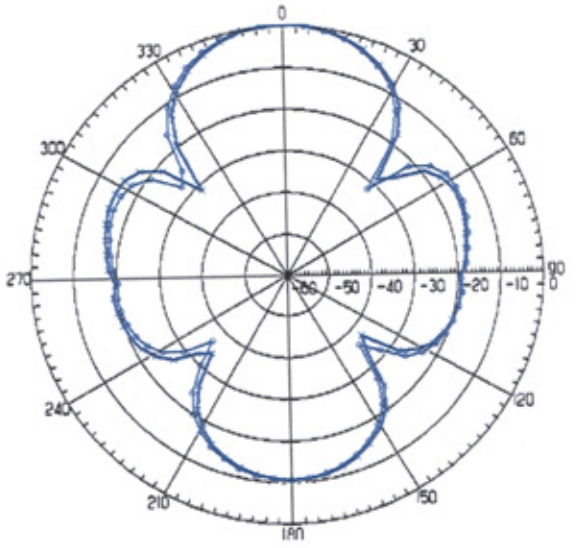

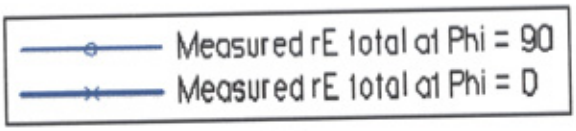

(a)

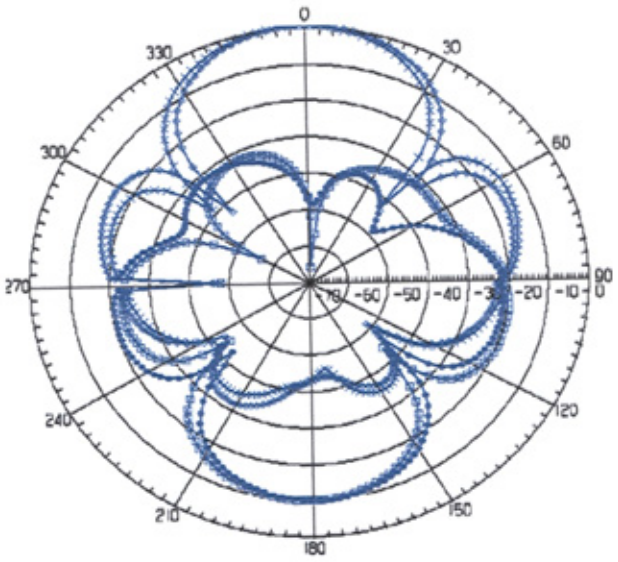

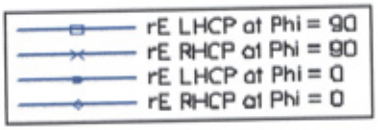

(b)

Figure 7.17: (a) Measured active array total radiation pattern, and (b) simulated (passive) radiation patterns of the broadband active array.

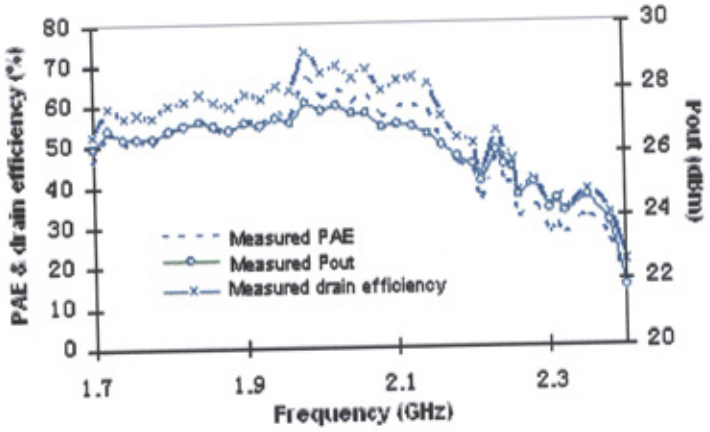

(a)

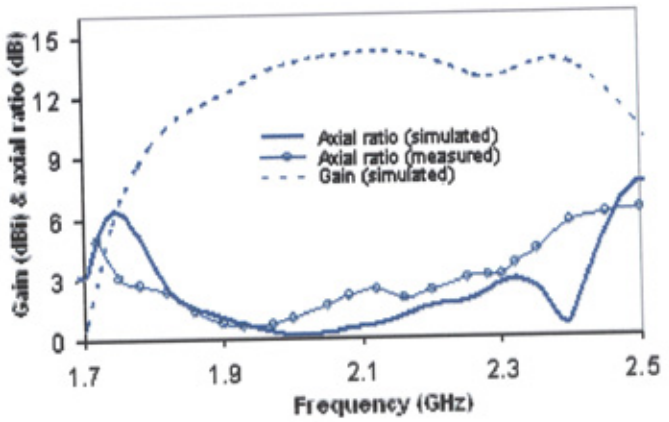

(b)

Figure 7.18: Frequency dependence of (a) Measured PAE, drain efficiency and power, and (b) measured and simulated axial ratio with simulated gain.

This antenna array was measured at the central frequency 2 GHz in anechoic chamber. The radiation pattern results are shown in Figure 7.17. The total radiation patterns shown in Figure 7.17(a) are measured atϕ = 0° and ϕ =90°. Simulated passive antenna patterns obtained from Ensemble are shown in Figure 7.17(b). Simulated results show that symmetric radiation patterns are obtained at both at ϕ = 0° and ϕ =90° and cross polarizations are well below -20 dB in the broadside direction. The frequency dependence of the PAE, drain efficiency and power output are shown in Figure 7.18. The calculation takes into account the losses in the cables. As shown in Figure 7.18(a), it achieves a peak drain efficiency of 71.35 %, and a

peak PAE of 64.8 %. The PAE is over 50 % within a 22.6 % bandwidth from 1.72 GHz to 2.16 GHz. The drain efficiency is over 60 % from 1.82 GHz to 2.14 GHz. The AR value below 3 dB is obtained over a 27 % bandwidth from 1.73 GHz to 2.26 GHz is shown in Figure 7.18(b) together with the simulated passive gain over the bandwidth. A close agreement is obtained between simulation and measurement.

7.4 Summary

This work presented novel designs of two broadband CP active antennas, a broadband high efficiency LP active antenna and a broadband high efficiency CP active array antenna. The broadband LP AIA was achieved a peak output power of 21.5 dBm and PAE is above 50 % over a 14.6 % bandwidth from 1.78 GHz to 2.06 GHz. The broadband CP high-efficiency active antenna was realized by integrating a broadband single-feed CP antenna with a pre-designed broadband class-E PA. The active antenna achieved an AR value below 3 dB within a 9 % bandwidth, i.e., from 1.84 GHz to 2.01 GHz. A bandwidth for PAE over 60 % was obtained. Finally, a 2×2 broadband high efficiency CP active array was realized by sequentially rotating the active antenna element. The PAE is over 50 % within a 22.6 % bandwidth from 1.72 GHz to 2.16 GHz. The AR value below 3 dB was obtained over a 27 % bandwidth from 1.73 GHz to 2.26 GHz. The active CP antennas reported here are of low cost, and achieved good performances in terms of broad bandwidth, high efficiency, thus useful for applications in satellite communications and other wireless systems.

CHAPTER 8

Conclusions and Future Work

8.1 Summary And Conclusions

The research work presented in this thesis proceeded from two primary motivations. The first is that RF PAs are one of the most power hungry components in a communication system and are very lossy in most applied applications. The second motivation is the need for bandwidth in a modern communication system. Past work on high efficiency AIA design has shown that high efficiency can be obtained in a narrow bandwidth.

The stated objective of this work is to extend and to implement the class-E design methodology into broadband high efficiency AIA design. An improved design technique to design the load network for broadband high efficiency class-E PA was investigated. Next, this improved design method is implemented to the broadband high efficiency AIA design. Toward this end, a new approach to design extended bandwidth AIA was investigated. Several LP and CP broadband high efficiency AIA

were reported. This includes the first reported high efficiency broadband CP AIA design.

Chapter 1 gave the background information and principal motivations for the work presented in this dissertation. The modern applications and limitations were briefly outlined. A list of contributions of this research work is discussed. A dissertation outline was given at the end of this chapter.

A general review of the broadband microstrip antenna is given in Chapter 2 which gives an over view of the different techniques employed to enhance the bandwidth.

An experimental study of broadband slot-coupled patch antenna is summarized in Chapter 3. Slot coupled feed antennas are used because of the potential of large impedance bandwidths and their ease of integration with an active circuit. Three single element broadband slot coupled patch antenna with a 2×2 slot-coupled array antenna are presented. By varying the shape of the ring slot, identical performance of 50 % impedance bandwidth is achieved by both two LP slot-coupled antennas. With the cross-slot feed, the broadband CP antenna achieves a 26 % bandwidth from 1.76 GHz to 2.29 GHz. The axial ratio bandwidth, defined as AR< 3 dB, is found to be 9.6 %, to further improve the axial ratio and impedance bandwidth, the cross-slot CP element is employed in a four-element sequentially rotated array. As the result, a VSWR<1.5 bandwidth is found to be 33 % The axial ratio bandwidth, defined as below 3 dB, is found to be 27.2 %.

A review study of class-E PA is presented in Chapter 4. The conventional PA classes are briefly discussed at the beginning. A detailed theoretical analysis of the class-E PA together with the experimental investigation of the circuit parameter effects, such as switch-on resistance and switch duty cycle, are studied.

CHAPTER 8 CONCLUSIONS AND FUTURE WORK

An experimental study of a broadband high efficiency class-E PA is presented in chapter 5. The class-E which utilizes the medium ATF-34143 device from Agilent® has a different design frequency and methodology, leading to performance variation. The first class-E PA design has a low design frequency with an improved load network which leads to a measured peak PAE of 66.5 % at 750 MHz with a 22.7 dBm output power at RF input power of 12 dBm. This design achieves a PAE above 50 %, within a frequency range between 540 MHz and 890 MHz. The second class-E PA increases the operating frequency to 2 GHz with a modified bias network and improved second harmonic termination load network, which achieves a peak PAE of 72.1 %, is measured at 1.95 GHz with 22.8 dBm output power. A bandwidth of 37 % of PAE>50 % is achieved. Further effort is taken to improve the efficiency and bandwidth. An improved design method is proposed. From the results, the third class-E PA is designed by using this design methodology. At most, a peak PAE of 82.1 % is measured at 1.99 GHz with 22.8 dBm output power for 12 dBm RF input power. The resulted bandwidth for a PAE of greater than 60 % is more than 12 %.

A general review of present AIA activities is summarized in chapter 6. The AIA is classified into three groups, which are oscillator type, amplifier type and frequency converter type. Some pioneering works in high efficiency AIA designs are outlined and the advantages and disadvantages of AIA are discussed.

The final contribution is the novel implementation of the improved design method in the broadband high efficiency AIA designs. A novel LP AIA element is presented at first. The concept of designing antennas designed to have the class-E load impedance over the wide frequency bandwidth is especially useful when the class-E impedance output mismatches that limited the peak efficiency and power available from the output of the PA. The measured PAE is above 50 % over a 14.6 %

bandwidth from 1.78 GHz to 2.06 GHz. A novel CP AIA element is presented in the following section. The same concept is implemented in this design. The results show the CP AIA achieves a PAE of over 50 % within a 14 % bandwidth from 1.92 GHz to 2.21 GHz. The axial ratio of the CP AIA is below 3 dB over a 9 % bandwidth from 1.99 GHz to 2.18 GHz. A cross slot is employed in the third broadband high efficiency CP AIA design. This novel AIA performs class-E amplification as well as radiating with a peak power output of 21.7 dBm. The CP AIA achieves an AR value below 3 dB within a 9 % bandwidth. Practical measurements show an output power flatness of 1dBm and drain efficiency above 60 % over a 15 % bandwidth. A peak drain efficiency of 73.3 % is achieved. A 12 % bandwidth for PAE over 60 % is obtained. In an effort to improve the CP AIA performance, the cross-slot element is employed into a 2×2 sequential rotated feed AIA array. A significant improvement of axial ratio and impedance bandwidth are resulted. It achieves a peak drain efficiency of 71.35%, and a peak PAE of 64.8 %. The PAE is over 50 % within a 22.6 % bandwidth from 1.72 GHz to 2.16 GHz. The AR value below 3 dB is obtained over a 27 % bandwidth from 1.73 GHz to 2.26 GHz.

In summary, the first goal of this research is satisfied with the designs of slot-coupled LP and CP broadband antenna. The second goal of class-E PA bandwidth and efficiency is satisfied, using the three class-E PA designs to cover the frequency bandwidth from 800 MHz to 2 GHz. The third goal is satisfied by the development of an improved design method together with the implementation of a 2 GHz class-E PA design. The final goal of this research work is satisfied with the demonstration of broadband CP and LP high efficiency AIAs and AIA array at 2 GHz.

8.2 Suggestions For Future Work

Base on the observations gathered while completing this thesis, the pertinent issue which adversely affect the performance of the broadband high efficiency AIA is the nonlinearity of the class-E PA. The high efficiency PA is limited in their usefulness if the signal distortion due to their inherent nonlinearity is not remedied.

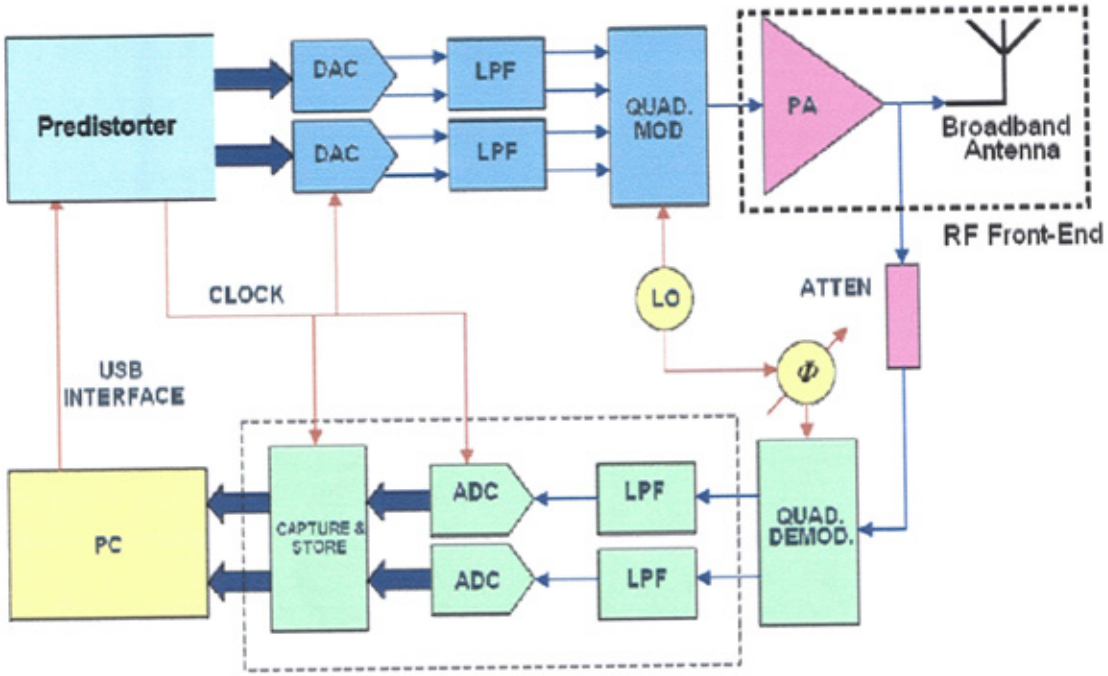

Figure 8.1 Block diagram of proposed advanced transmitter.

The need for increasing capacity in communications systems is placing high demands upon the linearity of transmitters, while the operating frequencies are also increasing with new generations of communications systems. A new level of sophistication is now required to meet the linearity requirements of future generations of communications systems. Hence, it is necessary to generate new architectures for future generations of communications transmitters, exploiting the latest microwave devices and advanced linearization techniques, offering improved channel capacity, power efficiency, spectral efficiency and cost. The wider RF/microwave community will benefit from increased awareness of the potential arising from integration of

highly linearised PA and microwave technologies. The block diagram of suggested research is shown in Figure 8.1.

Bibliography

[1] Y. Chung, and T. Itoh, "TAlGaN/GaN HEFT power amplifier integrated with Microstrip antenna for RF front-end applicationsT," *IEEE Trans. Microw. Theory Tech.*, vol. 51, no. 2, pp. 653-659, February 2003.

[2] S. Pajic and Z. Popovic, "An efficient X-band 16-element spatial combiner of switched-mode power," *IEEE Trans. Microwave Theory Tech.*, Vol. 51, Issue. 7, pp.1863-1870, July 2003.

[3] T. B. Mader and Z. Popovic, "Switch mode high efficiency microwave power amplifiers in a free space power combiner array," *IEEE Trans. Microw. Theory Tech.*, Vo. 46, Issue. 10, Oct. 1998, pp.1391-1397.

[4] H.A. Wheeler, "Small antennas," IEEE Trans. Antennas Propagat., vol. AP-23, pp.462-469, July 1975.

[5] J.R. Copeland, W. J. Roberston, and R. G. Verstraete, "Antennafier arrays," *IEEE Trans. Antennas Propagat.*, vol. AP-12, pp.227-233, Mar. 1964.

[6] H.H. Meinke, "Active antennas," *Nachrichtentech. Z.*, vol. 19, pp.697-705, Dec. 1966.

[7] P. Anderson, W. S. Davies, M. M. Dawoud, and D. E. Galanakis, "Notes on transistor-fed active-array antennas," *IEEE Trans. Antennas Propagat.*, vol. AP-19, pp.537-539, July 1971.

[8] M. M. Dawoud and A. P. Anderson, "Calculations showing the reduction in the frequency dependence of a two-element array antenna fed by microwave transistors," *IEEE Trans. Antennas Propagat.*, vol. AP-20, pp.497-499, July 1972.

[9] _____, "The performance of transistor fed monopoles in active antrennas," *IEEE Trans. Antennas Propagat.*, vol. AP-21, pp.371- 374, may 1973.

[10] M. I. Kontorovich and N.M. Lyapunova, "Active antennas," *Radio Eng. Electron. Phys.* Vol. 19, pp.126-127, 1974.

[11] T. S. M. Maclean and P. A. Ramsdale, "Short active aerials for transmission," *Int. J. Electron.*, vol. 36, pp.261-269, Feb. 1974.

[12] M. M. Dawoud and A. P. Anderson, "Experimental verification of the reduced frequency dependence of active receiving arrays," *IEEE Trans. Antennas Propagat.*, vol. AP-22, pp.342-344, Mar. 1974.

[13] P. K. Rangole and S. S. Midha, "Short antenna with active inductance," *Electron. Lett.*, vol. 10, pp. 462-463, Oct. 1974.

[14] J.P. Daniel and C. Terret, "Mutual coupling between antennas optimization of transistor parameters in active antenna design," *IEEE Trans. Antennas Propagat.*, vol. AP-23, pp.513-316, July 1975.

[15] B. Grob, Basic Electyronics, 6th ed. New York: McGraw-Hill, 1959, ch. 8.

[16] J. Lin and T. Itoh, "Active integrated antennas," IEEE Trans. *Microwave Theory Tech.*, vol. MTT-42, pp. 2186-2194, Dec. 1994.

[17] R. A. York and Z. B. Popovic, Eds., *Active and Quasi-Optical Arrays for solid-State Power Combining.* New York: Wiley, 1997.

[18] L. Wandinger and V. Nalbandian, "Millimeter-wave power combining using quasi-optical techniques," *IEEE Trans. Microwave Theory Tech.*, vol. MTT-31, pp. 189-193, Feb. 1983.

[19] J. W. Mink, "Quasi-optical power combing of solid-state millimeter-wave sources," *IEEE Trans. Microwave Theory Tech.*, vol. MTT-34, pp. 273-279, Feb. 1986.

[20] Kin-Fai Tong, Kwai-Man Luk, Kai-Fong Lee 'A broad-band U-slot rectangular patch antenna on a microwave substrate' IEEE transactions on antenna and propagation Vol, 48. No.6, June 2000

[21] Fan Yang, Xue-Xia Zhang, Xiao-Ning Ye,'Wide band E shaped patch antenna for wireless communication', IEEE transactions on antennas and propagation, Vol.49, No.7, July 2001

[22] S. Gao, L.W.Li, M.S.Leong, " wide-band Microstrip antenna with an H-shaped coupling aperture". *IEEE Transactions* Vol 51 no.1 January 2002.

[23] Stephen D. Targonski and David M. Pozar, 'Deign of wideband circularly polarized aperture-coupled Microstrip antenna', IEEE transaction on antenna and propagation, Vol.41,No.2, Feb .1993

[24] Wen-hsiu Hsu and Kin-Lu Wong 'A wideband circular patch antenna', Microwave and optical Technology letters, Vol. 25, no.5, June 5 2000.

[25] Jen-Yea Jan and Kin Lu Wong 'A broadband circular Microstrip antenna with two open ring slots', Microwave and optical technology letters, Vol. 23, No. 4, Nov 20 1999

[26] Shyh-Tirng Fang, Tzung-Wern Chiou, 'Broadband equilateral triangular Microstrip antenna with asymmetric bent slot and integrated reactive loading', Microwave and optical technology letters Vol. 23, No.3, Nov 5 1999

[27] G. kumar and K.C Gupta, ' Broadband Microstrip antennas using additional resonators gap-coupled to the radiating edges,' IEEE Transactions Vol AP-32, pp. 1375-1379, dec. 1984

[28] D.H. Schaubert ' Multilayer and parasitic configurations', *Hand Book Of Microatrip Antennas,* Vol 1, Chapter 6. 312-351.

[29] K.M. Luk, C.L. Chow, ' Broadband Microstrip patch antenna', Electronic letters 23rd July 1998 Vol. 34 No. 15

[30] Kin-Lu Wong, Tzung-Wern Chiou 'Broadband Single patch circularly polarizaed microstrip antenna with dual capacitively coupled feeds', IEEE transactions on antenna and propagation,Vol 49, No.1 Jan 2001.

[31] Wen-hsiu Hsu and Kin-Lu Wong, 'Broadband probe fed patch antenna with a U-shaped ground plane for cross polarization reduction', IEEE transactions on antenna and propagation Vol 50, No 3, March 2002.

[32] W.K.Lo, J.L. Hu, C.H.Chan, and K.M.Luk. ' L-shaped probe-feed circularly polarized microstrip patch antenna with a cross slot'. Microwave and optical technology letters. Vol. 25,No4, may 20/2000

[33] J.R James, P.S Hall; 'Handbook of microstrip antennas'. Peter Peregrinus Ltd. 1989

[34] Targonski, S.D.; Waterhouse, R.B.; Pozar, D.M.; 'Design of wide-band aperture-stacked patch microstrip antennas'. A P-Transactions IEEE , Vol: 46 Issue: 9 , 1998

[35] Tehrani, H.; T-Y Yun; K Chang; ' A multi-frequency microstrip-fed shorted square ring slot line antenna'. A P-S, 1999. IEEE Vol: 2, 1999

[36] Croq, F.; Papiernik, A.; 'Large bandwidth aperture-coupled microstrip antenna' Electronics Letters, Vol: 26 Issue: 16, 1990

[37] M. I. Aksun, Z. H. Wang, S. L. Chuang, and Y. T. Lo, "Double-slot-fed microstrip antennas for circular polarization operation," *Microwave Opt. Technol. Lett.*, vol. 2, no. 10, pp. 343–346, Oct. 1989.

[38] K.L. Wong and T.W. Chiou, "Broad-band single-patch circularly polarized microstrip antenna with dual capacitively coupled feeds" *IEEE Trans. Antennas Propagat.*, vol. 49, Issue. 1, pp. 41–44, Jan. 2001.

[39] P. S. Hall, "Application of sequential feeding to wide bandwidth, circularly polarized microstrip patch arrays," IEE Proceedings on Microwave, Antennas and Propagation, vol. 136, Oct. 1989, pp. 390–398.

[40] U. R. Kraft, "An experimental study on 2×2 sequential-rotation arrays with circularly polarized microstrip radiators," IEEE Trans. Antennas Propagat., vol. 45, pp. 1459–1466, Oct. 1997.

[41] K. L. Chung and A.S. Mohan, " A circularly polarized stacked electromagnetically coupled patch antenna", *IEEE Trans. Antennas Propagat.*, vol. 52, Issue 5, pp. 1365–1369, May. 2004.

[42] Herbert L. Krauss, Charles W. Bostian, Frederick H. Raab "Solid State Radio Engineering" John Wiley & Sons Inc, July 1979.

[43] Meyer, R.G.; Mack, W.D.; "A wide-band class AB monolithic power amplifier", *Solid-State Circuits, IEEE Journal of.* Volume 24, Issue 1, Feb. 1989 Page(s):7 – 12.

[44] N. O. Sokal and A.D. Sokal, "Class E – A new class of high-efficiency tuned single-ended switching power amplifiers," IEEE J. Solid-State Circuits, Vol. SC-10, pp.168-176, June 1975.

[45] F. H. Raab, "Idealized Operation of the Class E Tuned Power Amplifier," IEEE Transactions on Circuits and Systems, Vol CAS-24, No. 12, pp 725-735, Dec 1977.

[46] N. O. Sokal and A. D. Sokal, "Class E Switching-Mode RF Power Amplifiers__ Low Power Dissipation, Low Sensitivity to Component Tolerances (Including Transistors), and Well-Defined Operation," Proceedings

of the 1979 IEEE ELECTRO Conference, Session 23, New York, New York, 25 April 1979.

[47] M. K. Kazimierczuk and K. Puczko, "Analysis of Class E Tuned Power Amplifier at any Q and Switch Duty Cycle," IEEE Transactions on Circuits and Systems, Vol CAS-34, No. 2, pp 149-159, Feb 1987.

[48] N. O. Sokal, "Class E High-Efficiency Switching-Mode Power Amplifiers, from HF to Microwave," 1998 IEEE MTT-S International Microwave Symposium Digest, June 1998, Baltimore, Maryland,

[49] Ch. P. Avratoglu and N. C. Voulgaris, "A New Method for the Analysis and Design of the Class E Power Amplifier Taking into Account the QL Factor," IEEE Transactions on Circuits and Systems, Vol CAS- 34, No. 6, pp 687-691, June 1987.

[50] F. H. Raab and N. O. Sokal, "Transistor Power Losses in the Class E Tuned Power Amplifier," IEEE Journal of Solid-State Circuits, Vol SC-13, No. 6, pp 912-914, Dec 1978.

[51] N. O. Sokal and R. Redl, "Power Transistor Output Port Model for Analyzing a Switching-Mode RF Power Amplifier or Resonant Converter," RF Design, June 1987, pp 45-48, 50-53.

[52] N. O. Sokal and F. H. Raab, "Harmonic Output of Class-E RF Power Amplifiers and Load Coupling Network Design," IEEE Journal of Solid-State Circuits, Vol SC-12, No. 1, pp 86-88, Feb 1977.

[53] E. W. Bryerton, W. A. Shiroma, and Z. B. Popovic, "A 5-GHz High-Efficiency Class-E Oscillator," IEEE Microwave and Guided Wave Letters, Vol 6, No. 12, Dec 1996, pp 441-443.

[54] F. N. Sechi, "High Efficiency Microwave FET Amplifiers," Microwave Journal, Nov 1981, pp 59-62, 66. (Several "saturated Class B and Class AB"

amplifiers at 2.45 GHz, using several types of GaAs MESFETs: 0.97 W at 71% PAE, 1.2 W at 72% PAE, 1.27 W at 72% PAE.

[55] Mallet, D. Floriot, J. P. Viaud, F. Blache, J. M. Nebus, and S. Delage, "A 90% Power-Added-Efficiency GaIn P/ GaAs HBT for L-Band and Mobile Communication Systems," IEEE Microwave and Guided Wave Letters, Vol 6, No. 3, pp 132-134, March 1996.

[56] S. R. Mazumder, A. Azizi, and F. E. Gardiol, "Improvement of a Class-C Transistor Power Amplifier by Second-Harmonic Tuning," IEEE Transactions of MTT, Vol MTT-27, No. 5, pp 430-433, May 1979.

[57] J. J. Komiak, S. C. Wang, and T. J. Rogers, "High Efficiency 11 Watt Octave S/ C-Band PHEMT MMIC Power Amplifier," Proceedings of the IEEE 1997 MTT-S International Microwave Symposium, Denver, Colorado, June 8-13, 1997, IEEE Catalog No. 7803-3814-6/97, pp 1421-1424.

[58] J. J. Komiak, L. W. Yang, "5 Watt High Efficiency Wideband 7 to 11 GHz HBT MMIC Power Amplifier," Proceedings of the IEEE 1995 Microwave and Millimeter- Wave Monolithic Circuits Symposium, Orlando, Florida, May 15-16, 1995, IEEE Catalog No. 95CH3577-7, pp 17-20.

[59] W. S. Kopp and S. D. Pritchett, "High Efficiency Power Amplification for Microwave and Millimeter Frequencies," 1989 IEEE MTT-S Digest, IEEE Catalog No. CH2725-0/89/0000, pp 857-858.

[60] Bill Kopp and D. D. Heston, "High-Efficiency 5-Watt Power Amplifier with Harmonic Tuning," 1988 IEEE MTT-S Digest, pp 839-842.

[61] L. C. Hall and R. J. Trew, "Maximum Efficiency Tuning of Microwave Amplifiers," 1991 IEEE MTT-S Digest, IEEE Catalog No. CH2870-4/91/0000, pp 123-126.

[62] T. Mader, M. Markovic, Z. B. Popovic, and R. Tayrani, "High-Efficiency Amplifiers for Portable Handsets," Conference Record, IEEE PIMRC'95

(Personal, Indoor and Mobile Radio Communications), Sep 1995, Toronto, Ontario, Canada, IEEE publication 0-7803-3002-1/95, pp 1242-1245.

[63] T. B. Mader, "Quasi-Optical Class-E Power Amplifiers," PhD thesis, 1995, University of Colorado, Boulder, Colorado.

[64] Sowlati, Tirdad. "Low voltage, high efficiency GaAs class E power amplifiers for wireless transmitters", IEEE J. Solid-State Circuits, Vol 30,NO.10 (Oct 1995), 1074-1080

[65] Grebennikov "Switched-mode RF and microwave parallel-circuit Class E power amplifiers" Inter Journal of RF and Microwave, Vol 14 (January 2004), 21-35.

[66] T. B. Mader, Z. Popovic, "Switch mode high efficiency microwave power amplifiers in a free space power combiner array," IEEE J. transactions on microwave and techniques, pp.1391-1397, Oct. 1998

[67] Natalino, Camilleri "Monolithc Millimeter-Wave IMPATT Oscillator and Active Antenna" IEEE Transactions on MTT, vol36, No.12, December 1988

[68] J. Lin and T. Itoh, "Two-diniensional quasi-optical power-combining arrays using strongly coupled oscillators," *IEEE Trans. Microwme Theory Tech.*, vol. 42, pp. 734-741. Apr. 1994.

[69] J. Birkeland and T. Itoh, "Spatial power combining using push-pull FET oscillators with microstrip patch resonators,"IEEE *MTT-S Inr. Microwave Symp. Dig.*, vol. *3*, 1990, pp. 1217-1220.

[70] R. A. York and R. C. Compton, "Quasi-optical power combining using mutually synchronized oscillator arrays," *IEEE Trans. Micuowtrve Theory Tech.*, vol. *39*, pp. 1000-1009, June 1991.

[71] J. Birkeland and T. Itoh, "A 16-element quasi-optical FET oscillator power-combining array with external injection locking," *IEEE Truns. Microwuve Theon] Tech.*, vol. 40, pp. 475-481, Mar. 1992.

[72] Mortazawi, H. D. Foltz, and T. Itoh, "A periodic second harmonic spatial power-combining oscillator," *IEEE Trans. Microwave Theon Tech.*, vol. 40, pp. 851-856, May 1992.

[73] S. Kawasaki and T. Itoh, "40 GHz quasi-optical second harmonic spatial power combiner using FETs and slots," in *1992 IEEE MTT-S Int. Microwave Symp. Dig.*, vol. 3, June 1-5, 1992, pp. 1543-1546.

[74] H. Ohmine and A. Iida *ef a/.*, "An MMIC aperture-coupled microstrip antenna in the 40 GHz Band," in *Proc. ISAP*, pp. 1105-1 108, 1992.

[75] J. Lin and T. Itoh, "A 4 x 4 spatial power-combining array with strongly coupled oscillators in multilayer structure," *IEEE MU-S Inf. Microwuve Symp. Dig.*. vol. 2, Atlanta, GA, June 14-18, 1993, pp. 607-610.

[76] Mortazawi and B. C. DeLoach, "A nine-MESFET two-dimensional power-combining array employing an extended resonance technique," *IEEE Microwave Guided Wuve Lett.*, vol. 3, pp. 214-216, July 1993.

[77] S. Kawasaki and T. Itoh, "Second harmonic uniplanar active integrated antenna array with strong coupling," *23rd European Microwave Conf Procs.*, vol. I , Sept. 1993, pp. 204-206.

[78] S. Nogi, J. Lin, and T. Itoh, "Mode analysis and stabilization of a spatial power-combining array with strongly coupled oscillators," *IEEE Trans. Microwave Theon Tech.*, vol. 41, pp. 1827-1837, Oct. 1993.

[79] J. Lin, S. Nogi and T. Itoh, "Frequency tuning of a spatial power combining array using strongly coupled oscillators," *Proc. 1993 Asia- Par. Microwave Con$*, Hsinchu, Taiwan, Oct. 1993, pp. 1.26-1.29.

[80] S. Kawasaki and T. Itoh, "Quasi-optical planar arrays with FET's and slots," *IEEE Truns. Microwave Theonl Tech.*, vol. 41. pp. 1838-1844, Oct. 1993.

[81] Balasubra maniyan and A. Mottazawi, "Two-dimensional MESFET based spatial power combiners," *IEEE Microwuve Guided Wave Left.*, vol. 3, pp. 366368, Oct. 1993.

[82] R. Gillard, H. Legay, J. M. Floc'h, and J. Citerne, "Rigorous modelling of receiving active microstrip antenna,'' *Electron. Lett.*, vol. 27, no. 25, pp. 2357-2359, Dec. 1991.

[83] B. Robert, T. Razban, and A. Papiemik, "Compact amplifier integration in square patch antenna,'' *Electron. Lett.*, vol. 28, no. 19, pp. 1808-1810, Sept. 1992.

[84] D. J. Roscoe, A. Ittipiboon, and L. Shafai, "The development of an active integrated microstrip antenna," *IEEE AP-S In?. Symp. Dig.*, vol. I, June 24-28, 1991, pp. 48-51.

[85] R. Ken, P. H. Siegel and R. J. Mattauch, "A simple quasi-optical mixer for 100-120 GHz," *IEEE MTTSInt. Microwave Symp. Dig.*, 1977, pp. 96-98.

[86] K. D. Stephen, N. Camilleri, and T. Itoh, "A quasi-optical polarizationduplexed balanced mixer for millimeter-wave applications," *IEEE Trans. Microwave Theory Tech.*, vol. MTT-31, pp. 164-170, Feb. 1983.

[87] K. D. Stephen and T. Itoh, "A planar quasi-optical subharmonically pumped mixer characterized by isotropic conversion loss," *IEEE Trans. Microwave Theory Tech.*, vol. MTT-32, pp. 97-102, Jan. 1984.

[88] V. D. Hwang and T. Itoh, "Quasi-optical HEMT and MESFET selfoscillating mixers,'' *IEEE Trans. Microwave Theonl Tech.*, vol. MTT-36, pp. 1701-1705, Dec. 1988.

[89] J. Zmuidzinas and H. G. LeDuc, "Quasi-optical slot antenna SIS mixers," *IEEE Trans. Microwave Theory Tech.*, vol. 40, pp. 1797-1804, Sept. 1992.

[90] N. Camilleri and T. Itoh, "A quasi-optical multiplying slot array," *IEEE Trans. Microwave Theory Tech.*, vol. MTT-33. pp. 1189-1 195, Nov. 1985.

[91] Cynthia y. hang "high efficiency transmitter front-ends integrated with planar antennas and pbg" Microwave Conference, 2000 Asia-Pacific 3-6 Dec. 2000 Page(s):888 - 894